Investigating Cortical Reorganization Following Motor Cortex Photothrombotic Stroke In Mice

Zachary Eckert, MSc. Candidate in Neuroscience

Department of Cellular and Molecular Medicine

Faculty of Medicine

University of Ottawa

Abstract

Following a stroke, normal usage of the impaired limb guides spontaneous recovery across many months or even years; however, recovery is rarely complete. Pre-clinical tools are needed to investigate stroke-induced cortical reorganization over long periods. This thesis aims to characterize stroke impairment and spontaneous recovery in parallel with a battery of behaviour tasks in a mouse model of focal stroke. Young adult Thy1-ChR2 mice were implanted with a transcranial window over the intact skull permitting cortex visualization and enabling longitudinal assessments with light-based motor mapping and intrinsic signal optical imaging. Furthermore, mice were tested on sensorimotor behavioural tasks in parallel to the mapping experiments. These experiments allowed for the quantification of impairments in the sensorimotor cortex and forelimb function while identifying regions within the sensorimotor cortex that show re-mapping associated with behavioural recovery. Following primary motor cortex-stroke induction, both sensory and motor map impairments occurred. Sensory map transient impairments recovered within the same atlas-defined regions two weeks after a primary motor cortex stroke as identified by intrinsic signal optical imaging. In contrast, motor forelimb recovery was observed four weeks after the stroke in the peri-infarct region, the supplemental motor cortex, and the contralesional motor cortex. This recovery was identified through a combination of analyses, including changes in the mapped area and the amplitude of evoked forelimb movements using light-based motor mapping. Behavioural recovery occurred four to six weeks post-stroke, depending on the sensitivity of the task in forelimb impairment. Additionally, the contralesional hemisphere and forelimb did not show impairment acutely but evoked forelimb amplitude was significantly increased by post-stroke week four for both forelimbs. As the first study to conduct within-animal longitudinal spontaneous recovery sensory and motor map experiments using bilateral forelimb and hemispheric representations, we show that 1) photothrombotic stroke impacts both forelimb representations pertained within the ipsilesional hemisphere in LBMM experiments, 2) recovery of the impaired forelimb occurs ipsilesionally and contralesionally and, 3) impairments from stroke observed through motor mapping are functionally relevant and precede behavioural recovery ranging from zero to two or more weeks depending on the motor cortex's involvement in the behavioural task.

Table of contents

Page

List of Figures

List of Supplemental Figures

List of Abbreviations

CFA – Caudal Forelimb Area

LBMM – Light-Based Motor Mapping

M1 – Primary Motor Cortex

M2 – Secondary Motor Cortex

MCAO – Middle Cerebral Artery Occlusion

ICMS – Intracortical Microstimulation

IP – Intraperitoneal

ISOI – Intrinsic Signal Optical Imaging

iTBS – Intermediate Theta Burst Stimulation

LDI – Laser Doppler Imaging

PT – Photothrombosis

RFA – Rostral Forelimb Area

S1 – Primary Sensory Cortex

SEM – Standard Error of Mean

TMS – Transcranial Magnetic Stimulation

tPA – Tissue Plasminogen Activator

Acknowledgments

Though the last two years are only a blimp of my education, they are some of my most cherished and important years yet. I know I can always look back on my time here and be grateful that I decided to pursue this degree in the Silasi lab. For this reason, I would like to express my sincere gratitude to Dr. Greg Silasi for the opportunity to complete this degree in his lab. Through his mentorship and support, he provided an environment to explore and learn more about neuroscience and how stroke impacts the brain. Dr. Silasi enabled me to freely pursue my interests under the guidance of what would be best for my experiments.

Thank you to all the past members of the Silasi lab. Everything is a continuous growth story, and a lot of my data is based on their work to establish our pre-existing knowledge going into my study. For that reason, a special thank you to Sarah Zhang. I would also like to mention the members in the Silasi lab during my time here, Rana Abdelhalim, Beatriz Romero Quineche, Ségolène Chevallier Rufigny, Danya Alomar, Patrick Chary, Fiona Haugen, and Irina Morozov. Their guidance, skills, and lending ears have not only elevated my experience but also increased the quality of my work. I would like specifically to thank my lab mates: Eilia Dizgah for his help with the collection and analysis of behaviour data, Shafik Algharbi for helping with brainstorming and making workflow more efficient, as well as Katie Neale for mentoring me during my early time in the lab and aiding in establishing tools for motor mapping experiments.

A special thank you to Maxime Abran and Bruno Souza from LabeoTech for their software and hardware engineering support. Their support enabled me to collect data at a greatly increased pace, and I am incredibly grateful for their time and wisdom.

Thank you to my thesis advisory committee, Dr. Katalin Tóth, and Dr. Simon Chen, for providing unique viewpoints through their expertise in neuroscience.

Finally, I would like to thank my friends and family. To my friends for boosting my morale and listening to me figure out missing pieces of my work late at night, and my family and, most importantly, my wife Lauren Eckert for supporting me and ensuring I established proper and sustainable working habits.

1. Introduction

1.1. Clinical research on stroke recovery.

Stroke is a main concern in modern society, as stroke is Canada's third leading cause of death. In 2018, 878,500 Canadians suffered from stroke, with over 50,000 new cases yearly (Strokes in Canada, 2017; Ontario Stroke Network, 2020). More than 60% of all stroke cases produced lasting disability, often expressed as an impairment in sensorimotor function in the contralateral upper limb (Lee *et al.,* 2015; Rudd *et al*., 2017; Cramer *et al.*, 1997; Broughton *et al*., 2009; Hatem *et al*., 2016; Jones & Adkins, 2015). Sensorimotor impairments are common because ischemic strokes – the most prevalent form of stroke, accounting for 87% of all stroke cases (Saini *et al.,* 2021), often occur in the middle cerebral artery, the main blood vessel for the motor and sensory regions within the human brain (Nogles & Galuska, 2023). Although most motor recovery is spontaneous and occurs in the first three months, complete recovery of motor impairments through physical rehabilitation can take years, if ever at all (Stroke in Canada, 2017; Ontario Stroke Network, 2020). Furthermore, stroke impacts many countries financially since stroke most commonly restricts physical abilities and results in weakness or even paralysis of the contralesional side of the body (Kim, 2022). As a result, partial recovery from stroke impairments results in disability claims of over 30 billion dollars annually (Roger *et al.,* 2012). Therefore, a better understanding of stroke recovery is needed to optimize patient recovery and increase functional recovery reliably.

Regarding the sensorimotor cortex, stroke recovery is a spontaneous process that occurs over three to six months post-stroke through reintegrating the impaired regions functions over time (Lee *et al.,* 2015). Phases of recovery can be categorized as either acute (< three weeks), subacute (three weeks – six months), early chronic (six months – 18 months), and late chronic (> 18 months) (Ballester *et al.,* 2019; Bernheisel *et al.,* 2011; Duncan *et al.,* 2000; Donnan *et al.,* 2008; Kang *et al.,* 2004; Poh, 2013). Endogenous mechanisms that promote recovery peak in the acute phase and tamper in relative recovery until absent in the late chronic phase (Coleman *et al.,* 2017). During acute post-stroke recovery, edema and reperfusion of the ischemic penumbra, followed by neuronal plasticity reorganization, are

associated with functional recovery (Berber *et al.,* 1998; Hallett, 2001; Carmichael, 2005; Clark *et al.,* 2019). However, no rehabilitative interventions should occur in the first 24 hours, as it damages stroke recovery in animal models (Shen *et al.,* 2016). Depending on the severity of the stroke and the health of the patient, recovery can result in partial or complete recovery after six months (Lee *et al.,* 2015; Cassidy & Cramer, 2017; Duncan *et al.,* 1992; Poomalai *et al.,* 2023). However, because more than 60% of stroke cases do not recover, techniques to promote ideal recovery are being investigated.

1.2. Stroke impairment and recovery

Following a stroke, disruption in blood flow from atherosclerosis or plaque dislodgements diminishes blood flow, and neurons lack essential nutrients causing cellular stress. If the disruption in blood flow is prolonged, brain cells die, and the neural network is significantly disrupted (Broughton *et al*., 2009). Specifically, neurons are especially susceptible to hypoxia-induced stress as they are aerobic. In response to this crisis, cells' lack proper cell nutrients to maintain the cell charge, become overloaded with positive charge, and release glutamate to surrounding cells, which hyperstimulates nerve cells, ultimately resulting in the ischemic cascage (Deleglise *et al.,* 2018; Puig *et al.,* 2018; Yi & Hazell, 2006). Additionally, the surrounding tissue of an occluded blood vessel, known as the peri-infarct, has been observed to experience partial ischemia followed by reperfusion over time (Gerbaud *et al*., 2014. Cramer *et al*., 2006). This results in a cascade of events, including a temporary synaptic loss and neuronal dysfunction immediately following stroke onset, two weeks of increased tonic GABAergic levels (Clarkson *et al*., 2010), and a prolonged period (six weeks) of heightened synaptic plasticity following stroke (Brown *et al*., 2007; Jones *et al*., 1981; Murphy & Corbett, 2009; Jones & Adkins, 2015; Citri & Malenka, 2008; Nishibe *et al*., 2015; Pino *et al*., 2014).

One approach to improving post-ischemic stroke recovery involves thrombolysis, which aims to remove the blockage, restore blood supply, and minimize neuronal damage (Robinson *et al.,* 2011). One popular form is to inject tissue plasminogen activator (tPA), an endogenous protease which dissolves fibrin-based clots and restores blood flow (Gravanis & Tsirka, 2008). Although these are cost-effective and provide a great margin for success in decreasing stroke

effects, tPA must be administered within 5 hours of a stroke to be effective (Tung *et al.,* 2011). Furthermore, tPA has extensive exclusive criteria, which can cause many not to be eligible for treatment (Hughes *et al.,* 2023). An alternative technique involves thrombectomy, a mechanical intervention procedure designed to extract clots from the brain (Pilgram-Pastor *et al.,* 2021). This treatment is highly effective and can significantly enhance the acute and chronic performance of patients (Aghamiri *et al.,* 2022). However, thrombectomy demands swift and accurate diagnosis and treatment, akin to tPA (Pilgram-Pastor *et al.,* 2021). Additionally, thrombectomy tends to be costly (Patil *et al.,* 2009). It is important to note that thrombectomy is not suitable for all types of strokes; it's ineffective for hemorrhagic strokes and may not be applicable for certain clot locations and sizes (Chen *et al.,* 2023; Matthew & De Jesus, 2023). As a result, researchers also explore the phenomenon of stimulation-induced recovery during the subacute to chronic stages post-stroke to promote recovery to mitigate the effects of stroke.

Stroke rehabilitation research aims to identify brain regions implicated in recovery and reinforce their activity to promote cortical reorganization. To achieve this, techniques such as transcranial magnetic stimulation (TMS) are employed to investigate post-stroke reorganization of the motor cortex (Hoyer & Celnik, 2011). TMS is primarily utilized as either a therapeutic technique, where patterned or repetitive stimulation occurs in a controlled location to promote positive recovery (Huang *et al.,* 2005; Blumberger *et al.,* 2018; Tsuboyama *et al.,* 2019; Huang *et al.,* 2022), or as a probing technique to generate motor map representations (Nowak *et al*., 2008; Adkins *et al.,* 2006; Chail *et al.,* 2018; Basil *et al.,* 2005). To generate motor maps, single-pulse TMS is utilized to evoke motor potentials, an important biomarker in impairment and recovery trends post-stroke (Yarossi *et al.,* 2019; Włodarczyk *et al.,* 2022). However, several factors regarding stroke occurrence in a clinical population make it difficult to induce recovery within stroke rehabilitation patients reliably. First, stroke location varies significantly within and across clinical studies (Hui *et al*., 2021), making comparisons and conclusions on recovery challenging to analyze. Second, stroke size is often variable and can affect impairment and recovery differently. Third, recovery can be significantly influenced by underlying health conditions and comorbidities (such as diabetes, obesity, and depression), age, and lifestyle (Alawieh *et al*., 2018). Finally, inconsistencies in inducing recovery may stem from stimulating

the wrong regions, as research is inconsistent on locations to target following a stroke (Wang *et al*., 2019; Kubis, 2016; Veldema & Gharabaghi, 2022). Therefore, animal models allow one to study recovery mechanisms without the previously stated confounding variables. Additionally, non-invasive stimulation paradigms can be combined with the photothrombotic stroke model, commonly used to determine spatiotemporal recovery following localized stroke. Therefore, further understanding of spontaneous recovery is required to promote reliable and beneficial recovery in clinical environments.

1.3. Stroke and spontaneous recovery

Immediately following stroke, glutamate-mediated excitotoxicity results in neuronal death and disrupts the excitatory-inhibitory balance across hemispheres (Lai *et al*., 2014; Grigoras & Stagg, 2021). During the acute period, the increased GABAergic activity in the ipsilesional hemisphere (known as the interhemispheric inhibition model) is counteractive in promoting recovery. Clarkson *et al.,* 2010 demonstrated that decreasing peri-infarct GABAergic levels promoted recovery post-stroke in animal models. However, this maladaptive inhibitory process is currently understood to be essential for counteracting hyperacute glutamate-mediated excitotoxicity (Lai *et al*., 2014; Grigoras & Stagg, 2021). After excitatory and inhibitory balances are restored, neurons are responsive again. This end stage of the acute period recovery is considered a critical endogenous window for promoting recovery; however, results remain inconsistent.

Acute period spontaneous recovery can vary greatly in duration and location and is heavily influenced by stroke size. After a small-focal stroke, surviving peri-infarct neurons receive brain-wide connections from both up- and down-stream neural circuits to support restoration or compensation of lost functions (Harrison *et al*., 2013; Murphy & Corbett; 2009; Jones & Adkins, 2015; Buetefisch, 2015). Additionally, recovery occurs more rapidly when comparing a small-focal stroke against a stroke of a larger magnitude (Okabe *et al*., 2016; Zeiger *et al.*, 2021; Nishibe *et al*., 2015; Wang *et al*., 2009). After larger strokes encompassing entire functional regions, maladaptive recovery can strengthen the ipsilateral tract from the uninjured hemisphere while promoting learned non-use as a compensation technique (Cirillo *et al.,* 2019;

Takeuchi & Izumi, 2012). Although recovery happens spontaneously, the disruption of neural circuits usually prevents functional recovery to baseline levels for the impaired limb, but recovery can be promoted by learning and rehabilitation (Nudo, 2006, 2007). Therefore, plasticity plays an essential role in post-stroke recovery, where neuronal reorganization is theorized to be correlated with behavioural recovery (Hylin *et al.,* 2017).

1.4. The primary motor cortex

The primary motor cortex (M1) is a critical region for acquiring new motor skills and executing multiphasic and complex forms of coordinated movement (Papale *et al*., 2018). In healthy conditions, a movement intent descends from the motor cortex down the corticospinal tract to lower motor neurons in the ventral horns of the spinal cord for voluntary movement of the upper limbs (Van Wittenberghe & Peterson, 2023). The direct projecting Betz cells result in fast contralateral latencies from M1 and are useful for determining direct vs. indirect spinal tracts during movement (Taylor & Gandevia, 2004). However, 10% of Betz cells are directly ipsilaterally projecting and are believed to be important in movement planning and execution, as well as coordination of bimanual movements (Bundy & Leuthardt, 2019). The rubrospinal tract also is a pathway important for upper limb usage. However, the rubrospinal tract is traditionally associated with involuntary regulation for fine muscle control in distal regions (Lee & Muzio, 2022), thus coordinating with voluntary movements from the corticospinal tract to permit digit manipulation (Fujito *et al.,* 1995; Küchler *et al.,* 2002). Following a stroke, clinical work has demonstrated a strong correlation between the degree of corticospinal tract damage and motor impairment, suggesting that it may be a biomarker for recovery due to its importance in voluntary movements (Maraka *et al.,* 2014; Lin *et al.,* 2019). Therefore, injuries to M1 lead to upper limb impairments stemming from the disruption of motor neuronal tracts, including the corticospinal and rubrospinal tracts (Ito *et al.,* 2022).

When translating to non-human models, it became clear that the best option would be other non-human primates as the structural comparison in the neuroanatomy of the primary motor cortex is highly conserved, and primates have strong dexterous skills (Kwon *et al.,* 2015; Lemon *et al.,* 2019). However, it is not practical to use primates for many researchers due to

the strong ethical concerns, and alternative models such as mice which pertain to a rich history of genetic manipulation. As a result, rodents are an ideal model as the motor cortex hierarchical organization is highly conserved (Bakken *et al.,* 2021), and they have some degree of dexterous movements which permit object manipulation with their paws (Gu *et al.,* 2017; Lemon *et al.,* 2019). An important distinction is that rodents like mice do not possess direct cortico-motoneuronal connections. However, corticospinal tracts predominantly innervate spinal cord regions that control movements of the forelimbs, such as segmental interneurons (Moreno-Lopez *et al.,* 2021). In contrast, the human corticospinal tract is extensively developed and plays a significant role in controlling fine motor movements, particularly in the hands (Nathan, 1994; Krisa *et al.,* 2018). Although this distinction is primarily a concern for spinal lesion experiments, the difference in corticospinal tract representations should be considered.

Regarding the motor cortex, the functional representation of mouse forelimbs is divided into two key regions: the caudal forelimb area (CFA), analogous to M1, and the rostral forelimb area (RFA), equivalent to the supplementary motor cortex (M2) (Okabe *et al*., 2016; Tennant *et al.,* 2011). CFA characterization includes a high density of corticospinal and rubrospinal tract neurons (Neafsey *et al*., 1986) and is highly conserved across species (Ebbesen & Brecht, 2017; Bakken *et al.,* 2021). On the other hand, RFA is a unique region composed of a mix of M2 (agranular medial) and M1 (agranular lateral) structures (Tennant *et al*., 2011). Alike CFA, RFA also pertains both corticospinal tract and rubrospinal tract neurons, however RFA connects with different striatal and thalamic representations presumably due to its supplementary or pre-motor role (Rouiller *et al.,* 1993; Touvykine *et al.,* 2020). While CFA primarily governs basic motor functions, RFA is critical in more complex motor control, including fine-tuned manipulations (Brown & Teskey, 2014; Tennant *et al*., 2016).

Despite these functional distinctions, CFA and RFA send descending motor tracts to common locations along the motor axis, facilitating interactions between the hemispheres. This bilateral connectivity means one hemispheric motor representation impairment can impact contralateral and ipsilateral movements. CFA is often studied in experimental models involving lesions or strokes to assess the primary motor cortex's effects on basic motor behaviours, given its strong clinical relevance to M1 (Nishibe *et al.,* 2014) and dominant corticospinal tract

representations (Neafsey *et al*., 1986). Conversely, RFA has fewer interhemispheric connections than humans due to the smaller frontal cortex but more intrahemispheric circuits, presumably for processing sensorimotor information (Assaf *et al.,* 2020; Xu *et al.,* 2022). As a result, RFA is commonly investigated in experiments focusing on “higher-order” motor commands and complex motor recovery processes (Brown & Teskey, 2014; Tennant *et al*., 2016).

While mice may not possess the same level of dexterity as humans, mice provide a practical and valuable model for studying forelimb usage in motor mapping and behaviour and investigating impairments resulting from cortical damage, such as stroke. Furthermore, it is worth considering that fundamental questions related to corticospinal tract rewiring, hemispheric interactions, and cortical reorganization following developmental injuries can be thoroughly explored in "lower-order" model organisms like mice before advancing to more resource-intensive and costly primate or human experiments. This approach allows a deeper understanding of the underlying mechanisms and principles in a controlled and sustainable environment.

1.5. Intracortical microstimulation motor mapping

In order to assess the state of the motor cortex in animal models, motor mapping can be applied. Motor mapping was first introduced in 1870 by Fritsch and Hitzig (Fritsch & Hitzig, 1870). Fritsch and Hitzig utilized electrical stimulation from surface electrodes to evoke and record motor-induced muscle twitches, a novel finding in 1870. (Carlson and Devinsky, 2009). In more recent studies, intracortical microstimulation (ICMS) application directly inserts a stimulating electrode into the deep layers of the motor cortex. Muscle activity can be induced upon applying electrical current, producing movements in mammals through direct and indirect motor neurons (Asanuma & Sakata, 1966; Asanuma & Ward, 1970). Responses were generated based on the duration of the stimulation train; short trains of pulses evoked simplistic movements (Stephiewska *et al.,* 2011), whereas longer stimulation trains resulted in complex movements such as reaching and grasping (Graziano *et al.,* 2002; Kaas *et al.,* 2013). The resulting evoked movements were determined to be a proxy for the state of the motor cortex and are comparable to clinical techniques such as transcranial magnetic stimulation (Brown &

Teskey, 2014; Young *et al*., 2011; Corbett *et al.,* 2017). Additionally, ICMS motor maps are modulated by paired-pulse stimulation and permitted neural circuit dissections across structural regions by facilitating or inhibiting motor-evoked potentials (Lo *et al.,* 2020; Hanajima *et al.,* 1998; Touvykine *et al.,* 2020). Therefore, ICMS has proven valuable in assessing the state and connectivity of the cortex through evoked movements.

ICMS-evoked movements are precisely characterized based on muscle groups or specific anatomical regions, such as the wrist, elbow, or shoulder, as well as movement types like elevation, advancement, or retraction (Brown *et al.,* 2023). This comprehensive approach allows for a detailed analysis of motor cortex representations for a specific area, such as the upper forelimb. Alternatively, multiple motor regions such as the face, tail, forelimbs, and hindlimbs can be analyzed to provide a comprehensive motor cortex representation of an organism (Tennant *et al.,* 2011). Overall, ICMS-evoked movements permit for a proxy of motor cortex representations and can be essential in stroke impairment and recovery studies.

ICMS has since been applied in stroke models to monitor motor cortex neuronal reorganization responsible for controlling movement at baseline compared to different recovery time points (Nishibe *et al*., 2014; Boychuk *et al*., 2011; Shiromoto *et al*., 2017; Tennant *et al*., 2011). Many ICMS researchers analyze the contralateral forelimb motor map regions CFA and RFA comparisons to baseline conditions due to the clinical significance of upper limb impairments (Lee *et al.,* 2015). Following a lesion to CFA, RFA is observed to play a role in the recovery process post-stroke; however, lesion volume determines the role RFA executes. After a small-volume CFA stroke, plastic reorganization occurs in the peri-infarct space, ipsilesional RFA, homotopic contralesional CFA and potentially other functionally relevant locations (Nudo *et al.,* 1996; Nishibe *et al.,* 2015; Murphy & Corbett, 2009; Tennant *et al.,* 2011; Nudo, 2007; Jones & Adkins, 2015; Pino *et al*., 2014). In a large-volume CFA stroke, RFA compensates for complete connectivity loss at CFA, where RFA exhibits plastic recovery and increased spinal cord projections of the rubrospinal tract (Okabe *et al*., 2016; Jones & Adkins, 2015). Furthermore, distinctions in large and small volume CFA stroke result in a change in functional recovery, as observed in behavioural studies (Okabe *et al.,* 2016). As a result, the presence of the peri-infarct region in smaller-volume stroke cases has emerged as a noteworthy biomarker

for recovery. Alterations in the peri-infract space include: motor map plastic reorganization within the peri-infarct (Harrison *et al.,* 2013; Jones & Atkins, 2015), heightened peri-infarct excitability (Carmichael, 2012), expansion of motor maps (Nudo *et al.,* 1996; Kleim *et al.,* 2003), synaptic plasticity (Zeiger *et al.,* 2021; Brown *et al.,* 2007), and the integration of sensory information (Bice *et al.,* 2023). However, animal models have a particularly difficult task with investigating peri-infarct recovery longitudinally due to some limitations with ICMS.

Although ICMS has become a standard in the field for providing essential cortical representations of neural connectivity, it is limited by several methodological drawbacks. First, the methodology is invasive, requiring a highly invasive craniotomy surgery to expose the cortex. Permitting stimulating electrodes to penetrate deep output layers of the cortex (layer V) to activate a local population of neurons, inducing twitch-like movements (Cheney *et al.,* 2013). Electrodes are injected into multiple stimulation sites to record or induce neural circuits, resulting in the severe disruption of the cortex's natural state, ultimately leading to the sacrifice of the animal after map acquisition (Guo *et al.*, 2021). Therefore, when assessing stroke impairment and recovery trends, multiple cohorts of animals are required to assess overall trends in data representations, as longitudinal recordings are non-obtainable. Second, ICMS does not permit cell-type selective investigation when inducing movements, as electrode stimulation is an electric current. Third, due to the long-duration experimental protocol, only one hemisphere motor map to one forelimb interaction is typically performed during ICMS motor mapping. Therefore, it remains evident that non-invasive brain stimulation needs to be applied to “lower-order” model organisms to understand further spontaneous recovery, ultimately guiding clinical recovery strategies.

1.6. Rodent models for assessing post-stroke spontaneous recovery.

1.6.1. Light-Based Motor Mapping

During light-based motor mapping (LBMM), a brief light pulse induces a twitch-like motor movement to assess the condition of the motor cortex. To achieve this, light-sensitive cation channel, channelrhodopsin-2 (ChR2) from green algae (*Chlamydomonas reinhardtii*) expression occurs in a subpopulation of cortical neurons under the Thy-1 promoter. Thy-1 is

expressed in layer V pyramidal neurons (PN) (Arenkiel *et al*., 2007; Ayling *et al*., 2009), permitting for optogenetic stimulation of the large PN apical tufts with light at superficial layers of the cortex. This stimulation activates various descending motor pathways, including local circuitry, homotopic representations of the motor cortex, motor thalamic nuclei, the pons, the striatum, and directly to the spinal cord (Baker *et al.,* 2018; Hussin *et al*., 2015; Spruston, 2008; Jiang *et al*., 2020). Therefore, twitch-like motor movements can be induced in anesthetized animals to assess cortical movement control through the direct corticospinal tract and indirect rubrospinal tract representations.

An additional advantage of LBMM is that optogenetic stimulation may be applied through the intact skull of adult mice (Silasi *et al.*, 2016). Minimally invasive cortex visualization is achieved by surgically implanting a transcranial window that provides optical access to the entire dorsal cortex surface in both hemispheres. Permitting for bilateral non-invasive longitudinal stimulation of the cortex to represent post-stroke reorganization through LBMM. LBMM aims to utilize the non-invasive motor mapping from clinical studies with the control of animal models. Clinical depiction of motor recovery using transcranial magnetic stimulation lacks pre-stroke representations, as seeking non-invasive stimulation before a motor injury is impractical. Animal models have utilized alternative techniques, as applying traditional non-invasive stimulation to a small-scale rodent cortex is not plausible.

For this reason, ICMS has been a leading tool for investigating cortex reorganization within rat models, and more recently, mouse models as electrodes have become refined (Jeong *et al.,* 2016). However, when ICMS stimulates a site, current from the electrode spreads to affect a broader area of the cortex, resulting in imprecisions and overlap in functional areas (Han *et al.,* 2018). Due to the limitations of the functional parcellation of the cortex and the relatively small size of motor map representation in rodents, stimulation sites are spaced by cortical columns (0.3 – 0.5mm), resulting in less than 50 stimulation sites from the motor cortex, with around half giving evoked outcomes (Singleton *et al.,* 2021; Brown & Martinez). LBMM overcomes the issue of small cortex space by using a 50 µm laser diameter, creating motor maps with 350 stimulation sites, and two repetitions. The small-diameter laser increases the spatial resolution while maintaining the quality of short-burst ICMS (Neafsey *et al.,* 1986;

Young *et al.,* 2011). Importantly, LBMM does not alter the cortical representation of movements, which is a known effect of ICMS (Nudo *et al.,* 1990; Harrison & Murphy*,* 2013); thus, overlapping stimulation sites does not alter the recording of the following stimulation sites. Furthermore, the presence of evoked-forelimb movements can be used as a biomarker for impairment and recovery as seen in clinical studies (Escudero *et al.,* 1998; Boyd *et al.,* 2017; Cassidy & Cramer, 2016; Kowalski *et al.,* 2019; Hallett, 2007; Zhang *et al.,* 2022). Therefore, since optogenetic stimulation does not alter motor map representations, LBMM permits for potentially more precise analysis of the peri-infarct location during recovery by increasing repetitions and recording spontaneous recovery longitudinally following stroke.

The novelty of LBMM extends from the non-invasive longitudinal cortex recording. Since ICMS typically investigates only impaired forelimb to impaired hemisphere interactions, we aim to utilize bilateral forelimb recording with bi-hemispheric cortical representations to investigate further the peri-infarct reorganization pre- to post-stroke and interhemispheric reorganization. A research approach that, to our knowledge, has yet to be previously explored. Additionally, assessment of the sensory cortex is also permitted in this model, as LBMM is non-invasive and does not disrupt the state of the cortex. Therefore, LBMM can be combined with other non-invasive recordings to better understand the state of the cortex and reorganization following a motor cortex stroke.

One example of LBMM recording mice cortex reorganization is from Harrison *et al.,* 2013. Harrison *et al.* conducted longitudinal recordings of impairment and spontaneous recovery in the ipsilesional hemisphere following a PT stroke localized to the motor or sensory cortex. Their findings revealed decreased motor outputs during acute phase recovery and increased peri-infarct excitability during chronic phase spontaneous recovery. Therefore providing longitudinal recordings in peri-infarct recovery, and suggesting its role in spontaneous recovery. Notably, this study marked one of the first instances of performing longitudinal LBMM in mouse models; however, it focused solely on the ipsilesional hemisphere and did not include recordings from the nonimpaired forelimb. Since then, Zhang *et al. (*2021) have expanded on this research by utilizing LBMM with bi-hemispheric stimulations and bilateral forelimb recordings. Zhang *et al.* demonstrated how motor cortex PT stroke in a neonatal mice

model affects adult motor map outputs at a single time point in recovery while using a behavioural battery of sensorimotor tasks to measure functional recovery. Zhang *et al*. investigated how PT stroke in mice motor cortex during neonatal stages could impact motor map outputs in adulthood, examining a single LBMM time point in the recovery process. They also employed a battery of sensorimotor tasks to measure functional recovery. Their study revealed correlations between LBMM latency and area with functional behavioral recovery, suggesting the potential use of LBMM parameters as biomarkers for recovery.

In summary, LBMM to date has been utilized to longitudinally assess motor map impairment and spontaneous recovery in the ipsilesional hemisphere regarding the impaired forelimb or through bilateral bi-hemispheric motor mapping at the end of an experimental protocol with longitudinal behavioural assessment. This highlights a gap in knowledge regarding how adult mice's bilateral bi-hemispheric LBMM spontaneous recovery aligns with functional recovery in longitudinal experiments.

1.6.2. Intrinsic Signal Optical Imaging

Simultaneously assessing the sensory cortex can also provide useful information post-stroke, as typically, a stroke within regions such as the middle cerebral artery induces damage across the sensorimotor cortex (Gharbawie *et al.,* 2005). This notion is then exaggerated further in rodent animal models, as ~32 ± 3% of CFA overlap with the sensory cortex forelimb and hindlimb representations (Tennant *et al.,* 2011; Ayling *et al*., 2009; Hall & Lindholm, 1974). While functionally isolated, the overlapping space is illustrated by the structural fusion of sensory cortex layer IV with the dense concentrations of granular cells in the motor cortex (Tennant *et al.,* 2011). Additionally, because many cortico-cortical projections descend from the corticospinal tract bound within CFA, disruption in CFA can lead to an impairment in information flow, including sensory areas (Rouiller *et al.,* 1993; Kunori & Takashima, 2016; Hayley *et al.,* 2023). Specifically, RFA contains pre-motor-like functions, including pairing sensory and motor information and activity during the planning of movements (Chen *et al.,* 2017; Alyahyay *et al.,* 2023; Hayley *et al.,* 2023; Morandell & Huber, 2017; Nishibe *et al.,* 2010; Neafsey *et al.,* 1986). As a result, recent studies suggest that the sensory cortex is functionally

involved in motor recovery (Hayley *et al.,* 2023), similar to squirrel monkeys (Dancause *et al.,* 2005). Therefore, non-invasive imaging techniques such as Intrinsic Signal Optical imaging (ISOI) will provide valuable information in assessing sensory impairments through hemodynamic responses following a partial CFA localized stroke.

Sensory cortex mapping involves recording sensory-input responses to investigate superficial representations of sensory neuronal activity following afferent stimulation (Sunil *et al.,* 2023). A technique known as Intrinsic Signal Optical Imaging (ISOI) is employed in this process to visualize and analyze these sensory maps (Winship & Murphy, 2008, 2009). ISOI relies on changes in blood flow as a proxy for depicting neuronal activity by observing unique spectral patterns resulting from alterations in the oxygenation state of hemoglobin when neurons are activated (Lu *et al*., 2017; Frostig & Chen-Bee, 2009) to generate sensory maps on the dorsal cortex through a transcranial window (Silasi *et al.,* 2013). Specifically, different light frequencies can be used to differentiate between oxygenated and deoxygenated hemoglobin configurations (Lu *et al*., 2017), as greenlight relates to total hemoglobin, and red light relates to reduced hemoglobin (Lu *et al*., 2017; Frostig & Chen-Bee, 2009). As a result, ISOI has proven to be a valuable tool in the study of post-stroke reorganization, as it allows for non-invasive stimulation and recording of sensory cortical activity. Researchers have utilized ISOI to investigate how sensory representations change following a stroke, providing insights into the brain's adaptive processes and recovery mechanisms (Bauer *et al.,* 2014; Harrison *et a*l., 2013; Bice *et al.,* 2023).

Previous studies have presented evidence of impaired sensory-evoked cortical activity following stroke using ISOI (Frostig & Chen-Bee, 2009; Harrison *et al*., 2013; Lu *et al.,* 2017). Additionally, ISOI can be combined with the stroke models to assess the level of activity in the lesioned sensorimotor cortex compared to the intact hemisphere. Winship & Murphy, 2008, employed ISOI in conjunction with two-photon imaging to examine recovery, discerning macroscopic and cellular remapping following sensory forelimb cortex stroke. Winship & Murphy, 2008 shed light on how pre-stroke hard-wired neurons respond to stressors like local ischemia and recover. Notably, they found that neurons along the border of the sensory hindlimb and forelimb regions experienced heightened plasticity in response to stroke

reorganization during chronic phase recovery. Building upon this discovery, Brown *et al.,* 2009 extended the understanding of sensory map borders using ISOI, concurrently monitoring spine turnover via two-photon imaging and assessing behavioral recovery through the cylinder task. Their findings highlighted a strong correlation between sensory remapping in the peri-infarct region, increased synaptic turnover, and improved performance in the cylinder task. Consequently, the combined use of ISOI, two-photon imaging, and behavioral assessments has offered compelling evidence that peri-infarct recovery is intricately linked to the restoration of function in the affected forelimb post-stroke, particularly in longitudinal mouse models.

This study aims to investigate how sensory mapping through ISOI can provide additional insight into the state of the sensorimotor cortex when combined with LBMM. This combination aims to delve deeper into the mechanisms of spontaneous recovery within peri-infarct regions and interhemispheric plastic reorganization following stroke. The integration of non-invasive cortex reorganization techniques, such as ISOI and LBMM, with behavioural assessments holds great promise for advancing our comprehension of the functional implications of mapping results in a longitudinal model.

1.6.3. Pre-clinical stroke research

Animal models of stroke provide control over factors such as age of onset, comorbidities, and individual variability, which are challenging to manage in clinical studies. This level of control is crucial for generating reliable and consistent experimental data. Additionally, animal stroke models enable real-time and ex-vivo measurement of stroke induction using techniques like laser Doppler imaging (LDI) and Cresyl violet stains. These methods provide valuable insights into the extent and location of the stroke, allowing for precise assessments of stroke volume and the potential impact on peri-infarct synaptic plasticity during the recovery process (Cuccione *et al*., 2016; Leutenegger *et al*., 2011; Riva *et al*., 2011; Rousselet *et al*., 2012).

Two primary stroke techniques for ischemic stroke induction are middle cerebral artery occlusion (MCAO) and photothrombotic (PT) stroke. PT stroke allows for the precise and localized induction of stroke in a targeted brain area by activating a photosensitive dye, Rose

Bengal (Labat-gest & Tomasi, 2013; Watson *et al*., 1985). This approach offers the advantage of precise localization of stroke induction, allowing for consistent and reproducible results in location and volume by manipulating parameters such as light diameter and duration of the illuminating light beam (Wang *et al*., 2009). MCAO closely replicates the pathophysiology of human ischemic strokes, making it valuable for studying stroke mechanisms and potential treatments; however, it introduces greater variability, including subcortical damage (DeVries *et al.,* 2001; Liu & McCullough, 2011). A critical difference between models is PT stroke damage can be localized within functional regions in the cortex, which is significant considering that the MCAO model can also impact subcortical regions crucial for motor movements (Bolay & Dalkara, 1998; Navarro-Orozco & Sánchez-Manso, 2023). While the PT and MCAO stroke models offer unique advantages, the PT model emerges as the more suitable choice for this thesis, as stroke-induced damage is bound to a pre-determined localized region, such as CFA. Therefore, group effects can be assessed for spontaneous recovery following stroke using a controlled stroke induction site at CFA.

1.6.4. Longitudinal assessment of forelimb post-stroke

Behavioural measures provide functional context to mapping experiments (Nishibe *et al.,* 2015), where rehabilitative or experience dependent measures affect the state of the motor cortex (Nudo *et al.,* 1996). To gain a more comprehensive understanding of motor map impairments, it is imperative to quantify a battery of motor behavioral tests. However, the integration of motor mapping with behavioral assessments has been limited, primarily because traditional rodent motor mapping methods require sacrificing the animal (as discussed in section 1.5). Nevertheless, experiments utilizing ISOI and two-photon microscopy with behaviour suggest that recovery occurs at a similar pace across measures (Brown *et al.,* 2008, Winship & Murphy, 2009). Within this battery of tests, it is particularly valuable to include a detailed assessment of upper limb function, as upper limb impairments are prevalent among stroke patients (Ingram et al., 2021; Raghaven, 2015). Consequently, the combination of LBMM with a battery of behavioral forelimb tasks offers a comprehensive understanding of motor deficits and recovery.

Behavioural analysis is critical in assessing stroke recovery since behavioural tests offer functional representations of mapping results and clinical phenotypes. It is also worth considering that behavioural testing and associated training can act as a form of rehabilitation when applied correctly (Nishibe et al., 2015; Jones & Adkins, 2015; Hatem et al., 2016). Consequently, the tasks included in this behavioural assessment should minimally impact recovery. Several tasks, such as the grid walking task, the cylinder task, and the string-pull task, can fulfill this criterion (Chen et al., 2010; Allred & Jones, 2008; Schaar et al., 2010; Gharbawie et al., 2004; Blackwell et al., 2018; Inayat et al., 2020). For example, the grid walking task enables a quantitative assessment of skilled walking by counting missteps with the stroke-affected forelimb, providing a highly sensitive evaluation of sensorimotor impairment in a longitudinal model (Metz & Whishaw, 2009). The cylinder task measures spontaneous forelimb use preference, which is crucial in post-stroke recovery and allows for gross analysis metrics like forelimb use preference during exploration (Gharbawie *et al*., 2004). The string-pull task offers a precise kinematic assessment of motor coordination and function via hand-over-hand evaluation in a longitudinal model (Blackwell *et al.,* 2018; Blackwell *et al.,* 2021).

Since none of the mentioned behavioural tasks involve motor learning, a complex process known to influence the outcome of motor maps (Schlaug et al., 1994; Classen et al., 1998), it is reasonable to assume that the behavioural interventions should have minimal impact on sensorimotor recovery following stroke. The behavioural test battery was designed to assess various aspects of upper limb behavioural impairments following CFA-targeted PT stroke. Therefore, by combining the results of LBMM, ISOI, and behavioural assessments, we aim to advance our understanding of how small-scale PT stroke within CFA can influence map reorganization and the intricate relationship between impairment and spontaneous recovery concerning behavioural outcomes.

1.7. Experimental approach

Given the background presented, it becomes evident that there are still some notable gaps in the existing literature. First, there is a substantial difference between clinical and pre-clinical motor map research, primarily due to size limitations, as clinical techniques are bulky

and generate large stimulation sites in smaller organisms which would encompass the entire rodent motor cortex. As a result, ICMS research relies on disrupting the cortex primarily through electrodes to assess the state of the cortex. Although extensive stroke research has been conducted in clinical and pre-clinical literature, specific regions and time points critical during recovery remain elusive. Furthermore, motor map representations through ICMS rely on group comparisons, as stimulations modulate the cortex and ultimately lead to the sacrifice of the animal. This thesis will characterize within-group baseline motor maps and longitudinally investigate impairment and spontaneous recovery until the chronic recovery period to identify the critical time point for future therapeutic stimulation research.

Second, behaviour is a standard method for providing functional relevance to motor maps. However, the invasive nature of ICMS results in motor maps providing post-condition assessment and cannot be combined longitudinally. As a result, pre-clinical relationships of motor mapping and behaviour remain debated as longitudinal assessments are impractical due to pre-existing technical limitations. It is important to investigate further, as pre-clinical comparisons typically are applied to the assumed recovery profiles, but the direct relationship between motor map and behavioural recovery remains unknown.

Third, most research investigates a single limb-hemisphere interaction upon motor mapping. Although this approach is ideal for providing information on a specific topic, it is not practical for the cortex's complexity or movements' bilaterality. As a result, this thesis aims to further the work of LBMM performed by other researchers through bilateral and bi-hemispheric motor mapping post-stroke.

Finally, recent literature greatly emphasizes the role of sensorimotor dysfunction following CFA-targeted stroke in rodent models. Specifically, RFA recovery is critical for impaired forelimb function post-stroke, as identified by ICMS motor mapping. However, due to the substantial sensory cortex connections, further understanding of the state of the sensory cortex following a CFA stroke is required. As a result, the use of ISOI aims to address the state of afferent sensory representations to the sensory forelimb cortex through longitudinal post-stroke assessment.

Therefore, by leveraging mesoscopic imaging techniques like LBMM and ISOI and by integrating these findings with behavioural analyses, this thesis endeavors to provide a comprehensive characterization of post-stroke recovery and reorganization after partial primary motor cortex stroke, including the identification of critical regions and time points crucial for recovery.

2. Methods

2.1. General procedure and timeline

Ethical approval for all experiments was obtained from the University of Ottawa Animal Ethics and Compliance Board and conducted research followed the Canadian Council on Animal Care and Use guidelines. Male and female Thy1-ChR2-YFP mice (#007612 The Jackson Laboratory), totalling 29 animals. Data collection and analysis were conducted for 21 stroke mice (12 males: 3 months and 19 days ± 5.3 days, 9 females: 2 months and 25 days ± 3.0 days) and 4 sham mice (2 males: 3 months and 10 days ± 21 days, 2 females: 2 months and 30 days ± 10 days). The mice were housed on a 12-hour light/dark cycle and provided food and water *ad libitum*. Four mice were excluded from the study due to premature death (one due to stroke and three due to improper anesthesia injections resulting in death - one from the sham cohort and two from the stroke cohort).

Transcranial windows were surgically implanted on the intact skulls of adult mice to allow for longitudinal light-based motor mapping (LBMM), cerebral blood flow recording (LDI), and sensory mapping (ISOI). After the transcranial window surgery, the mice recovered for one week before baseline experiments commenced. Over the two baseline weeks, three ISOI, one LBMM, three grid walking tasks, three cylinder tasks, and seven string-pull tasks baseline data were collected (details for each task provided in section 2.3). Mice had either a stroke or sham induced, and data collection for post-stroke week one occurred on days four-seven. During subsequent post-stroke weeks, one of each behavioural task was conducted, except for string-pull, which took place at the beginning and end of each week relative to the stroke (Fig. 1B). Perfusion and brain extraction for lesion volume assessment transpired on post-stroke week seven.

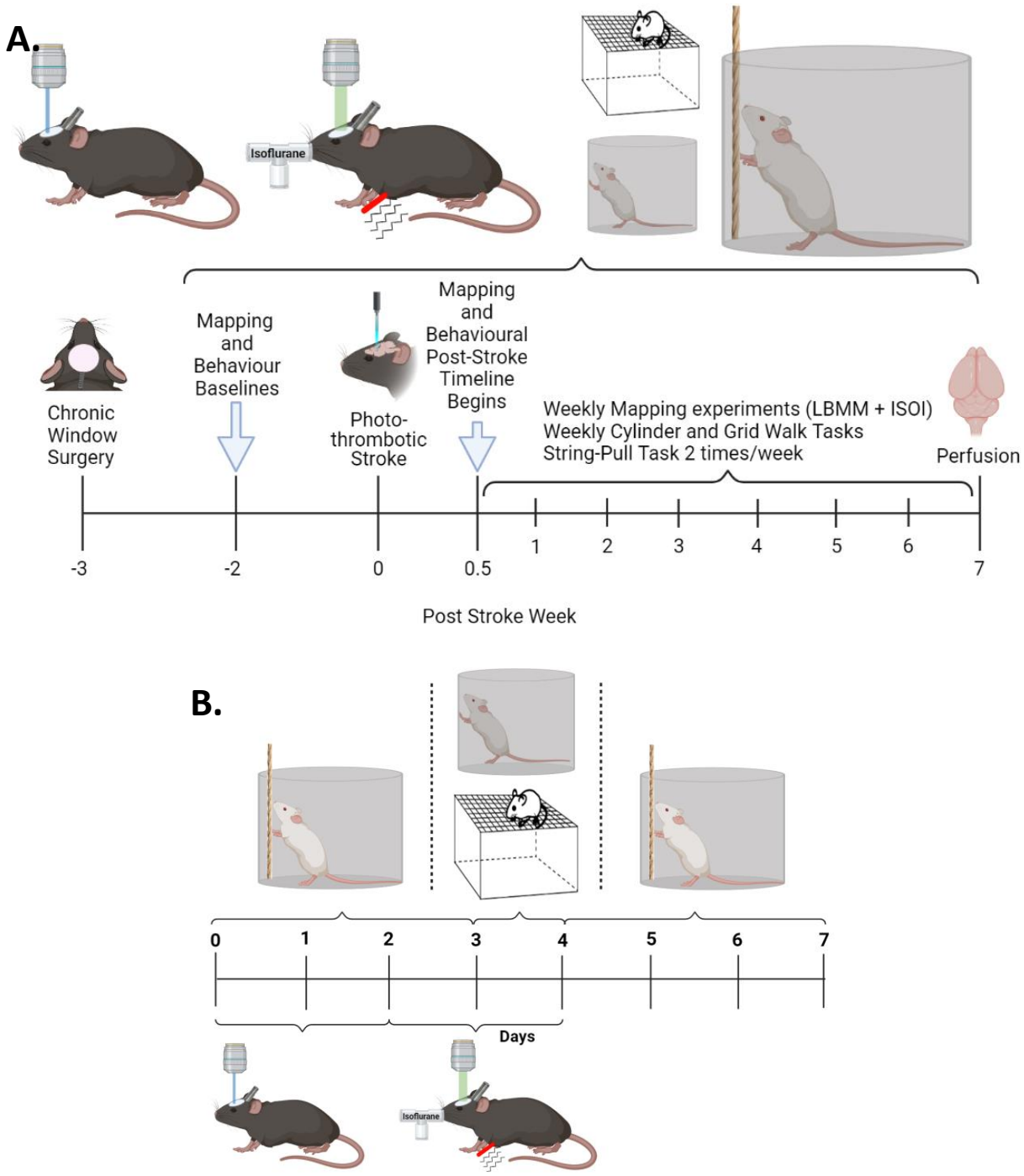

Figure 1. Experimental timeline. A) Experimental timeline overview. Adult mice underwent a series of imaging techniques, including three ISOI baselines and one LBMM baseline. Behavioural baseline assessments consisted of habituation to the string-pull task and seven baseline sessions, three baseline grid walk tasks, and three baseline cylinder tasks. Baseline imaging and behaviour occurred in the weeks leading up to the stroke (n=17-21) or sham (n=4) induction date. Photothrombotic stroke was induced on the right hemisphere at the CFA coordinates (+1.5mm, -0.5mm) in Thy1-ChR2-EYFP transgenic mice, and recovery was assessed for six weeks. The nonimpaired forelimb and baseline metrics were utilized as within-group controls, while the sham group (n=4) served as experimental controls. **B)** Weekly timeline for post-stroke weeks two-six. The weekly timeline illustrates the progression of events, with each tick representing the day relative to the stroke induction date.

2.2. Experimental surgeries

2.2.1. Surgical procedures - Transcranial chronic windows

Chronic transcranial window surgeries permitted longitudinal mapping and induction of stroke. Transcranial windows were implanted in mice one week before baseline experiments began. Mice were anesthetized with isoflurane (4-5% for induction and 1.5-2% for maintenance at a flow rate of 0.3 L/min oxygen flow) and maintained at 37°C with a thermal heating pad. Mice were regularly monitored for respiration rate and toe pinch responses to ensure appropriate anesthesia levels. The skin above the cortex was shaved using a beard trimmer (from eyes to ears) and then prepared with antiseptics and 70% ethanol. Mice were mounted in a stereotaxic frame, and Optixcare eye lubricant was applied to maintain cornea moisture. The scalp over both hemispheres was removed, the skull cleaned of debris, and dental cement (Parkell, Edgewood, NY, USA; Product: C&B Metabond, SKU: S380 https://brildent.in/product_10/) application for preservation of the skull and visualize the brain following the protocol described in Silasi *et al.,* 2016. A circular glass coverslip (deckgläser 8mm, Thomas Scientific, product #1217N78) was centred over Bregma and set immediately into dental cement. A head-fixing metal screw (McMaster-Carr, Los Angeles, CA, USA; Product #94355A216) was set in the dental cement over the point of lambda at a 30-45° angle. The metal screw had additional dental cement at the base for support. Once all dental cement had solidified (25 minutes), mice were injected with subcutaneous meloxicam (5mg/kg) and transferred to a heated incubation chamber until responsive (approximately 1 hour). Mice had a one-week recovery period before baseline experiments.

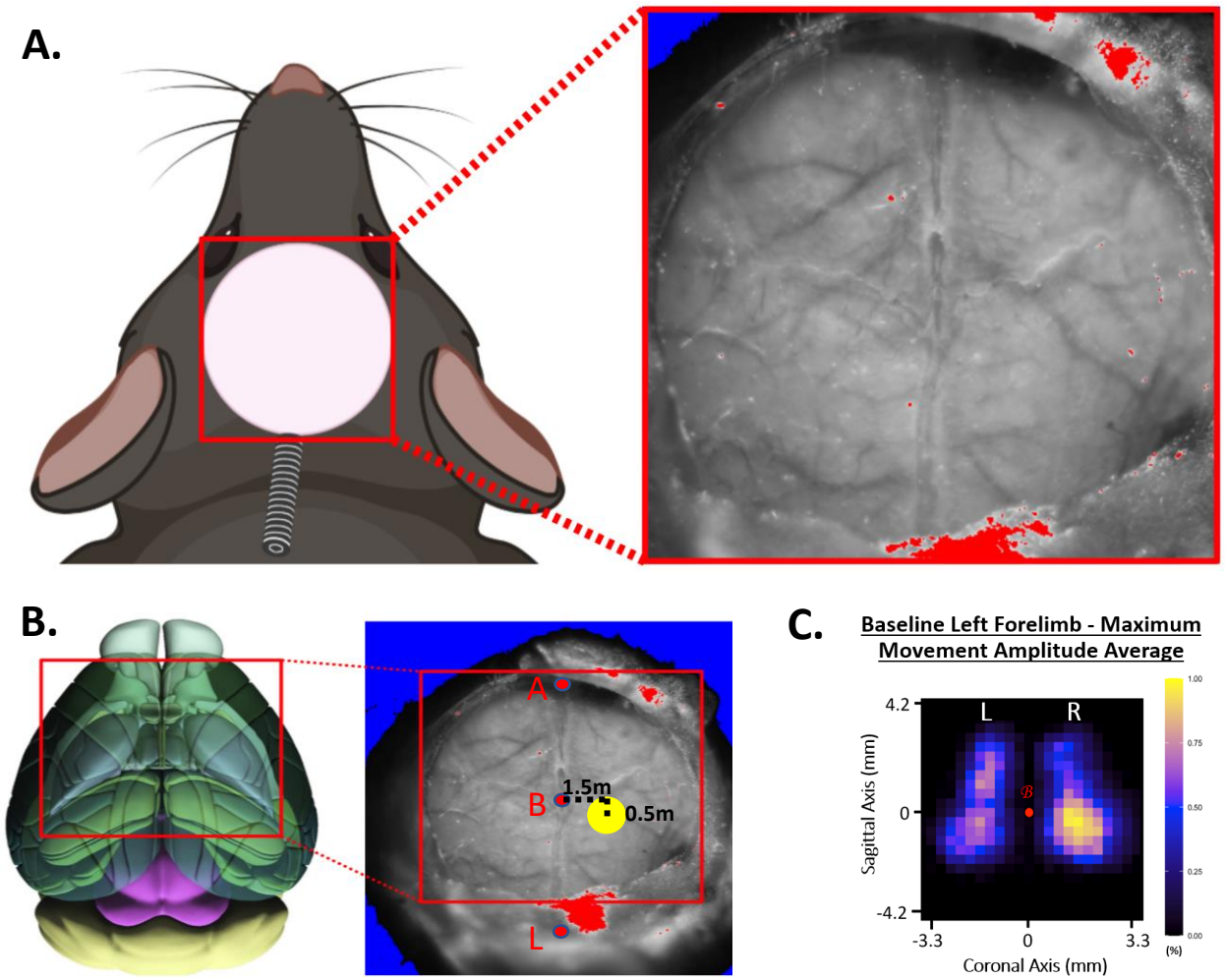

Figure 2. Surgical coordinates and transcranial window. A. Depiction of the transcranial window's position in relation to the mouse, accompanied by a green (520nm) fluorescence widefield image. **B.** Dorsal view of the Allen Mouse Brain Atlas (left) against a dorsal view of a transcranial window. Stroke (n=21) or sham (n=4) condition occurred on the right hemisphere CFA (ML: 1.5 mm; AP: -0.5 mm). Labels: A=Anterior Sinus, B=Bregma, L=Lambda approximation. **C.** Motor mapping utilized optogenetically evoked motor movements in the left forelimb at baseline. Anesthesia was induced with 40 mg/kg ketamine and 2 mg/kg xylazine in adult Thy1-ChR2-eYFP mice. Stimulation used a 50 µm laser in a grid of 300 µm spacing covering the entire motor cortex. Induced movements were recorded using a high-frame-rate camera and analyzed through MATLAB to obtain the induced maximum amplitude per stimulation site averaged across two repetitions. Motor maps were normalized to the maximum average amplitude site per session and averaged across conditions.

2.2.2. Photothrombotic stroke model

To induce photothrombotic (PT) stroke, mice were anesthetized with isoflurane (1.5% at 0.3L/min) and placed in a head-fixing mount with a heating pad to maintain body temperature at 37.0°C. To reduce the possible effect of the injection on cerebral blood flow, the needle containing Rose Bengal dye was pre-inserted intraperitoneally prior to recording baseline measures. A pre-stroke LDI scan followed the needle injection to generate a regional scan of blood flow, then 3-5 minutes of baseline LDI was recorded at the stroke induction site (AP: -0.5 mm; ML: 1.5 mm, relative to bregma). Rose Bengal dye (0.01g/mL) was slowly injected (100mg/kg) over 30 seconds, two minutes before laser illumination to allow the dye to circulate to the brain. A green laser (520nm, 1.1mm diameter, 22 mW of power) illuminated the cortex for 13 minutes to induce stroke. The stroke targeted the right motor cortex, specifically the centre of the CFA, as determined by group averaging data (Fig. 2B, AP: -0.5 mm; ML: 1.5 mm). LDI was used to continuously monitor cerebral blood flow at baseline, during stroke induction and for 15 minutes after the green laser was turned off (or until the LDI recording had plateaued). Post-stroke, an LDI regional scan assessed blood flow alterations, and the mice were returned to a heated recovery chamber until they became mobile. Sham animals underwent the same experimental procedure, but laser irradiation preceded the Rose Bengal injection.

2.3. Behavioural tasks

Adult mice performed non-learned behavioural tasks to minimize rehabilitative-like effects or motor learning-induced changes in motor maps. The Schallert cylinder task assessed spontaneous forelimb use preference and impairments, the grid walking task for skilled locomotion impairments, and the string-pull task to assess motor impairments and locomotion during bimanual coordinated pulling. Figure 1A, B demonstrates the experimental timeline.

Each week, one session of all behaviour data occurred in the middle of the week relative to the stroke induction (post-stroke day three-four, 10-11, 17-18, etc.) in the following order: cylinder task, string-pull task, then grid walking task. String-pull tasks' second session occurred with at least one-day separation from other behavioural recordings. Mice were video recorded

for offline analysis using a 3-megapixel HD Raspberry Pi camera with a wide-angle fish-eye lens. Mice were allowed at least 24 hours after receiving anesthesia before any behavioural experiments to minimize anesthesia effects.

2.3.1. Cylinder task

The cylinder task contained three baseline sessions, each lasting at least 7 minutes. The apparatus consisted of a well-illuminated transparent cylinder (20.5cm height x 9.5cm diameter) placed on an elevated piece of transparent plexiglass. A Raspberry Pi camera placed below recorded mice activity. If mice were inactive for the seven-minutes, they were encouraged to explore by applying sugar water along the cylinder's rim. Sessions were excluded if the mouse failed to perform ten bouts within a 15-minute window (one session for stroke, one session for sham). Quantified metrics for the cylinder task included: push-off limb, total wall contact, total wall contacts per limb, and limb landed on. The following equation determines individual forelimb usage: ((Contralesional Forelimb)／(Contralesional Forelimb + Ipsilesional Forelimb)) * 100%.

2.3.2. Grid walking task

The grid walking task consisted of three baseline sessions, each lasting 5 minutes. The apparatus consisted of a 33 cm x 20.5 cm horizontal grid with 1 cm square openings. The grid was elevated above the floor, and mice were allowed to explore the surface freely. Mice were recorded using a mobile phone camera (Samsung s20 or iPhone 13) placed at a 45-degree angle from the grid to assess forelimb depth for scoring forelimb missteps. Forelimb missteps were any instance where a mouse's forelimb slipped or missed a grid rod, causing at least the wrist to pass through the opening. Total steps with the impaired forelimb were counted for each session. A step was included if the forelimb moved at least one grid in distance. Forelimb asymmetry was calculated as ((% of contralesional forelimb missteps) - (% of ipsilesional forelimb missteps)) / ((% of contralesional forelimb missteps) + (% of ipsilesional forelimb missteps))

2.3.3. String-pull task

The string-pull task was conducted based on the protocol established by Blackwell *et al*., 2018, with slight modifications. Mice were habituated to sugar water presented on a string for two days in their home cage, then transferred to a home cage with 20 strings for pulling during task habituation. Strings varied in length from 30-100cm, with sugar water at the end of the string. Mice had one hour to pull the strings before removal from the task. Mice then underwent five consecutive days of the string-pull task, followed by two sessions staggered per week (post-stroke days three-seven, nine-14, 16-21, etc.). Three string-pull trials were recorded per session. The string was 1 meter in length and suspended into the apparatus, with the end doused in sugar water as a reward for task completion. Trials were completed within three minutes of string presentation or upon pulling the string to retrieve the reward. Forelimbs were analyzed offline and included one trial per day. Weekly results displayed the average of both days. Weekly exclusion from the experiment occurred when mice failed to complete one string-pull during either week-averaged session (n=ten stroke sessions, n=two sham sessions). Forelimb analysis manually scored the number of stride length-increasing instances and contacts for string pull. Forelimb stride length-increasing instances occurred when mice grasped the string, then repositioned the forelimb to a higher position on the string, breaking the alternating left/right pattern of forelimb use. Contacts for string pull were instances in which mice grasped and pulled the string during the task. Compensation recorded as: ((# Forelimb stride-length increasing instances) / (Contacts for string pull)) * 100%.

2.4. Cortical Imaging

2.4.1. Laser Doppler Imaging during stroke induction

Laser Doppler imaging (LDI) was performed using a commercially available system (MoorLDI2-IR; Moor Instruments, Axminster, Devon, UK) that utilizes an infrared laser beam to quantify blood flow in either a single location or across a scanned region. Mice were anesthetized with isoflurane (briefly, 4-5% for induction and 1.25% at 0.3 L/min for maintenance), and Optixcare eye lubricant was applied to the cornea to keep it moist during anesthesia. Mice were placed on a servo-regulated heating pad in a stereotaxic frame, with LDI

positioned at ~45 degrees to provide space for the stroke induction laser positioned directly overhead of the mouse. The infrared laser (785 nm, 1.2 mm diameter, 2.5 mW power) recorded cerebral blood flow at the site of photothrombosis (AP: -0.5 mm, ML: 1.5 mm relative to bregma) before, during, and after stroke induction. To determine the decrease in blood flow and blood concentration, the average values for a 2.5-minute segment after the green light was turned off were subtracted from the average reading of a 2.5-minute segment at baseline (before green light illumination) for stroke and sham animals. In addition, an area scan of both hemispheres was performed at baseline and repeated after stroke induction. LDI used flux recordings to depict cerebral blood flow across the transcranial window before and after stroke/sham induction. Analysis separated blood flow by hemisphere to analyze post-stroke/sham effects. Mice were transferred to a heated recovery cage until conscious and mobile before being returned to their home cages. Cortical imaging through LDI lasted 45-60 minutes per animal.

2.4.2. Intrinsic Signal Optical Imaging

ISOI allowed indirect measurements of cortical activity following sensory stimulation using light to measure hemodynamic alterations longitudinally. Mice were briefly anesthetized with 4% isoflurane, then maintained with light isoflurane (1.25% at 0.3 L/min oxygen) and head-fixed underneath the LabeoTech LightTrack Modular Optical Imaging System (OiS200) (Fig 3A). Optixcare eye lubricant was applied to the cornea to keep it moist during anesthesia. The isoflurane tube was set near the nose and mouth of the animal but did not touch any fur or whiskers. Mice had a linear resonant actuator placed underneath the paw to produce a vibrotactile stimulus, and their wrist was restrained with poly wax (Fig. 3A). Vibrotactile stimulation parameters consisted of a pulse width of 19.8 ms, a period of 20 ms, and an amplitude of 5V for three seconds in duration. Stimulation trials were separated by 30 s (Fig. 3B), and 20 trials were performed across an ISOI session (Fig. 3C). Red (630nm) and green (520nm) light pulses were cycled at 10 Hz and synchronized with the camera frame rate, thus providing a 5Hz temporal resolution for each colour. The camera exposure was set to 1 ms, and the image was binned 2x2 (on the sensor) to reduce file size. Three seconds of baseline data and eight seconds of stimulus effects were recorded for each stimulation trial.

Recordings were analyzed using custom MATLAB scripts as a plugin within UmIToolbox by LabeoTech. Images were aligned using Bregma as a reference and scaled using the eight mm window diameter. The responses were normalized to calculate relative change per stimulation, split into baseline and post-stimulation time points, and averaged across all 20 stimulation trials. A low-cut filter removed responses below zero Hz, and a high-cut filter removed responses above one Hz to reduce non-evoked noise. Responses were localized on the cortical surface using the Allen Mouse Brain Atlas (Wang *et al*., 2020) as a reference. Registration against an atlas allowed investigation of the size of the sensory response and the cortical regions. The response area and amplitude within each Allen Mouse Brain Atlas region of interest (S1_hindlimb, S1_forelimb, and M1 for both hemispheres) were analyzed. The median amplitude of all Atlas-defined regions was exported for group analysis. To localize the evoked area following stimulation, thresholding removed the bottom 55% ± 15% of values to determine the core regions evoked by the sensory stimulus. If an evoked response occurred on an atlas convergence point, then values on the convergence point were excluded to ensure confidence in atlas averages. For group visualization, the maximum evoked response frame was automatically determined. Group results separated the stroke and sham cohort, averaged all three baseline sessions, and averaged for each week following the condition.

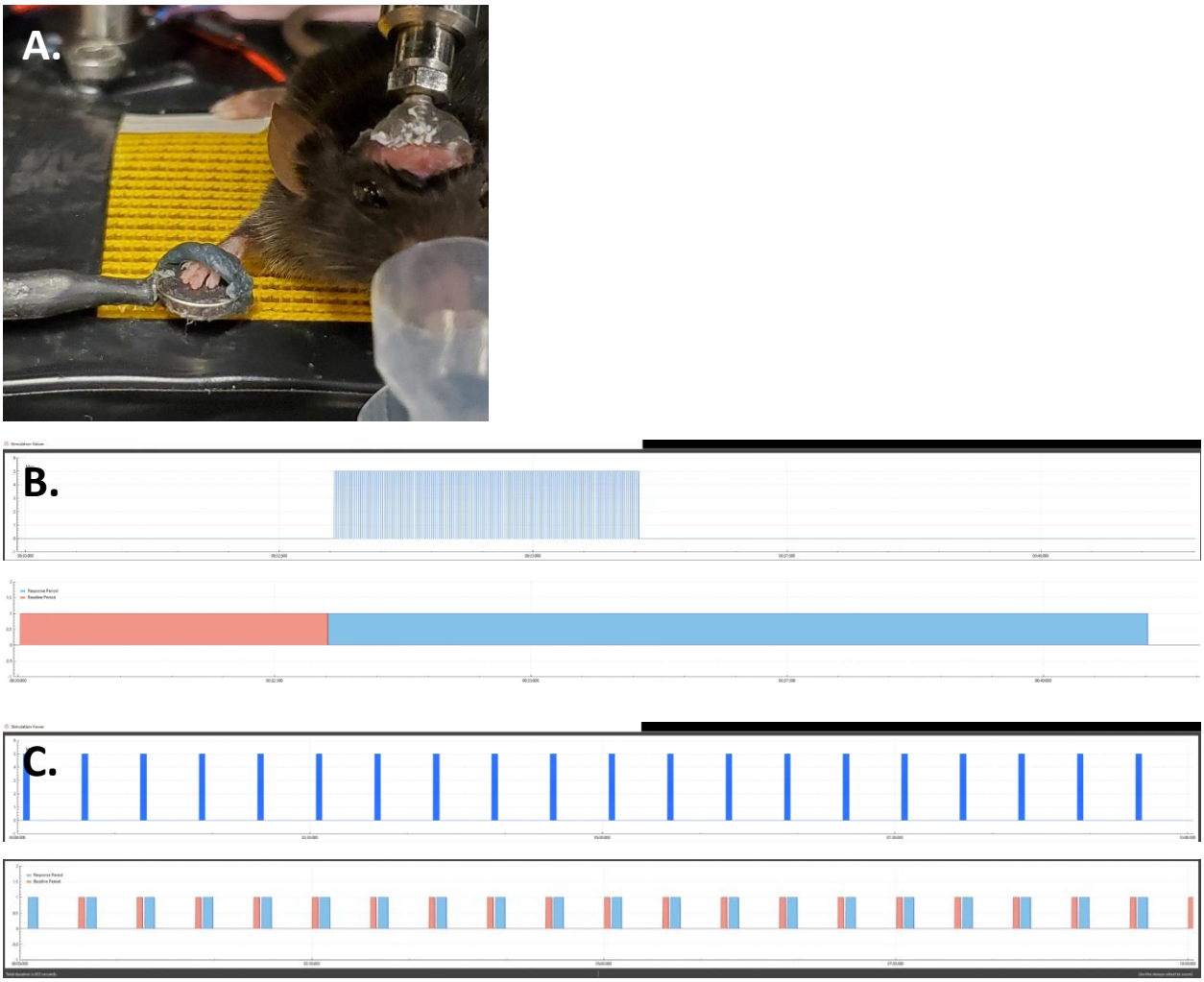

Figure 3. Intrinsic Signal Optical Imaging visualization. A. Experimental setup for intrinsic signal optical imaging. Mice were carefully positioned on a heating pad, and isoflurane (1.25% in 0.3L/min oxygen) anesthesia was administered under the OiS200 macroscope (not shown). A head-fixed screw mount enabled continuous assessment of blood flow responses through the transcranial window during the experiment Vibrotactile stimulation was applied under the paw, and the wrist was secured using poly wax. Computer interface control facilitated vibrotactile motor manipulation. **B.** Illustration of vibrotactile stimulation. A single-pulse vibration train (top) was applied for 3 seconds to activate the sensory cortex. Pre-stimulation recording (bottom, red) lasted for 3 seconds, followed by post-stimulus recordings depicted in blue. **C.** Overview of stimulation session. A zoomed-out view showcasing a 30-second loop repeated 20 times for subsequent analysis.

2.4.3. Light-Based Motor Mapping

Light-based motor mapping (LBMM) is an optogenetic tool that measures cortical reorganization following stroke by measuring longitudinally forelimb movement alterations. Mice were anesthetized with brief isoflurane exposure (4% in 0.3 L/min oxygen) followed by IP injections of ketamine (40mg/kg) and xylazine (2mg/kg), then relocated on a heating pad with thermoregulation set at 37.0°C. Optixcare eye lubricant was applied to the cornea to keep it moist during anesthesia. Mice were head-fixed, and their posture was linearly supported from the torso to the hindlimbs, with forelimbs symmetrically and freely suspended from an adjustable stage (Fig. 4A). This enabled unrestricted forelimb movement following cortical stimulation.

To ensure reliable and consistent motor maps, a range of laser intensities (1-4 mW of blue light at 470 nm, 5 ms duration, 50 µm in diameter) were sampled to establish an appropriate anesthesia level for effective mapping. After establishing the resting motor threshold, the minimal laser intensity required to evoke reliable forelimb movements in the relevant brain regions (RFA within both hemispheres) was determined per session. Subsequently, blue light stimulation was randomly applied throughout a grid with 300 µm spacing between stimulation points (approximately 375 stimulation sites per repetition; Fig. 4), comprehensively covering the sensorimotor cortex (AP: 3.9 mm, -1.8 mm; ML: 3.3 mm, -3.0 mm). Laser stimulation was delivered at an interstimulus interval of 0.5 seconds, with each stimulation site repeated twice to minimize variability. Each two-repetition map took approximately 7 minutes to complete.

During data acquisition, maps were reacquired if the anesthesia plane was unsuitable (e.g., too deep or too light) to ensure all motor maps were comparable in forelimb magnitude. The resting motor threshold was re-evaluated after each map to account for potential changes in anesthesia. Additional ketamine top-ups were provided for cortical stimulation if mice exhibited spontaneous movements. If mice regained consciousness during cortical stimulation, brief isoflurane application (5% in 0.3 L/min oxygen) prevented mice from becoming fully conscious. The entire process typically required approximately 120 minutes of anesthesia

usage. Mice were transferred to a heated recovery cage until conscious and mobile before being returned to their home cages.

Data analysis used a custom MATLAB script to generate heat maps analyzing forelimb movements relative to the cortical stimulation site. The inclusion criteria required forelimb movement to begin between 10-60 ms following stimulation, then the analysis of movements occurred until 100 ms after light stimulation. Following each stimulation site, motor evoked-forelimb movements analyzed each forelimb trajectory for maximum movement amplitude, the total distance travelled, and time to movement onset. Maximum movement amplitude is the maximum linear distance the forelimb is displaced during the analysis window (Fig 4E). The total distance travelled calculated the total forelimb displacement following stimulation (Fig 4F), where time to movement onset was the first continuous movement frame following stimulation (Fig 4F). For maximum movement amplitude, an exclusion criterion removed values smaller than 10% of the most significant evoked movement (Fig 4E). Regarding total distance travelled and the time to movement onset, movements were excluded if less than five continuous movement frames transpired during the 10-60 ms post-stimulation period (Fig. 4F, latency to 5-pixel threshold). The established criteria minimized spontaneous movements such as breathing.

For group analysis, individual stimulation sites were normalized to the largest evoked forelimb site in the session and averaged across the cohort. Group analysis compared baseline values against post-stroke week values to investigate impairments and spontaneous recovery. Additionally, functional movement analysis was depicted as the deviation from linear, calculated as [2*(Maximum Amplitude) / (Total Distance Travelled)] * 100%.

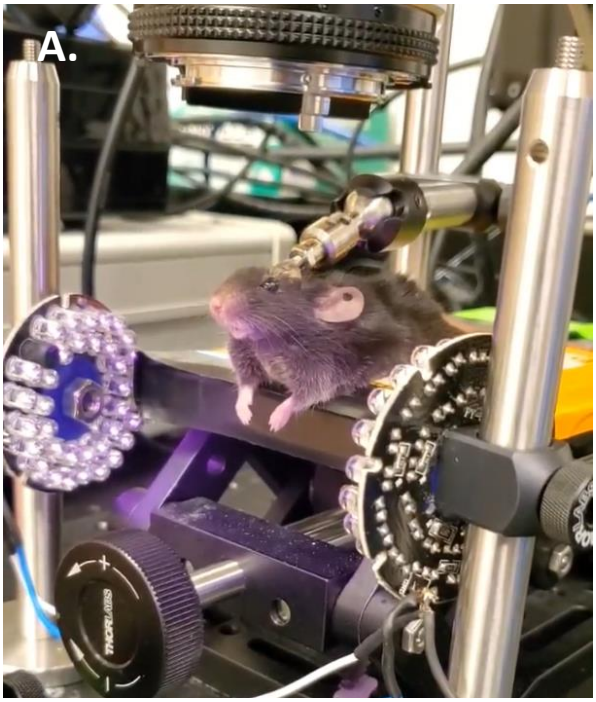
A.

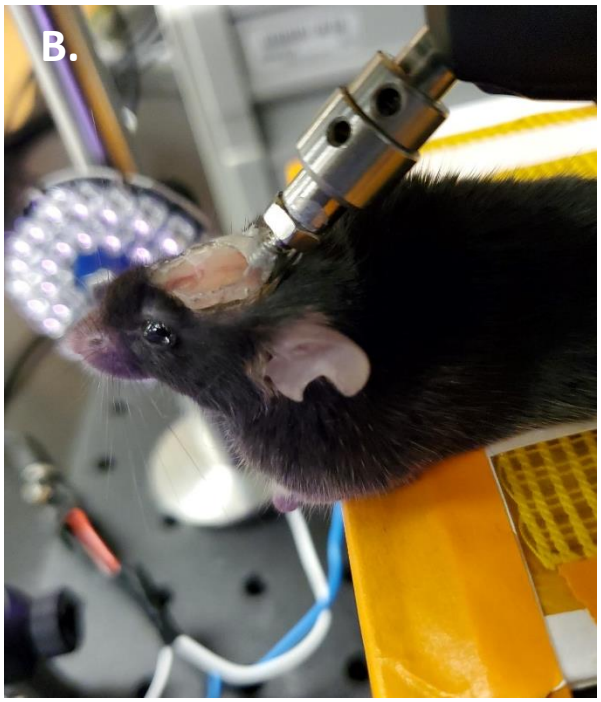
B.

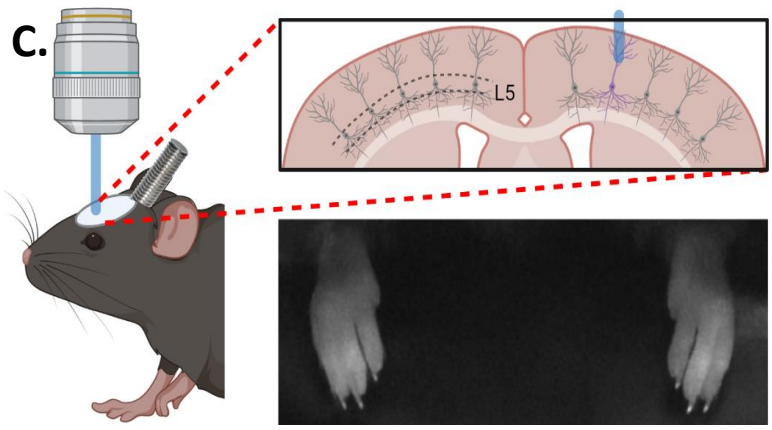
C.
L5

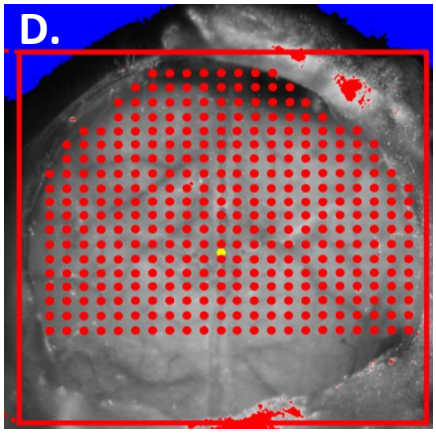
D.

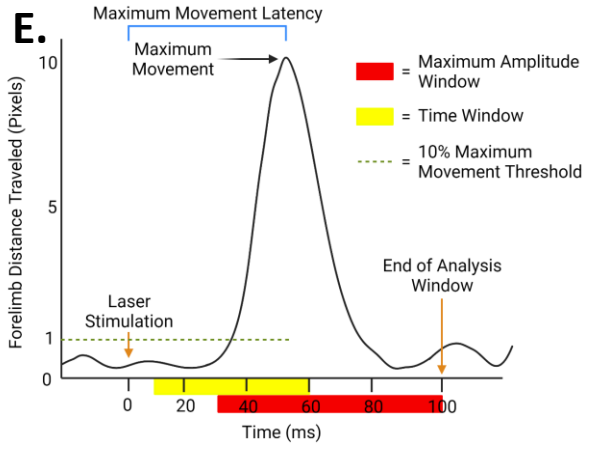
E.
Maximum Movement Latency
Maximum Movement
= Maximum Amplitude Window
= Time Window
= 10% Maximum Movement Threshold
End of Analysis Window
Laser Stimulation
Forelimb Distance Traveled (Pixels)
10
5
1
0
0
20
40
60
80
100
Time (ms)

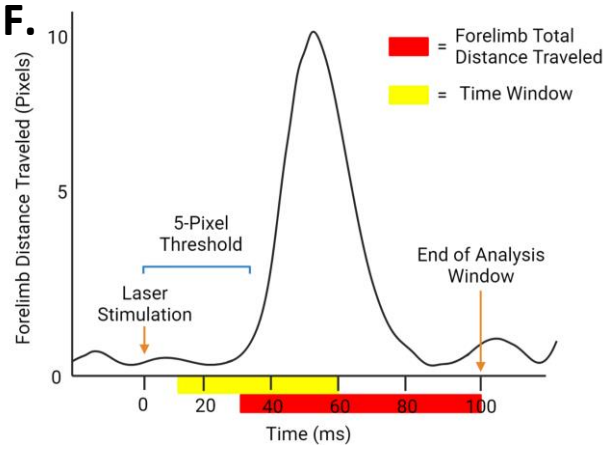
F.
= Forelimb Total Distance Traveled
= Time Window
5-Pixel Threshold
End of Analysis Window
Laser Stimulation
Forelimb Distance Traveled (Pixels)
10
5
0
0
20
40
60
80
100
Time (ms)

Figure 4. Light-Based Motor Mapping setup and exclusion criteria. A. Front view of the Light-Based Motor Mapping setup. An anesthetized and head-fixed mouse was positioned on the optogenetic rig (OiS200) under the macroscope's field of view on an adjustable stage. The forelimbs were free-floating, and the body was supported under the armpits. Body temperature was maintained by a thermal pad with a probe under the abdomen. Ultraviolet light illuminated the forelimbs and recorded using a 900Hz forelimb camera (not shown). **B.** Overhead view of the experimental setup to demonstrate mouse's head-fixing mount joint mechanism. **C.** Graphical depiction of light-based stimulation. Blue light (470 nm) from the OiS200 system stimulates the superficial cortex through the transcranial window, activating channel rhodopsin in the Thy1-ChR2-eYFP transgenic mice. Forelimb behavioural camera (bottom right) captured forelimb movements for analysis. **D.** Macroscope image (green light, 520nm) showed cortical stimulation sites (red) relative to Bregma (yellow dot). Stimulation sites were separated by 300 µm (motor map range = AP: 3.9 mm, -1.8 mm; ML -3.0 mm, 3.3 mm). **E/F.** Inclusion/Exclusion criteria. If movement latency onset occurred in the *Time Window* (yellow) then the forelimb was tracked during the *Analysis Window* (red). Time relative to the beginning of laser stimulation. **E.** Exclusion criteria for maximum amplitude. Any value <10% of the averaged maximum forelimb amplitude was excluded during Light-Based Motor Mapping per session. **F.** Exclusion criteria for forelimb latency (movement onset) and total distance travelled. Forelimb movement within the Time Window (yellow) must contain at least 5 continuous movement frames.

2.5. Histology and infarct volume

At the end of the experiment (post-stroke week seven), mice were deeply anesthetized with isoflurane (5% with 0.3 L/min oxygen), injected with euthanyl (i.p. 65 mg/mL concentration, 0.01 mL/g), and checked for any signs of responsiveness or reflexes. Mice were transcardially perfused with PBS, followed by 4% formalin (Cole-Parmer MasterFlex US) set at 3.2 mL/min for 10 and 5 minutes, respectively. Brains were extracted and post-fixed in 4% formalin for a minimum of 24 hours at 4°C. Brains were sectioned coronally on a Vibratome at 100 µm thickness, beginning at the front of the cortex and ending at the back of the thalamus (AP: 3.3mm, -3.7mm). Sections were mounted on 1% gelatin-coated glass slides.

Sections were dehydrated with ten dips of ethanol: 100%, 100%, 95%, 95%, 70%, then set in H2O for 1 minute for rehydration. Slides were immersed in 0.25% cresyl violet stain in 200 mM acetate buffer for 15 minutes. Slides were rinsed in distilled water, dehydrated again (70% then 95%), and differentiated in 0.25% glacial acetic acid in ethanol. Slides were dehydrated further (95% and 100%) and placed in Citrisolv clearing agent for at least 4 minutes prior to being cover-slipped (Fisherbrand #12541037CA) with Permount mounting media (Fisher Scientific, ADD).

Brightfield images were acquired using an Apotome.2 (Zeiss) microscope at 2.5x magnification through an Axiocam 105 colour camera. Sections were compared against Allen Mouse Brain Atlas (2008) to determine AP coordinates relative to Bregma. Sections were manually traced for cortical lesion damage by using the intact hemisphere to validate the natural curvature of the superficial cortex, then outlining the stroke as visible in cresyl-violet staining. Lesion volume was defined as: (Area of infarct on each section) * (Thickness of sections).

2.6. Statistical analysis

All analyses utilized GraphPad Prism 9 (GraphPad Software, La Jolla, California USA). Data were presented as mean ± SEM, and statistical significance was set at $p < 0.05$. Comparisons between groups and comparisons within groups' longitudinal measures were analyzed using a repeated measure ANOVA followed by Tukey's post hoc test for multiple comparisons.

3. Results

3.1. Blood flow reduction following stroke or sham.

Cerebral blood flow was measured with LDI during stroke induction and was expressed in units of flux and concentration (Supplemental Fig. 1B-D, Fig. 5). Quantification of blood flow was performed at a single point (stroke site) continuously before, during and after photothrombosis, as well as through area scans that covered both hemispheres. Area scans were performed at baseline and after photothrombosis. The single-point recordings at the stroke site showed a significant reduction in blood flux for both stroke ($p < 0.0001$) and sham groups ($p = 0.0102$) relative to baseline; however, blood concentration was only impaired in the stroke group ($p < 0.0001$) and not shams ($p = 0.9578$, Fig. 5B-D). Area scans of blood flow revealed a cortex-wide reduction in blood flux in the stroke group relative to baseline ($p < 0.0001$), with a greater decrease in the stroke hemisphere ($p < 0.0001$) than the nonimpaired hemisphere ($p = 0.0122$, Fig. 5D). Conversely, sham animals did not show a decrease in blood flux in the intact hemisphere ($p = 0.9998$) but surprisingly did show a significant decrease in the stroke hemisphere ($p = 0.0040$).

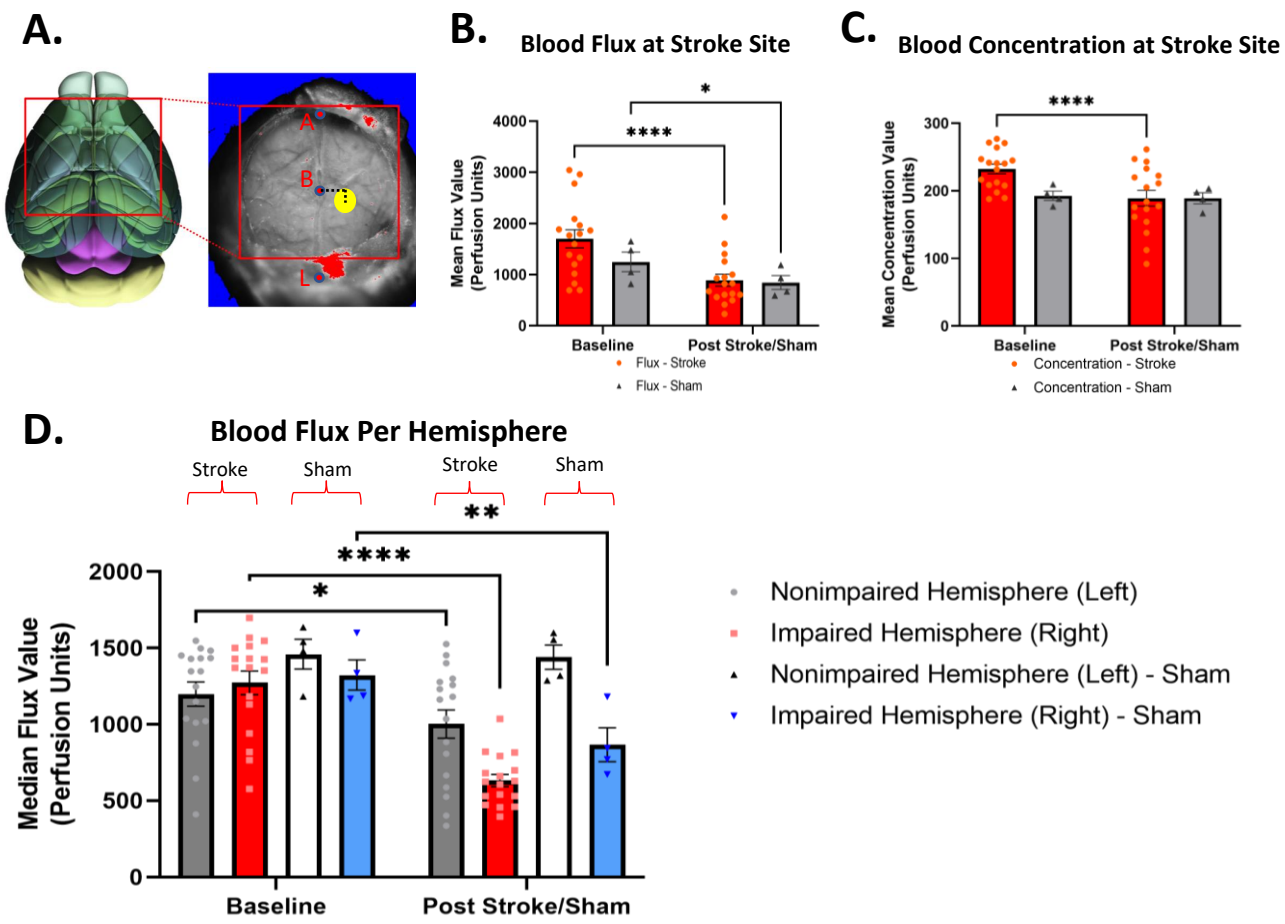

Figure 5. In-vivo Laser Doppler Imaging recordings of photothrombotic stroke. A. Dorsal atlas visualization of stroke site. The dorsal atlas from the Allen Mouse Brain Atlas is shown for reference (left) against the visualization of the stroke site (right) in yellow through the transcranial window. Stroke was induced 1.5 mm lateral and -0.5 mm posterior from bregma (B). A=Anterior Sinus, B=Bregma, L=Lambda approximation. **B/C.** Pre- and post-induction recordings of flux and concentration for the stroke (n=17) and sham (n=4) mice groups at the induction site. **B.** Blood flux recordings at the induction site. **C.** Blood concentration recordings at the induction site. **D.** Mean blood flux for both hemispheres pre- and post-induction condition. The data were extracted by separating hemispheres down the midline and averaging the mean values. All data was presented with a standard error of the mean (SEM). Statistical analysis was conducted using a repeated measures two-way ANOVA with Greenhouse-Geisser correction and Tukey's multiple comparisons tests. Significance indicated as * for comparisons between labelled regions. (*) $p < 0.05$, (**) $p < 0.01$, (***) $p < 0.001$, (****) $p < 0.0001$.

3.2. PT stroke results in CFA-localized stroke.

The PT stroke model generated consistent CFA localized stroke as determined by weekly functional mapping by LBMM (Fig. 7C) as well as lesion volume assessment at post-stroke week seven (Fig. 6B). Stroke was targeted to the centre of the CFA (averaged coordinate across all mice; Fig. 6C, AP: -0.5 mm; ML: 1.5 mm). Overall, the mean lesion volume was 1.06 +/- 0.16mm^3 (Fig. 6E). The majority of the sections showed damage through all cortical layers and in a subset of cases, there was some damage to the corpus callosum (Fig. 6B). Comparison of lesion volume and LBMM occurred by averaging lesion volume along the anterior-to-posterior axis (300 µm) in coronal sections and aligning these values with the LBMM amplitude values for the same region. Stroke volume aligned with the centre of the CFA (contralateral motor map: RFA = 1.28 +/- 0.015 mm^2, 3.0 – 1.5 mm anterior of Bregma. CFA = 5.93 +/- 0.015 mm^2, 1.2 – -2.1 mm anterior of Bregma; Lesion localization at 1.2 – -1.5 mm anterior of Bregma; Fig. 6C/D). Sham animals had no detectable tissue damage in cresyl violet-stained sections.

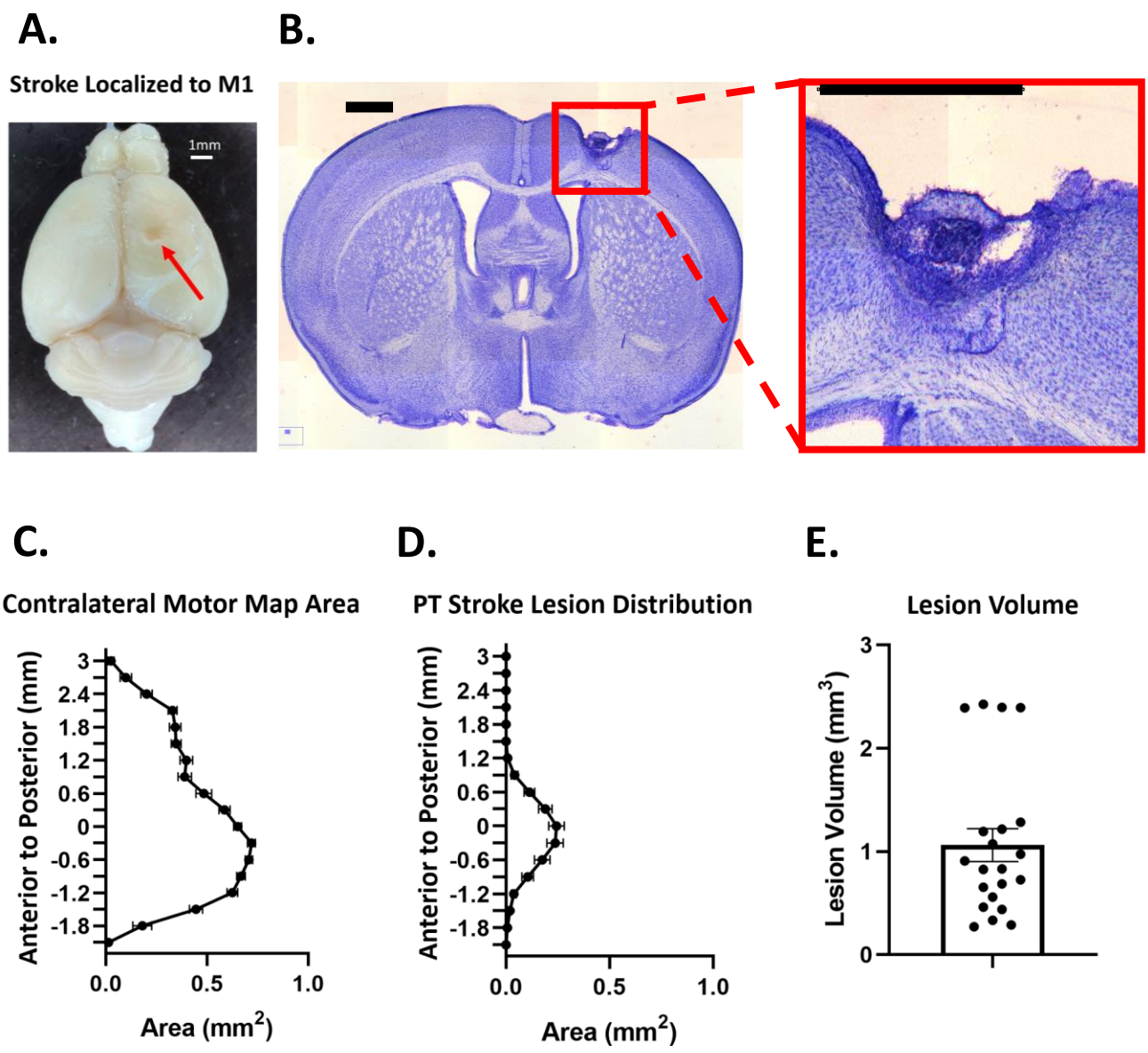

Figure 6: Photothrombotic stroke analysis. Photothrombotic stroke and ex-vivo analysis was performed following the experimental protocol at post-stroke week seven. **A.** Dorsal view of perfused and fixed brain following experimental protocol. Stroke infarct (0.85 mm^3) labelled by red arrow, scale bar (1.00 mm^2) in white. **B.** Example section of typical cresyl-violet stain. B. Representative cresyl-violet stained section. The scale bar (1.00 mm^2) depicted in black. Image analysis was performed using FIJI. Cresyl Violet stain was outlined for infarct and peri-infarct damage (determined by the absence of cresyl violet stain). **C/D**. Photothrombotic stroke of stroke (n=21) mice. All values depicted along the anterior to posterior axis were averaged per 300 µm relative to bregma. **C.** Contralateral motor map area illustrated the area that evoked forelimb movement following stimulation at baseline. All horizontal values were averaged across the stroke group. **D.** Stroke relative to the motor map. Manual lesion volume averaged three 100 µm sections per 300 µm. **E.** Stroke group lesion volume. The average lesion volume depicted (1.06 ± 0.16 mm^3). All data was depicted as mean ± SEM.

3.3. Forelimb motor amplitude and area are impaired by PT stroke and recover partially four weeks after injury.

LBMM permitted visualization of the forelimb movement representation in both hemispheres (Fig. 7C). Mice had baseline motor maps generated one to two weeks before stroke induction. Map area (number of responsive sites, Fig. 7C, F-G) and movement amplitude (Fig. 7 C-E) were summed per hemisphere, and latency (time to movement onset, Fig. 9) was averaged per hemisphere to illustrate hemisphere-wide changes following CFA-targeted PT stroke. Baseline motor maps were bilateral (Fig. 7C, F, G) but demonstrated significantly larger values for contralateral CFA motor map amplitude ($p \leq 0.0001$) and area ($p \leq 0.0133$) when compared to ipsilateral CFA representations (Fig. 7, 8). However, differences in forelimb trajectory shape ($p \geq 0.3805$) and movement latency ($p \geq 0.5613$) were not significantly distinguishable in the contralateral hemisphere at baseline ($p \geq 0.5613$; Figure 9, 10). Sham animals were comparable in motor map size ($p \geq 0.7145$) and amplitude ($p \geq 0.6828$) at baseline to stroke animals. Longitudinal assessment of the sham group was stable in the forelimb area ($p \geq 0.1801$) and amplitude ($p \geq 0.7136$) across the six weeks relative to baseline (Supplemental Fig. 2). At post-stroke week one, both forelimb movements were significantly decreased in the impaired hemisphere for the area ($p < 0.0001$) and amplitude ($p < 0.0001$) relative to the baseline. Alternatively, the contralesional hemisphere had no significant decrease in movement amplitude ($p \geq 0.7324$) or area ($p \geq 0.4807$) following stroke. This indicated that forelimb movements from each hemisphere changed differentially after the stroke, and impairment occurred in the ipsilesional hemisphere.

Both forelimb representations in the ipsilesional hemisphere increased significantly by post-stroke week four for evoked amplitude ($p \leq 0.0004$) and area ($p \leq 0.0011$). Distinctions in ipsilesional recovery were observed between the forelimbs, as the evoked amplitude of the nonimpaired forelimb was comparable to baseline ($p \geq 0.6813$), but the impaired forelimb remained significantly decreased ($p \leq 0.0118$). Conversely, ipsilesional map size was comparable to baseline for post-stroke weeks four to six in the impaired ($p \geq 0.12$) and nonimpaired ($p \geq 0.3267$) forelimbs. With regards to the contralesional hemisphere, a significant increase in impaired and nonimpaired forelimb evoked movement amplitude ($p \leq 0.005$) and map area ($p <$

0.0001) was observed when post-stroke week four was compared to baseline. In conclusion, differences in motor recovery profiles were observed ipsilesionally for the impaired and nonimpaired forelimbs, with greater recovery recorded in the nonimpaired forelimb than in the impaired forelimb.

LBMM amplitude values were summed into horizontal groups per hemisphere for both forelimbs, and every group was assessed longitudinally. Horizontal averages were averaged into acute (post-stroke weeks one-three, $p \geq 0.1799$) and chronic (post-stroke weeks four-six, $p \geq 0.6151$) period spontaneous recovery due to a lack of significance from within acute and chronic period recovery for all periods (Fig. 7D-G, Fig. 8). For acute recovery, the ipsilesional hemisphere (Fig. 8A, C) was significantly reduced in CFA ($p \leq 0.0001$) for both forelimbs evoked amplitude compared to baseline. Conversely, ipsilesional RFA remained unchanged for both forelimbs ($p \geq 0.1250$) when acute period recovery was compared to baseline. When the contralesional hemisphere was analyzed, no differences were observed in RFA or CFA for the impaired forelimb, whereas the nonimpaired forelimb was significantly increased in both anterior CFA (0.3 mm – 0.6 mm, $p \leq 0.0386$) and most of RFA (1.5 mm – 2.4 mm, $p \leq 0.0154$). Therefore, during the acute recovery period, we saw increased nonimpaired forelimb - contralesional hemisphere evoked amplitude and decreased ipsilesional amplitude in CFA for both forelimbs.

For the chronic stages of recovery, ipsilesional recovery of both forelimbs was primarily anterior of the stroke (anterior CFA and RFA; -0.6 mm – 2.4 mm, $p < 0.0001$) when compared against acute period recovery (Fig. 8A. Significance not shown). Significant decreases for both forelimbs remained in ipsilesional CFA for chronic phase recovery against baseline CFA ($p < 0.0001$). Regarding the contralesional hemisphere, impaired forelimb amplitude was significantly larger in ipsilaterally evoked forelimb movements (-2.1 mm – 2.7 mm, $p \leq 0.05$, Fig. 7B) for chronic period recovery relative to baseline. Whereas nonimpaired forelimb amplitude was significantly increased in contralesional RFA (1.5 mm – 2.7mm, $p < 0.001$, Fig. 8D) and anterior CFA (0.3 mm – 1.2 mm, $p < 0.05$, Fig. 8D). Although the sham group suggested some impairment in the sham-induced hemisphere, the results were insignificant when acute or chronic period recovery was compared to baseline (Fig. 8E/F, Supplemental Fig. 3). Overall,

ipsilesional recovery was primarily anterior of the stroke site, and contralesional responses were larger for both forelimbs.

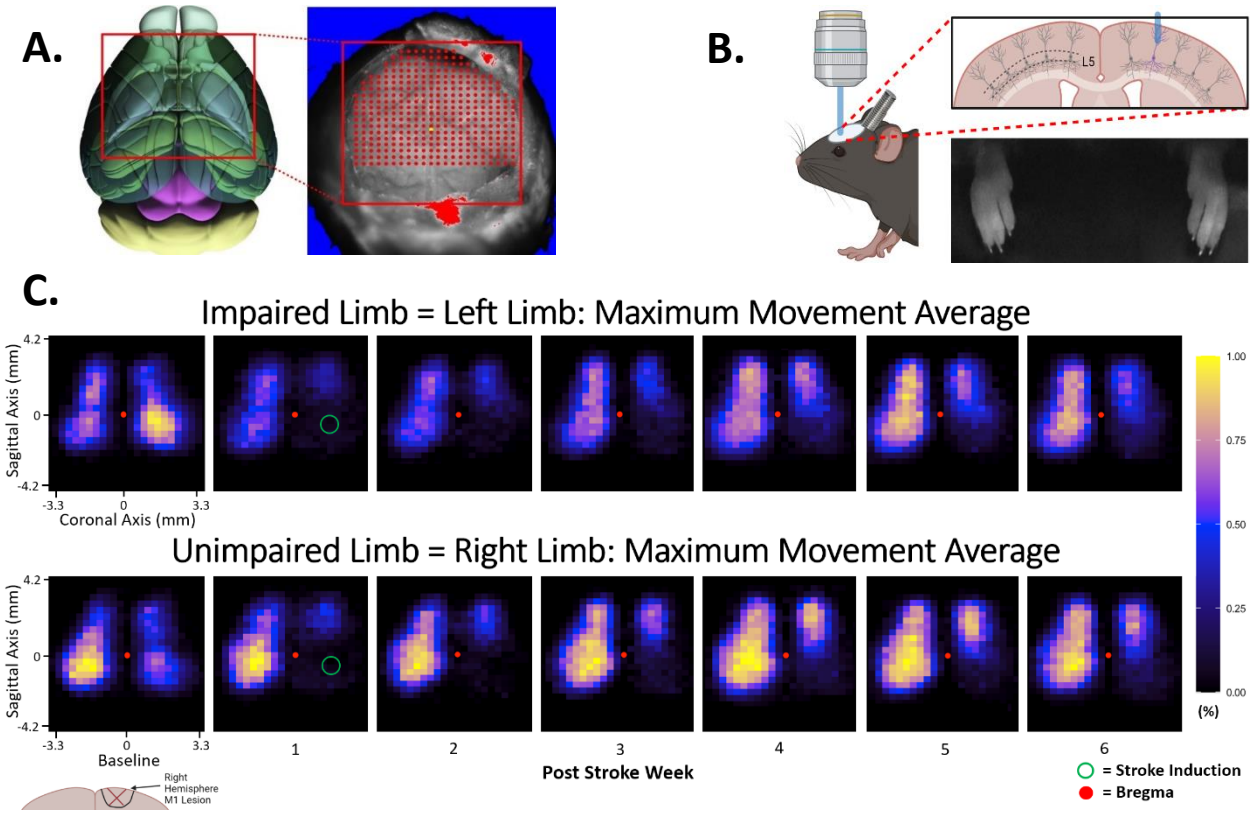
A.
B.
L5
C.
Impaired Limb = Left Limb: Maximum Movement Average
Sagittal Axis (mm)
Coronal Axis (mm)
Unimpaired Limb = Right Limb: Maximum Movement Average
Baseline
Post Stroke Week
(%)
= Stroke Induction
= Bregma
Right Hemisphere M1 Lesion

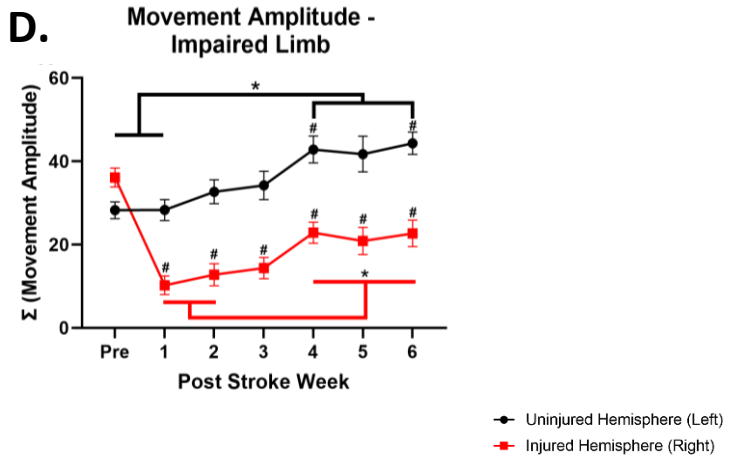
D.
Movement Amplitude - Impaired Limb
Σ (Movement Amplitude)
Post Stroke Week
Uninjured Hemisphere (Left)
Injured Hemisphere (Right)

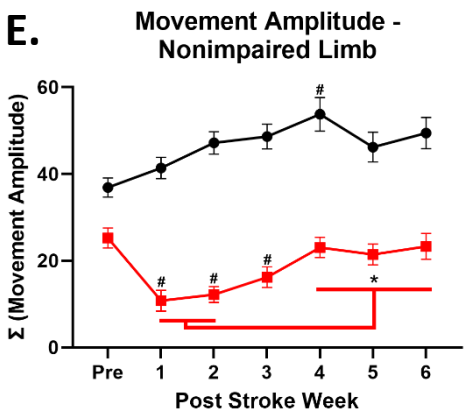
E.
Movement Amplitude - Nonimpaired Limb
Σ (Movement Amplitude)
Post Stroke Week

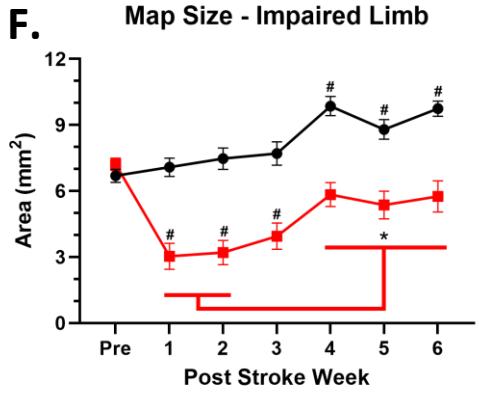
F.
Map Size - Impaired Limb
Area (mm²)
Post Stroke Week

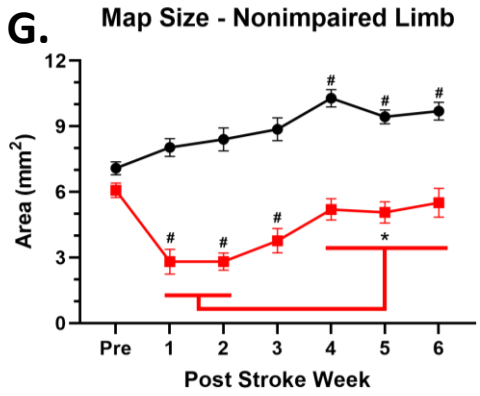
G.
Map Size - Nonimpaired Limb
Area (mm²)
Post Stroke Week

Figure 7. Light-Based Motor Mapping evoked forelimb analysis. Adult Thy1-ChR2-eYFP mice (n=21) were anesthetized with 40 mg/kg ketamine and 2 mg/kg xylazine. **A.** Motor sites were stimulated with a 50 µm laser at each grid point with a spacing of 300 µm (red). Bregma is indicated in yellow. **B.** Forelimb-evoked movement was quantified to determine the maximum movement per stimulation site. Forelimb movements were recorded using a high-frame-rate camera and analyzed through MATLAB to obtain averaged evoked responses per stimulation site. **C.** Motor maps were normalized to the maximum response per session, averaged per timepoint, and normalized per timepoint. Bregma was indicated as a red dot. The photothrombotic stroke site (ML: 1.5 mm; AP: -0.5 mm) was labelled in green at post-stroke week one. **D-G.** Data was summed per hemisphere and presented as mean ± SEM. **D.** Hemisphere-summed movement amplitude for the impaired forelimb. **E.** Hemisphere-summed movement amplitude for the nonimpaired forelimb. **F.** Hemisphere-summed map size for the impaired forelimb. **G.** Hemisphere-summed map size for the nonimpaired forelimb. Statistical analysis was performed using repeated measures two-way ANOVA with Greenhouse-Geisser correction and Tukey's multiple comparisons tests. * indicated significance per the labelled time point. # indicates significance within the hemisphere relative to baseline.

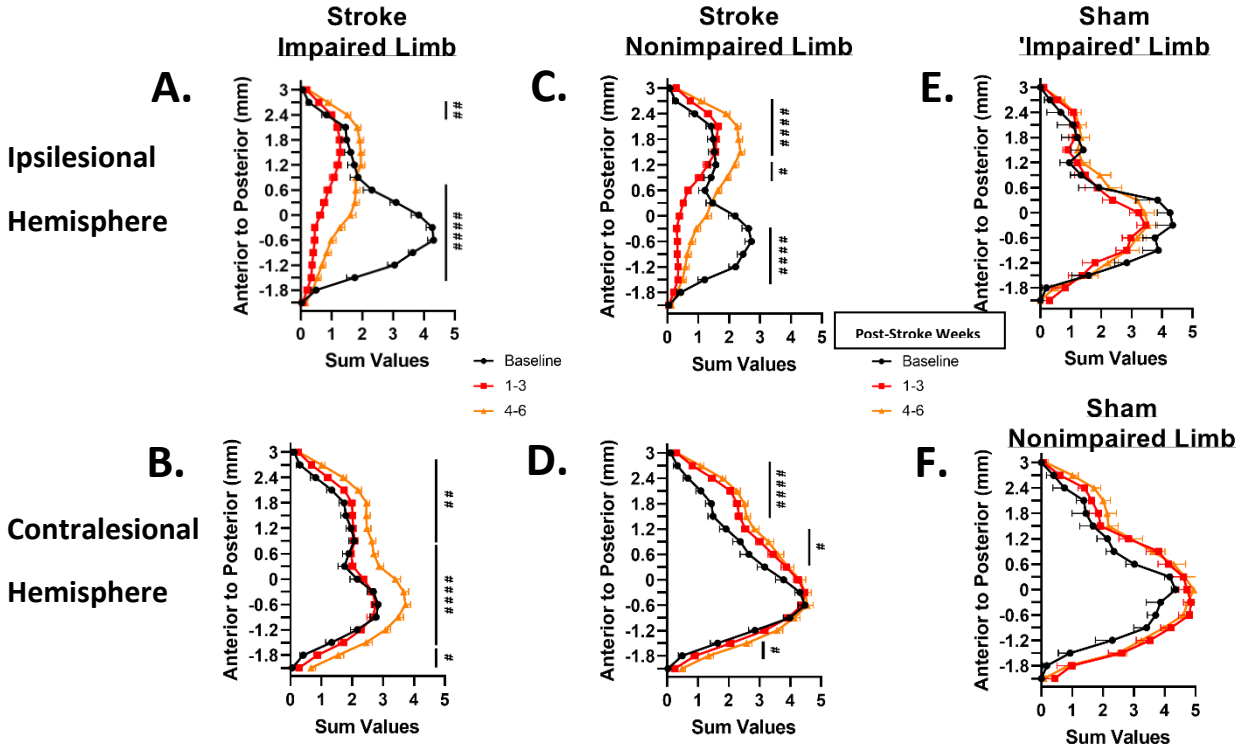

Figure 8. Anterior to posterior scanning of Light-Based Motor Mapping. Maximum amplitude values were summed per horizontal group and averaged per timepoint (baseline, post-stroke weeks one-three, and weeks four-six; n=21 stroke, n=4 sham mice). Each depiction represents the interaction between one hemisphere and one paw. Photothrombotic (PT) stroke was induced at 0.5 mm posterior of Bregma with an average lesion of 1.06 mm^3. **A.** Impaired forelimb-ipsilesional hemisphere. **B.** Impaired forelimb-contralesional hemisphere. **C.** Nonimpaired forelimb-ipsilesional hemisphere. **D.** Nonimpaired forelimb-contralesional hemisphere interaction. **E.** Sham group 'impaired' forelimb-induced hemisphere. **F.** Sham group nonimpaired forelimb-noninduced hemisphere. Statistical analysis was conducted through a repeated measures two-way ANOVA with Greenhouse-Geisser correction and Tukey's multiple comparisons tests. Significance indicated as: (#) $p < 0.05$, (##) $p < 0.01$, (###) $p < 0.001$, (####) $p < 0.0001$. The significance demonstrated depicts comparisons between post-stroke weeks four-six and baseline.

3.4. Motor map forelimb trajectory recovery is observed contralesionally.

In addition to movement amplitude and area, the evoked forelimb movement trajectory was quantified by determining how nonlinear the forelimb trajectory was in two-dimensional space for each stimulation site (Fig. 7,9, described in section 2.4.3.). Measures of linearity were averaged per hemisphere, and each hemisphere was separated into RFA and CFA. Importantly, CFA was also subsampled to match the size of the RFA (CFA – Local). At baseline, RFA stimulation produced linear movements (Fig. 9A, top right), whereas CFA stimulation produced more ellipsoid or non-linear movement (Fig. 9A, bottom right). The linearity of movements was not significantly different at baseline between contralateral and ipsilateral hemispheres for both CFA – local ($p \geq 0.381$) and RFA ($p \geq 0.9069$, Fig. 9B). Following stroke induction, the ipsilesional hemisphere forelimb trajectory was more linear. Regarding ipsilesional CFA – local, acute period recovery of the forelimb trajectory was significantly more linear for both the nonimpaired ($p < 0.0011$) and impaired ($p < 0.0078$) forelimbs when compared to baseline (Fig. 9 C, D). Concerning the ipsilesional RFA, there was an observed trend of increased linearity in the impaired forelimb trajectory during acute period recovery, although this change did not reach statistical significance for either the impaired forelimb ($p = 0.0599$) or the nonimpaired forelimb ($p = 0.4778$) compared to the baseline. The Forelimb trajectory for both forelimbs in the ipsilesional hemisphere did not improve by chronic period recovery for RFA ($p \geq 0.4002$) or CFA – local ($p \geq 0.767$) when compared to acute period recovery (Fig. 9C, D, right side).

Regarding the contralesional hemisphere, acute period recovery of the impaired forelimb elicited increased linear forelimb trajectories for CFA – local ($p = 0.0496$) relative to baseline (Fig. 9C, D, left side). However, increased linear forelimb trajectory of the impaired forelimb was not observed in contralesional RFA ($p = 0.6721$) relative to baseline. In chronic period recovery, the impaired forelimb contralesional projections were significantly more circular for both RFA ($p < 0.0433$) and CFA – local ($p < 0.0312$) relative to acute period recovery. Chronic period recovery of the nonimpaired forelimb trended on being more nonlinear in movement trajectory for both RFA ($p > 0.2235$) and CFA – local ($p > 0.3324$) but was insignificant (Fig. 9D, left side). Overall, forelimb trajectory analysis suggests that the impaired

forelimbs' ipsilateral representations exclusively recovered, whereas impaired forelimb contralateral representations remained impaired.

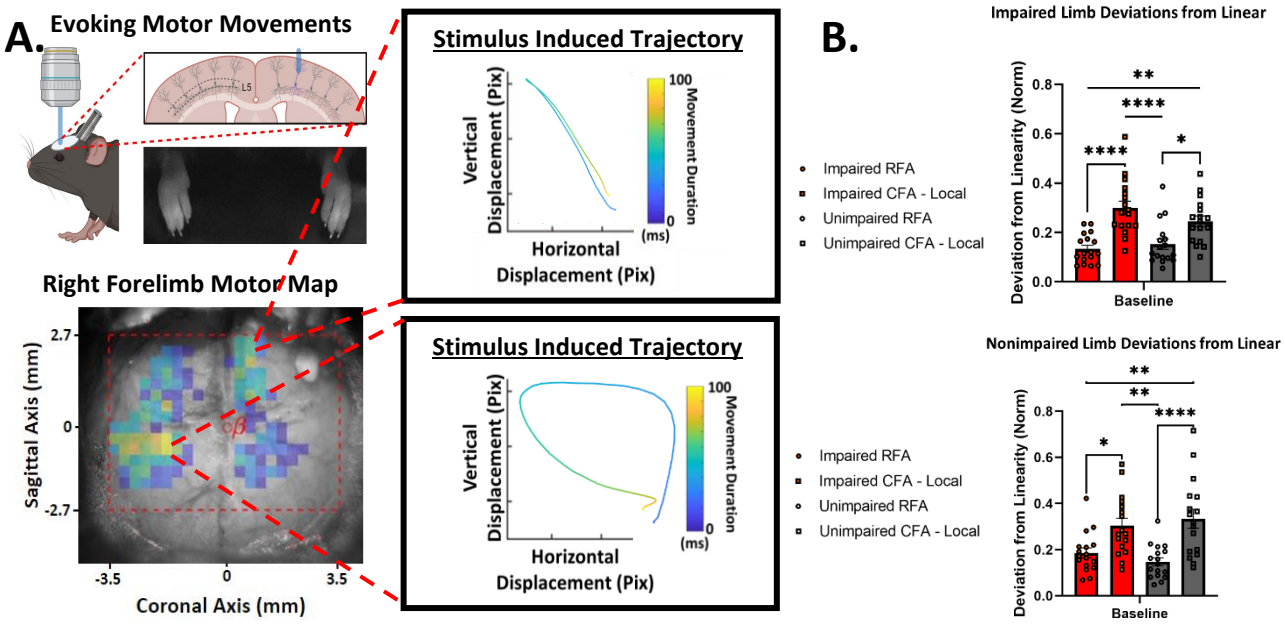
A.
Evoking Motor Movements
L5
Right Forelimb Motor Map
Sagittal Axis (mm)
2.7
0
-2.7
-3.5
0
3.5
Coronal Axis (mm)
Stimulus Induced Trajectory
Vertical Displacement (Pix)
Horizontal Displacement (Pix)
100
0
Movement Duration (ms)
Stimulus Induced Trajectory
Vertical Displacement (Pix)
Horizontal Displacement (Pix)
100
0
Movement Duration (ms)
B.
Impaired Limb Deviations from Linear
Impaired RFA
Impaired CFA - Local
Unimpaired RFA
Unimpaired CFA - Local
Deviation from Linearity (Norm)
Baseline
Nonimpaired Limb Deviations from Linear
Impaired RFA
Impaired CFA - Local
Unimpaired RFA
Unimpaired CFA - Local
Deviation from Linearity (Norm)
Baseline

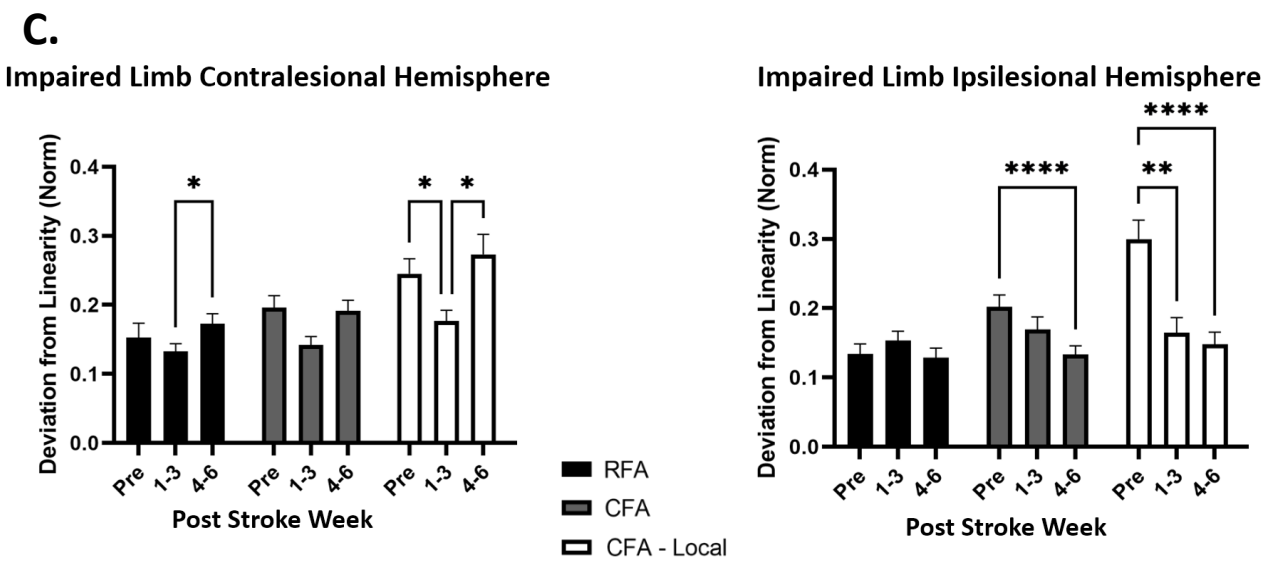
C.
Impaired Limb Contralesional Hemisphere
Deviation from Linearity (Norm)
Pre
1-3
4-6
Post Stroke Week
RFA
CFA
CFA - Local
Impaired Limb Ipsilesional Hemisphere
Deviation from Linearity (Norm)
Post Stroke Week

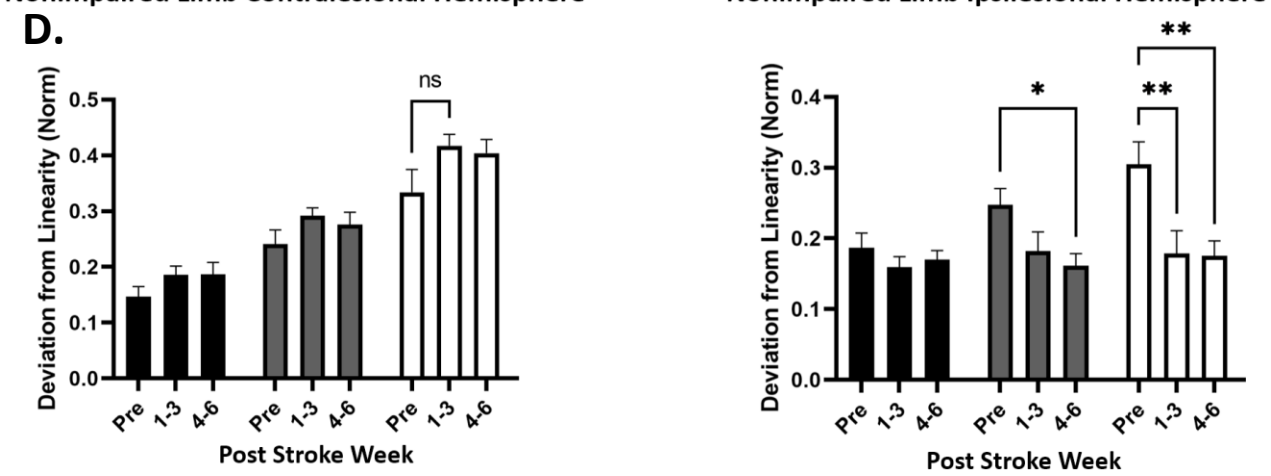
Nonimpaired Limb Contralesional Hemisphere
D.
Deviation from Linearity (Norm)
ns
Post Stroke Week
Nonimpaired Limb Ipsilesional Hemisphere
Deviation from Linearity (Norm)
Post Stroke Week

Figure 9. Light-Based Motor Mapping forelimb trajectory analysis. A. Top left: light-based motor map representation. Bottom left: representative baseline forelimb amplitude map of the right forelimb. Top right: two-dimensional forelimb tracking following stimulation in RFA. Colour scale depicted the time since stimulation. Bottom right: forelimb tracking following stimulation in CFA. Colour scale depicted time since stimulation. **B.** Baseline analysis of movement per forelimb. Deviation from linear calculated per stimulation site as [2 (maximum amplitude)] / total distance. Values were normalized to the largest nonlinear movement per session to minimize anesthesia effects. Analysis was grouped per functional motor region (RFA and local CFA) for both hemispheres. Local CFA was 1.8mm^2 to compare with RFA size. **C/D.** Post-stroke analysis of acute (post-stroke weeks one-three) and chronic (post-stroke weeks four-six) period spontaneous recovery. **C/D.** Contralesional hemisphere (left) and Ipsilesional hemisphere (right). Impaired forelimb (top) and nonimpaired forelimb (bottom). Data depicted as mean ± SEM. Statistical analysis was conducted through repeated measures two-way ANOVA with Greenhouse-Geisser correction and Tukey's multiple comparisons tests. Significance indicated as: (*) $p < 0.05$, (*) $p < 0.01$, (***) $p < 0.001$, (****) $p < 0.0001$.

3.5. Motor map latency recovery is observed predominantly contralesionally.

The final metric used in motor map analysis was movement latency, or the time for movement onset. At baseline, movement onset was fastest from the center of the contralateral CFA, and forelimb latency increased from the center of the CFA to the map's perimeter (Fig. 10A). No significant decrease in movement latency for the contralateral CFA compared to ipsilateral CFA was recorded at baseline ($p = 0.9876$), presumably due to large variations in movement onset at the center of CFA and CFA map borders. Following a stroke, a general trend displayed longer movement latencies for the impaired forelimb across both hemispheres but remained intact for the nonimpaired limb (Fig. 10B/C). During chronic phase recovery, the impaired forelimb evoked latency was the fastest from contralesional CFA (Fig. 10B), suggesting impaired forelimb movement latency reorganized in the contralesional hemisphere. Conversely, nonimpaired forelimb latency remained visually consistent across time. Motor map latency for the sham group was qualitatively consistent with stroke animals at baseline, where post-sham motor map latency appeared stable (Supplemental Fig. 4B/C). It should be noted that longitudinal assessment of the sham-induced hemisphere did fluctuate more than the noninduced hemisphere post-sham. However, the effects of sham on LBMM remain unknown. Overall, no conclusive results can be depicted from motor map latency, but general trends suggest a recovery in the contralesional hemisphere.

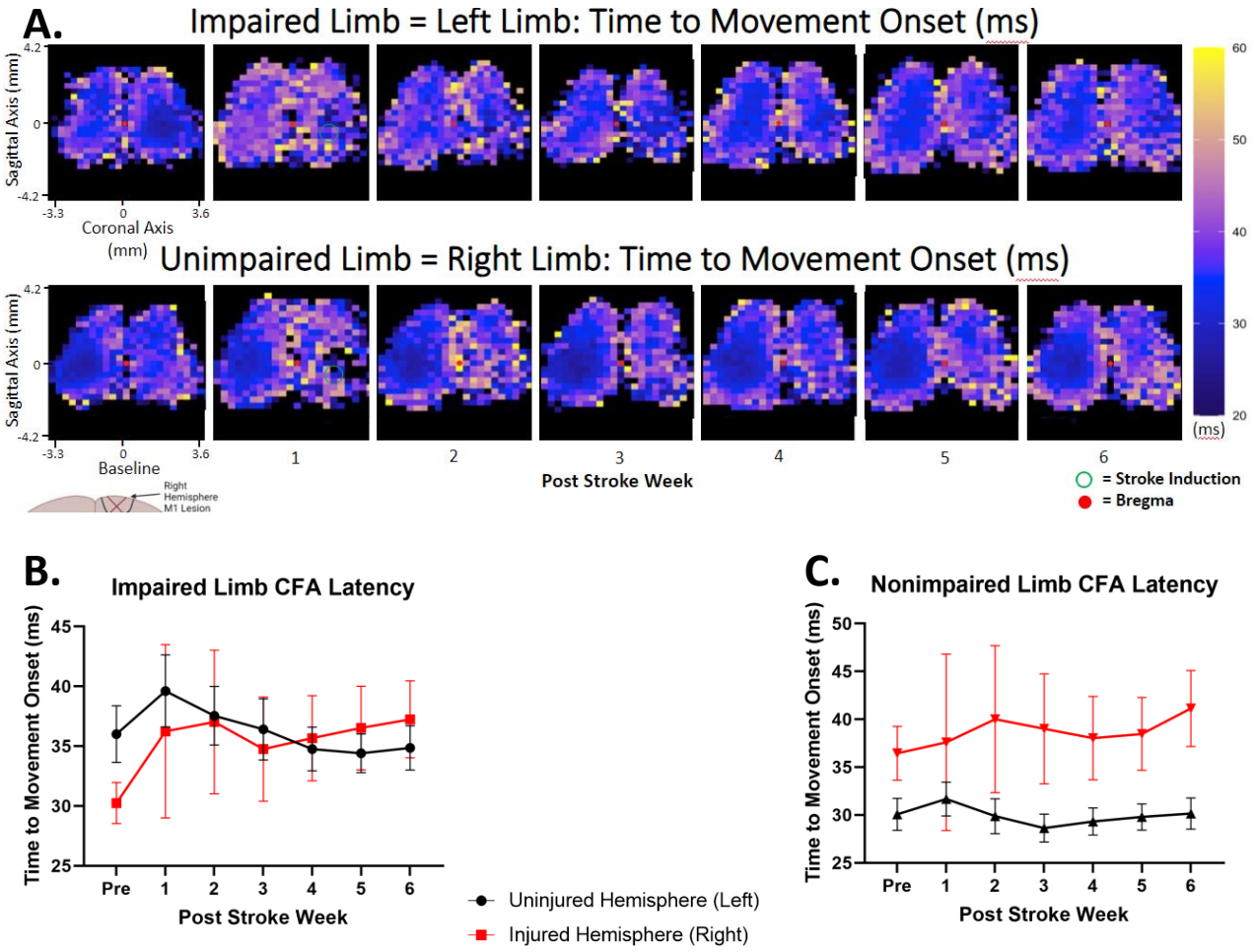

Figure 10: Averaged latency for motor maps following photothrombotic stroke. Adult mice (n=21) time to movement onset following light-based motor mapping stimulation. Movement was considered valid if it was continuous for at least 5 frames within 10-60 ms post-stimulation. **A.** Movement latency was averaged across two repetitions then were averaged per timepoint. Stroke was induced at ML: 1.5 mm, AP: -0.5 mm relative to Bregma (in red). **B.** Time to movement onset for the impaired forelimb in CFA. Data included the interior half of CFA. **C.** Time to movement onset for the nonimpaired forelimb in CFA. Data depicted as mean ± SEM. Statistical analysis was conducted through a mixed-model two-way ANOVA with Greenhouse-Geisser correction and Tukey's multiple comparisons tests.

3.6. Intrinsic signal optical imaging revealed a transient impairment in the sensory cortex.

In conjunction with LBMM, ISOI was employed to create longitudinal sensory maps, enhancing the assessment of cortical impairment following stroke by quantifying changes in blood flow elicited by sensory stimulation. Forelimb sensory maps were generated and registered to the Allen Mouse Brain Atlas. Sensory maps were analyzed for evoked amplitude and area in the following Atlas regions: sensory forelimb ("FL"), sensory hindlimb ("HL") and the primary motor cortex ("M1") and were displayed as the contralesional (eg. FL_C) or ipsilesional

(eg. FL_I) hemispheres. Baseline measurements demonstrated significant contralateral (verses ipsilateral) responses for both sensory evoked area ($p < 0.0001$) and amplitude ($p < 0.0001$). Within the contralateral hemisphere, the evoked area was significantly distinct from all other atlas regions ($p < 0.0001$), whereas amplitude was only significant when compared against M1 ($p \leq 0.0074$) but not the sensory hindlimb cortex ($p \leq 0.3591$) for both forelimbs.

The induction of stroke at the center of the CFA motor map led to a transient impairment in sensory maps. The representation of the sensory forelimb is located posterior-lateral to the stroke core, which was likely disrupted following an M1-targeted stroke. Following stroke induction, the impaired forelimb exhibited broader and less localized responses that extended beyond the boundaries of the target sensory forelimb region for both area ($p > 0.7455$) and amplitude ($p > 0.1735$), particularly when compared to the adjacent M1 atlas region in the first week after stroke (Fig. 11B, C). By post-stroke week three, the impaired sensory forelimb area exhibited significant recovery within the designated atlas location ($p < 0.0160$). Moreover, the evoked amplitude demonstrated significant recovery by post-stroke week four for HL_I ($p < 0.0057$), FL_I ($p < 0.0165$), M1_I ($p < 0.0034$), and FL_C ($p < 0.0491$) when compared against post-stroke week one amplitude values. Although the evoked response returns to the same atlas region, qualitatively, it appears slightly more lateral in the ipsilesional cortex (Fig. 11A). Additionally, the nonimpaired forelimb had no significant impairment or recovery across time for either amplitude or area following stroke, but did lose significance against the hindlimb sensory cortex for post-stroke weeks one and four (Fig. 11C). The sham group was additionally analyzed to determine the stability of sensory responses longitudinally. Shams did not have a significant time–Atlas region effect for the area ($p \geq 0.1940$) or amplitude ($p \geq 0.9562$) when investigated across the experiment (Supplemental Fig. 6).

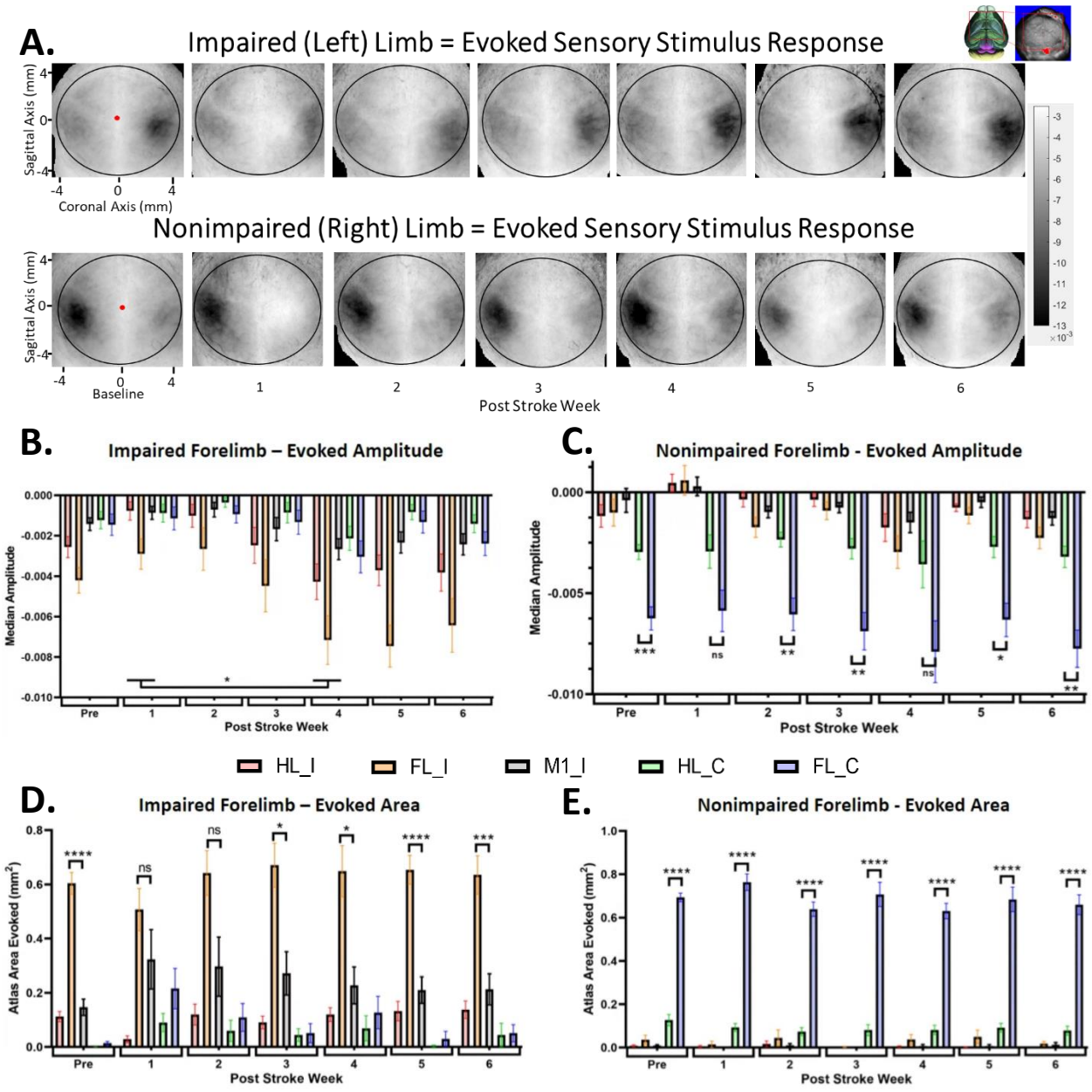

Figure 11. Intrinsic Signal Optical Imaging following motor cortex photothrombotic stroke. Evoked blood flow following sensory stimulation. The analysis frame was automatically generated as the maximum signal amplitude change relative to baseline. Images were aligned to Bregma (red label), stretched to overlap, and averaged across the stroke group (n=17). The stroke was induced at ML: 1.5 mm, AP: -0.5 mm relative to bregma. **A.** Impaired forelimb (top) and nonimpaired forelimb (bottom). The average window location was represented as a black outline. **B-D.** Atlas-defined regions of interest were displayed for each forelimb as a predetermined mask per individual animal transcranial window. Impaired forelimb (left side), nonimpaired forelimb (right side). **B/C.** Maximum signal amplitude relative to the baseline. Data is depicted as median amplitude ± SEM. **D/E.** The threshold area evoked is displayed per atlas region. Threshold was set to 55% ± 15% of the maximum amplitude per session average. Displayed as mean area evoked ± SEM. Statistical analysis was conducted through repeated measures two-way ANOVA with Greenhouse-Geisser correction and Tukey's multiple comparisons tests. Significance is indicated as follows: (*) $p < 0.05$, (*) $p < 0.01$, (***) $p < 0.001$, (****) $p < 0.0001$.

3.7. String pulling task performance was not impaired following motor cortex stroke.

The string-pull task was utilized to quantify deficits in non-learned complex motor movements. From the initial introduction of the task, mice could perform the task but had to learn the reward association. Over 80% of pulling events at baseline exhibited bimanual hand-over-hand behaviour (Fig. 12D). Importantly, this spontaneous behaviour at baseline did not include forelimb repositioning movements that extend the stride length of a particular pulling movement. Following the stroke, the number of forelimb stride length extensions significantly increased in the nonimpaired forelimb ($p < 0.0485$) relative to baseline (Fig. 12D). This trend led to a decrease in the number of bouts per session, although the change was not statistically significant (Fig. 12B). Interestingly, mice exhibited relatively similar performance in the string-pull task both before and after stroke induction, and there was no observed decrease in their participation rate following the stroke (Fig. 12C). The number of stride length extensions significantly decreased by post-stroke week three ($p < 0.0243$) when compared to post-stroke week one. Additionally, sham animals did not demonstrate any deviation from the baseline in forelimb extensions or participation rate (Fig. 12E). Overall, the stroke group exhibited no disruption in the impaired forelimb, while the nonimpaired forelimb demonstrated significantly more repositions to a higher position on the string following stroke induction, potentially to increase stride length.

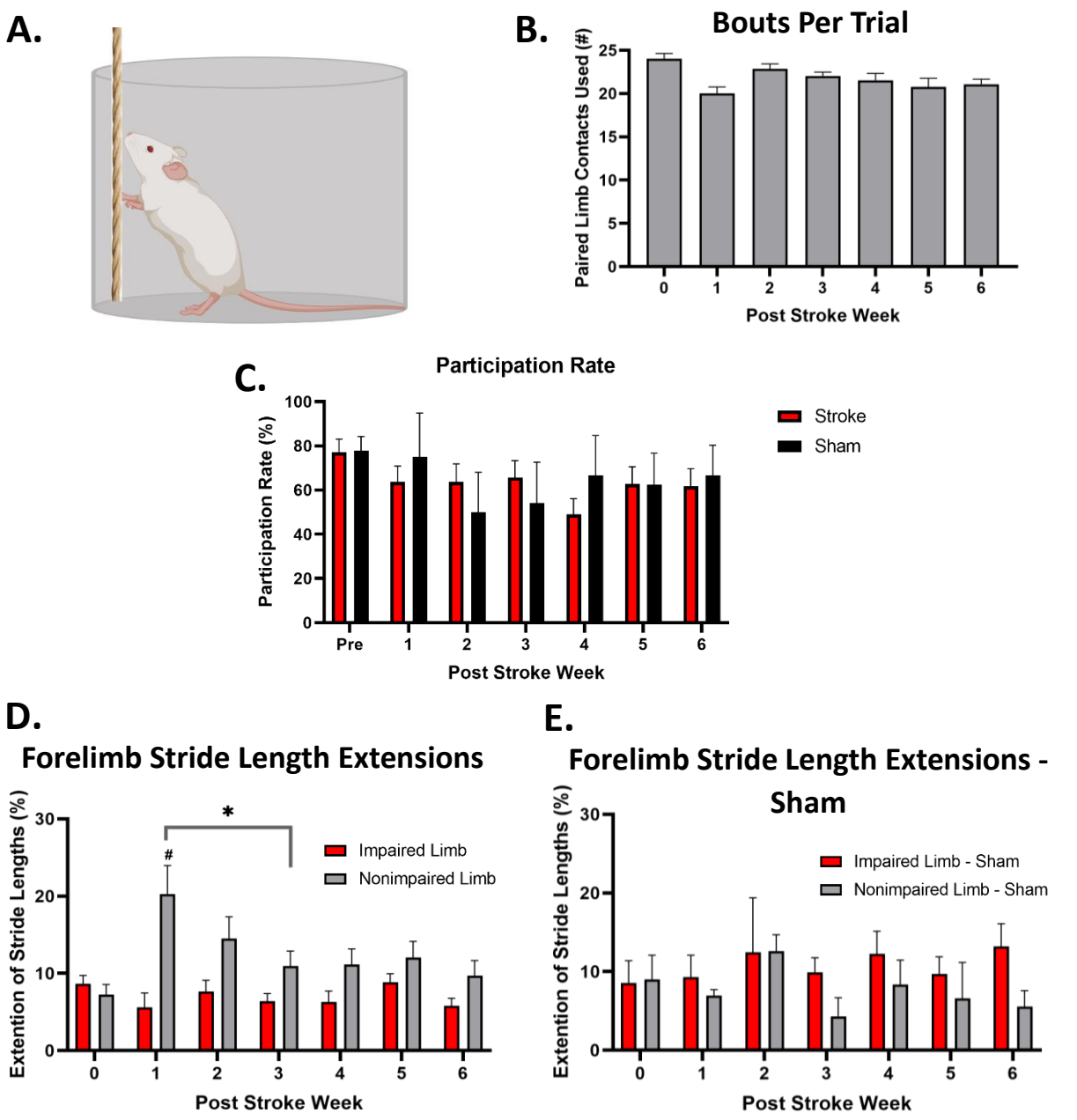

Figure 12. String-pull task analysis. Mice were habituation for 2 days to sugar water strings in their homecage, followed by one session of 20 strings in a homecage environment for an hour. Five consecutive baseline string-pull task sessions were conducted, then 2 sessions per week for the experiment duration. **A.** Graphic representation of the string pull task. **B.** Number of bimanual coordination occurrences required to pull a 1-meter string across stroke cohort (n=17). **C.** Task participation rate longitudinally for stroke (n=17) and sham (n=4) animals. Values averaged across the last three baseline sessions and both sessions per week post-condition. Sessions displayed as the number of completed trials divided by the total number of trials per session (three), where a completed trial was when the entire one-meter string was pulled. **D/E.** The number of occurrences where one forelimb extends to a higher position on the string after contacting the string divided by the total number of bouts (B) for the stroke (**D.**) and sham groups (**E.**). Data depicted as mean ± SEM. Statistical analysis was conducted through a repeated measures two-way ANOVA with Greenhouse-Geisser correction and Tukey's multiple comparisons tests. Significance is indicated as follows: * denotes significance per labelled timepoint, and # denotes significance within the forelimb relative to baseline.

3.8. Photothrombotic stroke induces long-term impairments in spontaneous limb use and grid walking.

In the cylinder task, mice exhibited an approximately equal usage of their impaired and nonimpaired forelimbs during baseline exploration. Following stroke induction, the stroke group had a significant decrease in impaired forelimb usage for pushing off the ground ($p < 0.0001$, Fig. 13C), wall contacts ($p < 0.0012$, Fig. 13F), and landing on the ground ($p < 0.0225$, Fig. 13D) when compared to baseline. Relative forelimb usage during total wall contacts significantly differed until post-stroke week five ($p \leq 0.0066$). Similarly, relative forelimb usage during total wall contacts showed significant differences until post-stroke week five ($p \leq 0.0066$), and relative forelimb usage for pushing off the ground demonstrated significant differences until post-stroke week six ($p \leq 0.0096$). During bouts of wall exploration, the number of contacts per rear was significantly reduced ($p \leq 0.0039$, one-way ANOVA with Tukey's multiple comparisons tests) from baseline and did not recover by post-stroke week six (Fig. 13B). This same depiction was also observed as a decrease in both forelimb usage during total wall contacts ($p \leq 0.0003$, Fig. 13E), even though the number of rears per task was unchanged (data not shown). When analyzed through the cylinder task, stroke impairments range from two-six weeks post-stroke.

In the sham group, the push-off forelimb and the relative forelimb usage during wall contact were consistent over the experiment (Supplemental Fig. 8C, F). Interestingly, the relative number of wall contacts per rear showed a numerical decrease, similar to the stroke group was not significant ($p \leq 0.1660$, Supplemental Fig. 8B, E). The relative usage of the sham-induced forelimb during landing was significantly reduced ($p < 0.0372$) at post-sham week one, accompanied by a significant forelimb-time interaction ($p = 0.0317$). Overall, signs of impairment were evident in the sham group, characterized by a sudden reduction in exploration and the emergence of a time-forelimb effect.

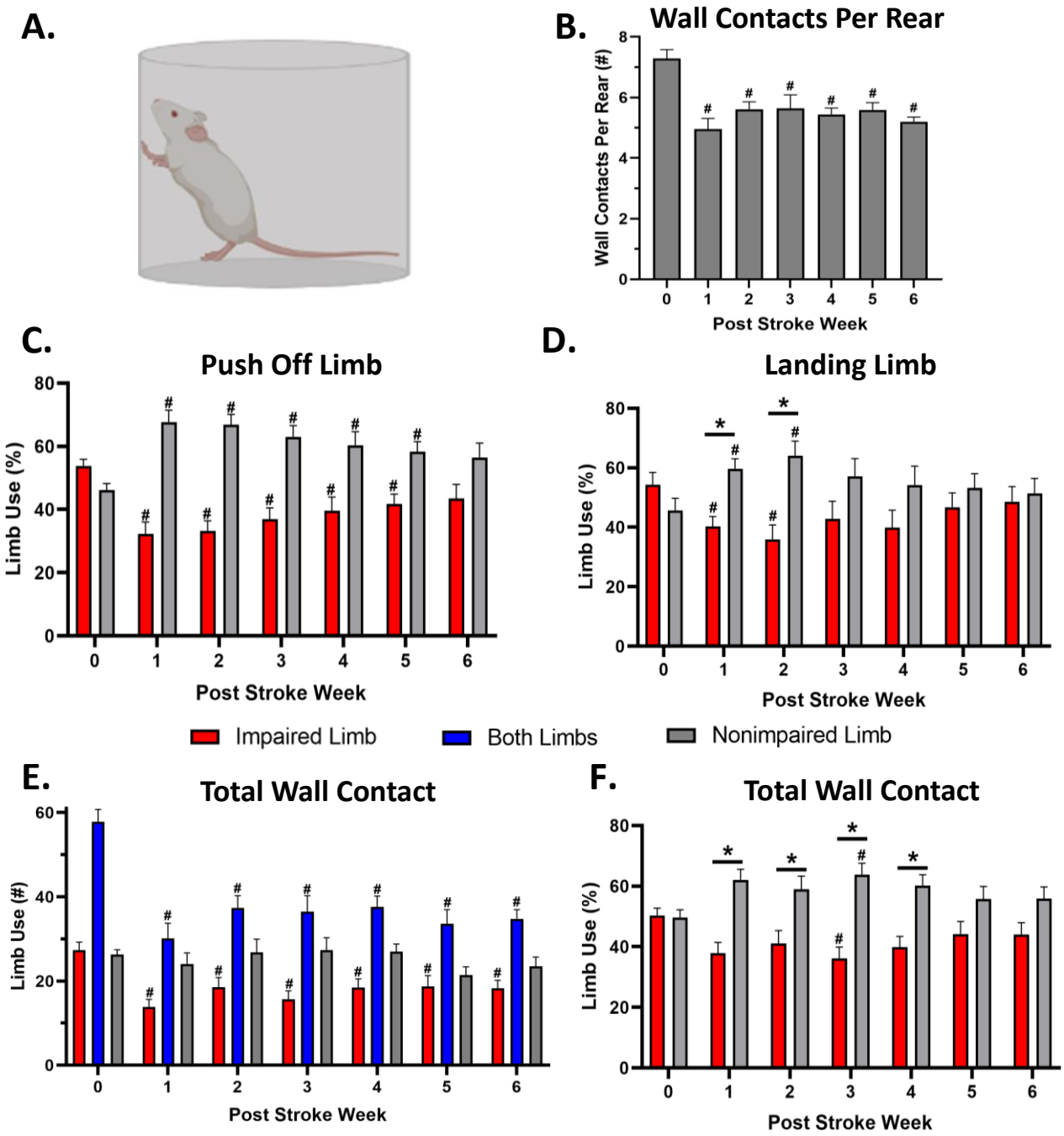

Figure 13. Cylinder task forelimb usage post-stroke. Adult mice (n=17) were analyzed for three baselines followed by weekly sessions post-stroke. Each session was a minimum of 10 rears, with a maximum of 25 rears analyzed. **A.** Graphic representation of the cylinder task. **B.** The average number of wall contacts per rear. **C.** Percentage of each forelimb last in contact with the ground at the start of a rear. **D.** Percentage of each forelimb first in the contact with the ground when landing from a rear. **E.** Total number of wall contacts per individual and combined forelimb-wall contacts. **F.** The total wall contacts displayed as a relative left-right forelimb usage. All data was depicted as mean ± SEM. Statistical analysis was conducted through a repeated measures two-way ANOVA with Greenhouse-Geisser correction and Tukey's multiple comparisons tests. * indicated significance per labelled timepoint. # indicated significance relative to baseline.

In the grid walking task, mice were specifically monitored for forelimb missteps and total steps taken during five-minute sessions. Baseline assessments revealed a nearly identical number of forelimb missteps among mice (Fig. 14B), along with consistent steps taken across all baseline sessions (data not shown). Following stroke induction, the stroke group significantly increased impaired forelimb missteps ($p < 0.0001$) post-stroke week one relative to baseline. Significant recovery occurred by post-stroke weeks four-six ($p \leq 0.0305$) against post-stroke weeks one to two. Furthermore, the stroke group did not exhibit significant forelimb missteps relative to baseline by post-stroke week six ($p = 0.0798$). The nonimpaired forelimb did not result in any significant number of forelimb missteps post-stroke ($p \geq 0.1922$) relative to baseline. Forelimb asymmetry emerged at post-stroke week one against baseline ($p < 0.0001$, One-way ANOVA with Tukey's multiple comparisons tests. Fig. 13C.) and did not recover by post-stroke week six ($p \leq 0.0036$). The amount of exploration across tasks was significantly decreased at post-stroke week one ($p = 0.0046$) and remained significantly decreased at post-stroke week six ($p = 0.0009$, Fig. 13D).

The sham group forelimb missteps indicated a three-week trend for the sham-induced forelimb but did not demonstrate statistical significance in forelimb missteps ($p \geq 0.5633$) or a forelimb–time effect ($p = 0.1305$, Supplemental Fig. 9). No impairments occurred for the nonimpaired forelimb post-sham, and there were no substantial alterations in asymmetry post-sham induction. The total steps taken also showed a decreased post-sham trend but was insignificant ($p \geq 0.1064$, One-way ANOVA with Tukey's multiple comparisons tests). Overall, the sham group appeared minimally damaged in the afflicted forelimb but was insignificant in any recorded metric.

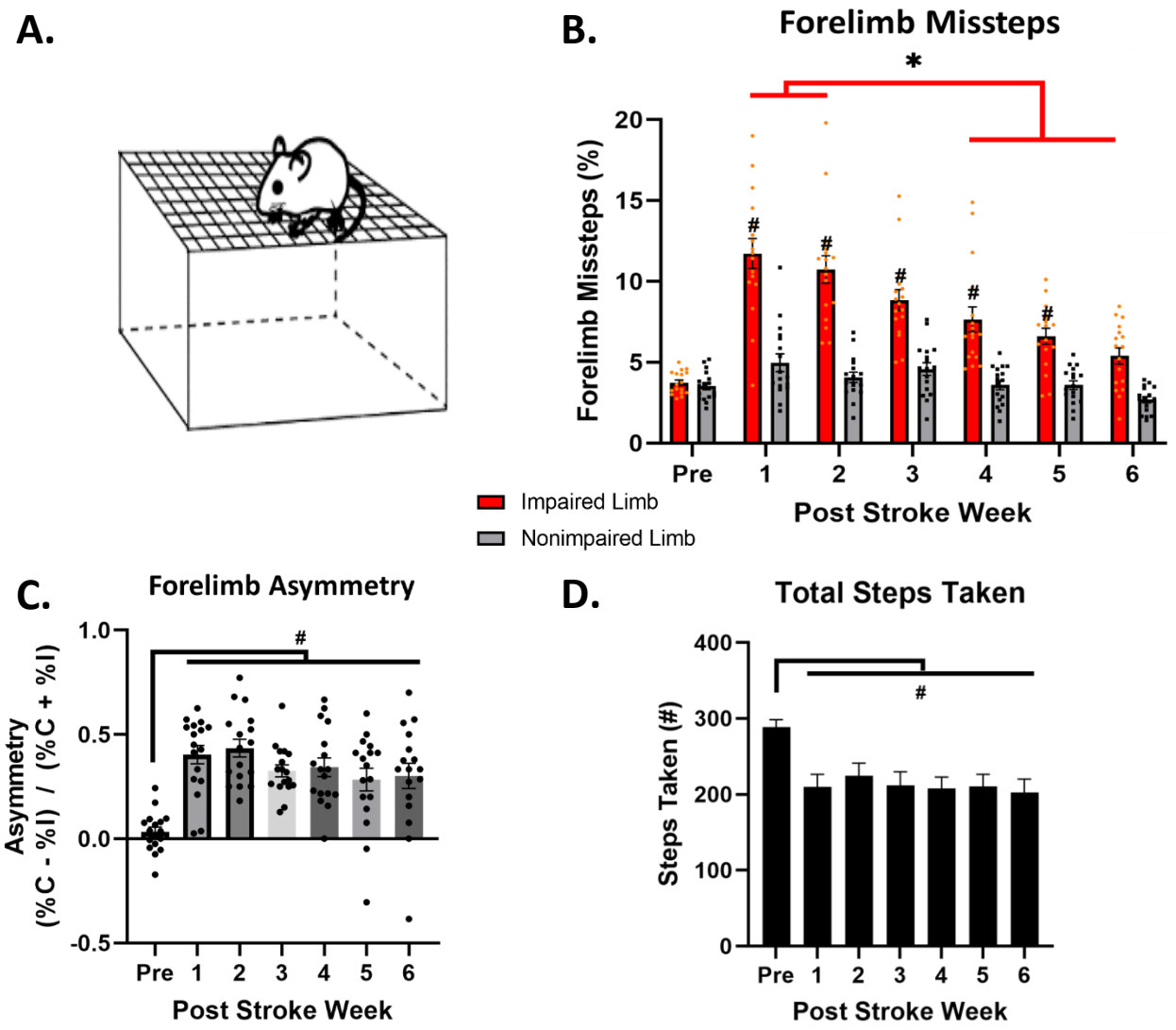

Figure 14. Grid walking task forelimb analysis post-stroke. Adult mice (n=17) were placed on a thin mess wire for five minutes and recorded for forelimb missteps. Three baseline sessions were averaged followed by one post-stroke session per week. A minimum of 75 steps was required. **A.** Graphic representation of the grid walk task. **B.** The number of forelimb missteps over the total session steps taken. Missteps were included if the wrist went past the wire mesh. Steps were counted if the forelimb moved at least 1 mesh square in distance (1.0 cm). **C.** Forelimb asymmetry was the difference in forelimb missteps as a percentage divided by the summed forelimb percent missteps as a percentage. **D.** The total number of steps taken was manually counted using the impaired forelimb post-stroke. All data are depicted as mean ± SEM. Statistical analysis was conducted through repeated measures two-way ANOVA with Greenhouse-Geisser correction and Tukey's multiple comparisons tests. Significance is indicated as follows: * denotes significance per labelled timepoint, and # denotes significance within the forelimb relative to baseline.

4. Discussion

Minimally invasive Light-Based Motor Mapping (LBMM) assessed longitudinal stroke impairment and spontaneous recovery of motor maps in mice. LBMM identified key time points involved in the spontaneous recovery of motor forelimb representations, where recovery progression was not observed for the first two weeks post-stroke, and recovery plateaued at post-stroke week four. LBMM demonstrated bilateral plastic recovery in motor maps at chronic time points, with recovery of forelimb trajectory and forelimb amplitude in the contralesional hemisphere. In addition to LBMM, we quantified motor behaviour pre- and post-stroke and found that the recovery of motor map representations precedes behavioural recovery. Motor maps in sham mice showed some fluctuations but were not significantly different across time points in our experiment. Interestingly, forelimb sensory stimulation evoked brain activity that was initially impaired after stroke but recovered before any recovery in motor maps. Lastly, LDI recordings suggested alterations in blood flow may occur during our sham procedure in Thy1-ChR2-eYFP mice. To our knowledge, this is the first study to longitudinally investigate bilateral motor and sensory mapping while also monitoring sensorimotor behavioural recovery.

4.1. Spontaneous ipsilesional recovery assessment by Light-Based Motor Mapping.

Utilizing LBMM, stroke damage was quantified, and recovery was recorded weekly for six weeks post-stroke. At baseline, the LBMM area for the impaired forelimb was 7.22 ± 0.28 mm^2 along the dorsal cortex's surface, 1.28 ± 0.015 mm^2 RFA, and 5.93 ± 0.015 mm^2 CFA. Stroke volume was recorded at 1.06 ± 0.16 mm^3 and localized within the anterior CFA of the motor map (Fig 6 C-E). RFA is considered a higher-level cortex processing region than CFA and is considered analogous to supplemental or premotor cortices (Neafsey *et al.,* 1986; Deffeyes *et al.,* 2015). Additionally, RFA is primarily upstream of CFA; therefore, more significant impairments are expected as it feed-forwards information and intent into CFA for execution (Rouiller *et al.,* 1993; Hira *et al.,* 2013; Deffeyes *et al.,* 2015). Knowing all this, we targeted CFA as our primary objective was to determine the impact of stroke on cortical sensorimotor representations and how this relates to behavioural recovery. Since CFA comprised over 80% of the motor map, it was a key target to achieve this goal (Neafsey *et al*., 1986; Neafsey & Sievert,

1982). We targeted the center of CFA specifically as it consistently produces forelimb movement when stimulated and minimally overlaps with the sensory cortex, unlike posterior-lateral CFA (Tennant *et al*., 2011). Of note, our stroke model produced only partial injury to CFA (approximately 20-25% by post-stroke week seven); however, our lesions penetrated all layers of the cortex but avoided white matter damage (Fig. 6).

During the first three weeks after stroke, we showed that ipsilesional motor maps had a reduction in movement amplitude and area and produced more linear movement trajectories at a longer latency for both forelimbs (Fig. 7-10). Interestingly, recovery of motor representations was minor for the first two weeks post-stroke, but began changing in week three, then immediately plateaued by weeks four to six in terms of both map area and movement amplitude (Fig. 7C-G). One possibility for the delay of recovery is that photothrombotic stroke initially impacts a wide area, impacting tissue more than four-fold of the core lesion (Kuroiwa *et al.,* 2008; Labat-gest & Tomasi; 2013; Zeiger *et al.,* 2021). At one-day post-stroke, the photothrombotic stroke model has a substantially larger lesion volume, accompanied by brain edema and blood-brain barrier edema. Throughout the first two weeks, neovascularization, glucose metabolism, inflammatory cells, and astrocyte infiltration relative levels increase, whereas infarct volume, brain edema and the blood-brain barrier permeability decrease towards baseline as described in Liu *et al.,* 2017. As a result, most of the CFA was likely impacted following photothrombotic stroke, but lesion volume refined to less than 25% of CFA by post-stroke week seven. Research has shown that by post-stroke day 14, vascularization around the lesion recovers to 50% of baseline and continues recovering until reaching baseline blood flow at post-stroke week five (Liu *et al*., 2017; Kuroiwa *et al*., 2008; Schrandt *et al*., 2015). As a result, neovascularization may contribute to behavioural recovery after stroke by restoring blood flow to peri-infarct regions (Williamson *et al.,* 2020). Our data shows that although there were slight changes in motor maps during the third-week post-stroke, these changes were not yet significant. It appears, therefore, that vascular reorganization precedes motor map recovery (post-stroke week four, Fig. 7,8), suggesting that partial repair of stroke-associated vascular damage is a precursor for peri-infarct neuronal recovery.

In addition to vascular changes, stroke-induced neuronal excitability alterations may contribute to our observed results. For example, within the acute period (post-stroke weeks one-three), long-range projections from the intact hemisphere (through the corpus callosum) may over-inhibit the ipsilesional cortex. A review from Grigoras and Stagg, 2021 states that the peri-infarct cortex may be inhibited due to increased GABAergic signalling during the acute phase after stroke. In contrast, contralesional representations display decreased GABA levels in the homotopic region. Recent research supports this claim as decreasing $GABA_A$ receptor activity with benzodiazepine increased motor recovery in grid walking and skilled reaching in rodent models of focal stroke (Alia *et al.,* 2016; Clarkson *et al.,* 2010). Additionally, The Bauer Lab recently showed that enhancing contralesional activity during the acute period can negatively impact recovery (Bice *et al*., 2022). This effect may be due to the overactive contralesional hemisphere exerting excessive inhibition on ipsilesional (peri-infarct) regions. Overall, our findings of acute period loss of motor representations within the injured hemisphere align with models of recovery that suggest excessive inhibition originating from the intact hemisphere.

Our findings of motor map reorganization in the peri-infarct (CFA and RFA) and contralesional CFA (Fig. 8A/D), are also consistent with previous findings showing the brain's capacity for adaptive change and neuroplasticity post-stroke (Nudo *et al.,* 2001; Okabe *et al.,* 2016; Nishibe *et al.,* 2014). Additionally, we found that movement representation for the nonimpaired forelimb within the ipsilesional hemisphere also decreased significantly. Most previous mapping studies have only quantified the contralesional forelimb representations. One reason for this is that techniques such as ICMS disrupt the cortex during the mapping procedure, thus leaving a limited time window for stimulating “healthy” brain tissue. These terminal experiments lead to the animal's sacrifice and require long protocol durations (Clark *et al.,* 2011; Tehovnik, 1996). As a result, ICMS studies rely on between-subject comparisons to compare motor representations at critical timeframes, such as acutely, chronically, or after promoting recovery (Okabe *et al.,* 2016). Using LBMM, we addressed this limitation by investigating bilateral and bi-hemispheric forelimb motor maps. This approach allows us to perform longitudinal experiments, similar to clinical studies (Traversa *et al.,* 1997; Cicinelli *et*

al., 1997), with the advantage of having controlled experimental manipulations possible in rodent models (Jones & Adkins, 2015). We found that although nonimpaired ipsilesional forelimb representations decreased acutely, chronic period recovery returned to baseline levels for the area and amplitude surrounding the stroke site (Fig. 8C). Conversely, the impaired forelimb recovered but did not reach baseline levels for forelimb amplitude (Fig. 7D, 8A). The difference in impaired- and nonimpaired-forelimb recovery ipsilesionally is likely because of the importance of contralateral representations for direct corticospinal tract forelimb movements in mice (Liu *et al.,* 2009), which is clinically relevant (Buetefisch *et al.,* 2023). As a result, forelimb movements were a valuable biomarker for impairment and recovery within the peri-infarct space, demonstrating a more remarkable recovery observed in the nonimpaired forelimb (Jeffers *et al.,* 2020; Prabharkaran *et al.,* 2007).

One benefit of LBMM is that it facilitates longitudinal investigation of forelimb motor representations, permitting comparisons with other longitudinal techniques such as multiphoton imaging. Recent findings state that surviving neurons in the peri-infarct cortex are strengthened (Zeiger *et al*., 2021). Supporting research by Okabe *et al*., 2017 demonstrates that recovery following CFA photothrombotic stroke results in increased RFA corticospinal axonal remodelling when imaged ex-vivo, which is thought to be functionally relevant (Liu *et al.,* 2009; Buetefisch *et al.,* 2023). Furthermore, Brown *et al*., 2007 showed that spine turnover increased significantly post-stroke, as spine turnover is elevated (five-eight-fold) the first two weeks after stroke and remains significantly increased until post-stroke week six in the motor cortex. In comparison, LBMM forelimb amplitude and area recovery plateaued by post-stroke week four. It is possible that motor regions likely undergo prolonged reorganization after stroke to remove redundancy and generate ideal synaptic circuits; however, these subtle changes may not be detectable by LBMM. The microscopic imaging performed in studies of synaptic spines are inherently more likely to detect ongoing reorganization on a smaller scale, while cortical mapping approaches likely only detect changes on a mesoscopic scale. In conclusion, the increase in peri-infarct CFA and RFA forelimb representations likely occurs due to the strengthening of neuronal connections, which can be directly visualized through microscopic imaging or examined on a mesoscale level through cortical mapping experiments.

Due to the acutely stagnant recovery followed by significant recovery, which plateaued suddenly for both forelimbs (Fig. 7), we analyzed changes in forelimb trajectory at acute (post-stroke weeks one-three) and chronic time points (post-stroke weeks four-six. Fig. 8-9). Importantly, evoked forelimb movements in CFA displayed a circular pattern at baseline, while RFA exhibited a significantly more linear trajectory (Fig. 9). Upon acute period recovery, forelimb trajectories from CFA became significantly more linear, resembling those of RFA. However, in the chronic recovery phase, neither forelimb displayed restoration of peri-infarct CFA forelimb trajectory (Fig. 9-10), despite the reestablishment of forelimb representation in area and amplitude (Fig. 7-8). Additionally, forelimb latency was contralateral at baseline and did not recover ipsilesionally (Fig. 10). This distinction suggests that latency and forelimb trajectory are independent metrics from area and amplitude that recover at differential rates after stroke. Specifically, recovery of movement trajectory and latency does not occur in chronic periods within the peri-infarct cortex. One possibility for these findings is that the contralesional hemisphere compensates following stroke, which can lead to functional changes.

Some limitations involved in motor mapping include using light ketamine and xylazine anesthesia. Although this is standard in rodent mapping techniques, such as ICMS, it requires the manual generation of a stable anesthetic plane. Although strict protocols were in place to ensure similar motor map anesthetic planes across animals, it should be noted that this work was not blinded, as results were analyzed in real-time, and stroke could be visualized through the transcranial window. Additionally, mice underwent LBMM sessions weekly, where due to the repetitive exposure to ketamine and xylazine, mice reacted to anesthesia differently from baseline versus experimental endpoints. As a result, criteria were set to ensure that mice were stable before motor mapping, which increased experimental duration. Future work is investigating using LBMM with automatic ketamine top-ups to address the potential bias in investigator-determined mapping plane effects.

4.2. Bilateral motor maps – baseline and post-stroke recovery.

At baseline, we confirmed that each forelimb has a bilateral forelimb movement representation (Silasi *et al.,* 2013), whereas most motor mapping literature shows represents

unilaterally forelimb representation pre-clinically (Nudo *et al.,* 1996; Kleim *et al.,* 2004; Boychuk *et al.,* 2016). Although LBMM was significantly more contralateral for movement amplitude (Fig. 7) and latency (Fig. 10) than the ipsilateral hemisphere, ipsilateral representations were present in all animals before stroke (Fig. 7-10). There could be many reasons our maps were bilateral. One explanation is that other research groups do not typically record bilateral forelimb data. ICMS-derived motor maps often use invasive electromyography (EMG) signals, typically only inserted contralateral to the stimulated hemisphere (Teskey *et al.,* 2002; Tennant *et al.,* 2011). Other ICMS studies that generate motor maps based on manual observations of movements often focused on just the contralateral forelimb (Graziano *et al.,* 2005; Cooke *et al.,* 2003; Baldwin *et al.,* 2016), so they may not have reported ipsilateral movements. The other potential scenario is that LBMM exclusively activates glutamatergic layer-V pyramidal neurons in the neocortex (Arenkiel *et al*., 2007). As a result, light stimulation could bypass natural excitatory-inhibitory balance and simultaneously evoke direct (corticospinal tract; Muñoz-Castañeda *et al.,* 2021) and indirect motor movements (rubrospinal tract; Liang *et al.,* 2012), resulting in both contralateral and ipsilateral motor movements from one stimulation site in the motor cortex. In the human motor system, 8% of evoked responses are ipsilateral (Grafton *et al.,* 1996; Kim *et al.,* 1993), so although our motor maps are more bilateral, healthy populations can also express some degree of bilateral movements. Therefore, LBMM analysis permits a unique recording for bilateral bi-hemispheric motor mapping through layer-V pyramidal neuron activation.

Utilizing LBMM, the contralesional hemisphere forelimb area and amplitude significantly increased during chronic period recovery for both forelimbs (post-stroke weeks four-six). Traditionally, peri-infarct reorganization is thought to be the most important for recovery, but the role and importance of the contralesional motor cortex remain elusive (Buetefisch, 2015). Clinical research suggests that during hand movement, the contralateral hemisphere to the active hand inhibits the ipsilateral hemisphere through transcallosal fibres, although can vary by hand dominance and task processes (short-interhemispheric inhibition model; Meyer *et al.,* 1998; Kurth *et al.,* 2013; Ferbert *et al.,* 1992; Daskalakis *et al.,* 2002; Bütefisch *et al.,* 2003; Newton *et al.,* 2004; Morishita *et al.,* 2022). After a stroke, there is a loss of inhibition of the

intact hemisphere, and the contralesional hemisphere is hyperactive, theorized to contribute to poor recovery (Bütefisch *et al.,* 2003; Bütefisch *et al.,* 2008; Takeuchi & Izumi, 2012). One theory suggests that increased contralesional hemisphere activity can result from nonspecific motor outputs, where bilateral projections become more dominant than unilateral projections (Dodd *et al.,* 2017). Therefore, promoting a normalized hemispheric balance should achieve ideal motor recovery and reduce bilateral movements through rehabilitative means (Hoyer & Celnik, 2011).

These theories align with our findings since we do not promote recovery, and our selected behavioural tasks were for non-learned forelimb movements (Fig. 11-13). Additionally, many research groups have recorded improved benefits in bilateral use therapy as being effective in preventing learned non-use of the injured side (Summers *et al.,* 2006; Stoykov *et al.,* 2009; Theresa Jones, 2017; Takeuchi & Izumi, 2012). This approach is particularly important since learned non-use can promote maladaptive recovery (Allred & Jones, 2009), decreasing recovery to the impaired forelimb and increasing ipsilateral reliance. In our study, we utilized bilateral tasks through string-pull and grid walking tasks, where through participation in these tasks, the probability of maladaptive recovery occurring in the peri-infarct space was decreased. Therefore, while motor maps predominantly displayed contralateral patterns regarding forelimb amplitude at baseline, they also exhibited bilateral recordings. The ipsilesional and contralesional motor map recoveries corresponded with the impaired forelimb's observed recovery in functional behavioural outcomes.

4.3. Motor map recovery precedes behavioural recovery.

A battery of sensorimotor behavioural tasks was used to evaluate the functional role of motor map changes. These behavioural measurements permitted the assessment of stroke-induced sensorimotor impairments and recovery during our longitudinal experiment. The reasons for choosing the behavioural tasks were deliberate: string pull task to assess complex non-learned motor movements following an M1-localized stroke (Fig. 12), cylinder task to assess forelimb preferences during spontaneous exploration (Fig. 13), and grid walking task to assess sensorimotor coordination during locomotion (Fig. 14). It remained crucial that we

minimized any effects of motor learning, as studies have shown motor learning alters motor map organization (Kleim *et al*., 1998; Kleim *et al*., 2004; Nudo *et al.,* 2001; Tennant *et al*., 2012). Furthermore, this is a unique opportunity for the experiment, as many studies utilize longitudinal behaviour and correlate findings to maps derived at the end of the experiment. Non-invasive stimulation paradigms such as LBMM and ISOI can run parallel to behavioural recordings to determine the relationship of maps to behaviour, providing a unique insight into reorganization and recovery that remains unreported.

Surprisingly, complex non-learned motor movements remain intact in the string pull task. The lack of motor impairment is likely due to the potential involvement of the striatum, a subcortical basal ganglion motor region theorized to hold motor engrams relayed acquired from the motor cortex (Hwang *et al*., 2022; Lemke *et al*., 2019; Lemke *et al*., 2021; Guo *et al*., 2021). Although several metrics of string-pulling behaviour were analyzed, the only significant impairment we observed was one week following a stroke. Stroke mice performed significantly more forelimb repositions with the nonimpaired limb to extend stride length during bouts of pulling (Fig. 11C). This effect was not observed in sham mice (Fig. 12D). In the cylinder task, a two-week increase in the nonimpaired forelimb for landing was observed following stroke, impaired forelimb usage was significantly distinct for four to six weeks during wall exploration, and relative forelimb usage was distinct until post-stroke week six. Forelimb preference during wall exploration as a percentage is the most common measurement for cylinder task (Magno *et al.,* 2019), which in our findings demonstrates that recovery was no longer significant by post-stroke week five. Additionally, although exploratory behaviour generally decreases with repeated testing (as displayed in Fig. 13B), reduced wall contacts at chronic phase recovery are presumed to be a participation effect because of weekly exposure. Therefore, when presented as a percentage, this does not impact the overall damage, justifying the differences observed in Fig. 13E/F.

The grid walking task showed an increased frequency of missteps with the impaired forelimb until post-stroke week six and displayed a linear recovery (Fig. 14B). Additionally, mice do not recover in the overall asymmetry of missteps, as the impaired limb remains continuously dominant in the number of forelimb missteps for all six weeks post-stroke (Fig. 14C). Overall,

our findings relay that motor map reorganization precedes behavioural recovery by at least one week depending on the task utilized. These findings suggest that motor map reorganization is functionally relevant to sensorimotor behaviour. A review article from Tim Murphy and Dale Corbett in 2009 suggests four weeks of heightened plasticity following a stroke, whereas Brown *et al.,* 2007 found an increase in spine turnover for six weeks post-stroke. As a result, modulations during this time of heightened plasticity promoted functional recovery dependent on behavioural engagement (Biernaskie *et al.,* 2004). For example, synaptic circuits may rewire using pre-existing circuits to form stable connections as mice use the impaired forelimb in tasks (Kleim *et al*., 2004; Zeiger *et al.,* 2021). Future experiments using LBMM could investigate motor-learning or rehabilitative behaviour to investigate the effects of such interventions on motor map recovery. Additionally, unique opportunities specific to optogenetics could be utilized, where recording longitudinal motor map alterations to pharmaceuticals or teasing out contralesional-ipsilesional transcallosal fibres could be conducted. the behavioural results suggest that neuronal reorganization, as detected through LBMM, precedes consistent behavioural recovery across tasks. Specifically, tasks like the grid walking task exhibit delayed recovery, likely due to the high level of precision required to perform this task, whereas the cylinder task likely demonstrated slightly earlier recovery due to the more simplistic approach of the task.

One potential limitation to these findings is the weekly repetitive administration of anesthesia. Although repetitive ketamine-xylazine administration is not known to affect behaviour or grimace (Hohlbaum *et al*., 2018), repetitive isoflurane does affect grimace score and home cage exploration (Hohlbaum *et al*., 2017), as well as learning, memory, and recovery (Lee *et al*., 2014; Rothstein *et al*., 2008; Bajwa *et al*., 2019). Additionally, ketamine increases neuroplasticity when applied in subanesthetic doses. However, the effects that weekly anesthetic doses of ketamine have on post-stroke recovery remain unknown. Ketamine, xylazine, and isoflurane were administered weekly in all animals and presumably impacted behavioural recovery, while the effects on motor or sensory map outputs remain unclear. However, the relatively stable longitudinal sham animals and comparisons with previous literature suggest that repetitive exposure does not negatively impact longitudinal motor or

sensory map output (Grigoras & Stagg, 2021). Additionally, isoflurane exposure occurred before any behavioural recordings, as transcranial window implantation was the first step in the experiment (Fig. 1A), therefore any effects in initial isoflurane exposure was present throughout the experiment for pre- and post-stroke analysis.

4.4. Transient sensory impairment and recovery distinctions from motor recovery.

The utilization of optical techniques, such as intrinsic signal optical imaging (ISOI) and LBMM, provided valuable insights into cortex reorganization following M1-localized photothrombotic stroke induction. Since functional forelimb motor and sensory regions are proximal anatomical regions and 33% overlap through cytoarchitecture zones (Tennant *et al*., 2011), motor cortex stroke impacts the sensory cortex substantially. The overlap zone consists of the hindlimb, forelimb, and shoulder region in the motor cortex and primarily the hindlimb and forelimb in the sensory cortex (Tennent *et al*., 2011), which matches our forelimb motor and sensory mapping data (Supplemental Fig. 5). As a result of M1 stroke, ISOI showed a decrease in intensity and area (non-significant) for two weeks post-stroke, then significant recovery by post-stroke week three for area, and week four for intensity (Fig 11C/E). Since the evoked area was a percentage, impairment was determined as a change relative to the atlas area at baseline and post-stroke week one. This was designed to localize the core area activated by stimulation. However, future analyses will require determining the area as two standard deviations change from the baseline average to relay decreases in the relative area evoked. This will prove more useful in determining the absence of signal demonstrated initially following stroke induction. Interestingly, the initial decrease recorded one-second following stimulation is absent in post-stroke week one and did not recover across the experiment (Supplemental Fig. 6), where the nonimpaired forelimb maintains this activity.

One possible explanation for why sensory maps recovered before motor maps is that the sensory forelimb cortex is positioned posterior-lateral to the motor cortex (Supplemental Fig. 5). Therefore, any repair in the vasculature that might occur would impact lateral regions first as the vessels travel in a lateral to medial orientation (Williamson *et al.,* 2020). Therefore, the return of evoked activity in the sensory cortex recorded by ISOI preceding peri-infarct

stroke regions (anterior and medial CFA, LBMM) is likely related to the vascularization recovery profile. This is likely a root cause of the transient damage, as Sunil *et al.,* 2023 have recently demonstrated how neurovascular coupling is preserved following PT stroke using ISOI when combined with widefield fluorescence imaging. Alternatively, the recovery may stagnate for two weeks by disruptions to the excitation-inhibition balance following stroke, where long-range connectivity primarily through the corpus callosum is over-inhibiting the ipsilesional cortex as described prior. Conversely, ISOI demonstrated stable nonimpaired forelimb representation, with no change across time for the response amplitude or threshold activation area. Sham animals also were relatively stable across the cohort longitudinally.

Following stroke recovery, evoked sensory cortical responses occur within the same structural region for ISOI sensory mapping. Therefore, ISOI recovery was distinct from LBMM recovery, where ISOI returned to the original anatomical forelimb regions, and LBMM recovery was in peri-infarct space and homotopic structural regions. This finding aligns with Harrison *et al.'s* 2013 published findings, stating that motor stroke did not increase shared motor-sensory overlap. This is particularly interesting, as Harrison *et al.,* 2013 also demonstrated that sensory stroke results in the expansion of sensory neurons in the motor cortex during chronic period recovery. Therefore, a hierarchical reorganization order is present and partially reiterated here. Regarding the sensory impairment, although the sensory hemodynamic recordings significantly decreased for two weeks, the impairment was only transient and did not have permanent effects. This also would be supported by the vascularization studies where ISOI responses reoccur in a similar location as the stroke core lesion does not envelop them (Williamson *et al.,* 2020). Additionally, this finding could provide context to RFA increases in motor amplitude post-stroke, as ipsilesional sensory forelimb impairments are nonsignificant by post-stroke week three and still providing tactile responses to RFA for sensorimotor coordination (Hayley *et al.,* 2023). Indicating a potential role for RFA in somatosensory processing alongside its motor functions due to RFAs known connections with S1 forelimb, and its potential role as a pre-motor cortex (Rouiller *et al.,* 1993; Hayley *et al.,* 2023). Overall, sensory forelimb metrics were transiently impaired, and recovery occurred within the functionally defined forelimb sensory cortex.

4.5. LBMM as a tool for guiding stimulation therapy.

Although a popular notion, many researchers find inconclusive or contradicting results when applying stimulation therapy clinically or pre-clinically to promote functional recovery. Many believe these inconsistencies occur due to improper time, location, or type of stimulation therapy. Too early (hyper-acutely) can be damaging, too late (chronic) can be reduced in effect, improper location can further impair neuronal imbalance, and improper stimulation type can be null in producing change (Bice *et al*., 2022; Shen *et al.,* 2016; Coleman *et al*., 2017; Jones, 2017; Murphy & Corbett, 2009; Nudo *et al*., 2001; Wahl & Schwab, 2014). Additionally, clinical studies are burdened with variables that are difficult to control for, such as lesion location, lesion size, age, lifestyle, and more. As a result, animal models can be used as a platform for testing clinically relevant non-invasive brain stimulation paradigms. Using LBMM, brain stimulation can occur longitudinally post-stroke because the skull remains intact, and the cortex remains preserved. Since LBMM generates mesoscopic maps of the motor cortex, LBMM is an ideal technique for generating comprehensive and rapidly acquired motor maps to determine how the cortex adapts to neurological damage, such as stroke. Additionally, short-burst randomized stimulation patterns utilized in LBMM do not evoke plasticity, as either sensory pairing (paired-associative stimulation: Stefan *et al.,* 2000; Castel-Lacanal *et al.,* 2008; Carson & Kennedy, 2013) or stimulation trains (intermittent theta burst stimulation (iTBS): Huang *et al.,* 2005; Blumberger *et al.,* 2018; Tsuboyama *et al.,* 2019; Huang *et al.,* 2022) are typically required for stimulation-induced plasticity (Diao *et al.,* 2022; Dickins *et al.,* 2015). LBMM can be combined with stimulation paradigms such as iTBS or rehabilitative-like behavioural tasks such as the pellet grab and reach task to promote recovery. For example, Bice *et al*. 2022 performed chronic period contralesional excitation to investigate the effects on sensory cortex recovery. LBMM could be the ideal paradigm for investigating where and when to use recovery-promoting agents, such as iTBS stimulation therapy. From this study, we identified that motor map recovery was not visible by mesoscopic imaging with LBMM in post-stroke weeks one-two but then suddenly plateaued by post-stroke week four. Therefore, stimulation could be performed during this time gap to promote motor map alterations by promoting recovery to an early time point or increasing peri-infarct recovery, which could benefit sensorimotor

behaviour. Furthermore, because LBMM is longitudinal, individual stroke damage could be assessed for variability and customized treatment applied per stroke condition. As a result, LBMM could add control to non-invasive brain stimulation experiments to aid in stroke recovery.

4.6. Photothrombotic stroke and blood flow changes.

Our study utilized photothrombotic (PT) stroke induction to mimic cerebral ischemic events. PT stroke induction was recorded through Laser Doppler Imaging (LDI). LDI permitted recording at a fixed laser location before, during, and after stroke, which was then adjusted to scan blood flow and generate blood flow maps (Nilsson *et al*., 1980; Webber *et al*., 2022). As expected, PT stroke induction resulted in a decrease in LDI blood flow maps and flux recordings (Fig. 5B). To our surprise, sham mice also had a reduction in blood flow in the afflicted hemisphere (Fig. 5D), specifically after the injection of the rose Bengal dye (Supplemental Fig 1E). Comparatively, the PT stroke induced a more significant reduction in blood flow in both hemispheres (Fig. 5B) than the sham group (Supplemental Fig 1B/C).

Additionally, blood concentration was decreased exclusively in PT stroke animals as identified through LDI single-point recordings at the stroke core (Fig. 5C, Supplemental Fig. 1D/E). Although the post-stroke blood concentration equals pre-sham values, we do not believe this is induced damage. Blood concentration varies across stroke subjects (187-276PU), where a decrease in percent change is consistent in the stroke cohort. However, sham animals do not alter from their baseline, although it should be noted that sham animals had a lower blood concentration than stroke mice. Overall, LDI results suggest that blood flow and concentration can be used to measure different degrees of ischemia due to the range in selectivity. LDI permits recording all blood or red blood cell flow exclusively at a fixed location (Välisuo *et al.,* 2015). As a result, although the injection of rose Bengal may alter blood flow, it does not impact the red blood cell concentration. Comparison against stroke animals' longitudinal data suggests that sham animals do not have ischemia but may experience a change in vascular contraction with rose Bengal absorption into light-compromised epithelial cells (Efron *et al*., 2012).

The comparison between stroke-induced mice and sham animals validated the photothrombotic stroke model. The significant differences observed between the stroke and sham groups confirmed the specificity of the motor and sensory impairments to the stroke condition. This validation strengthens the reliability and relevance of our findings in knowing that the effects were not because of the Rose Bengal dye, the laser for stroke induction, or the longitudinally sustained anesthesia usage. One intriguing observation was that sham animals appeared different than a hypothetical naïve animal, as motor and sensory maps were non significantly altered in the sham-induced hemisphere, and the landing limb in the cylinder task and forelimb missteps in the grid walking task also showed trends toward impairments. Although channel rhodopsin (ChR2) is selective to blue light (470 nm; Klapoetke *et al.,* 2014; Lin, 2011), the long duration (13 minutes) and high intensity (22 mW) of green light exposure may result in mild damage to neurons at the sham site. In addition to increasing the number of sham mice used in this study, adding a naïve group would be essential in determining sham animal effects following photothrombotic stroke. Future experiments could explore the use of middle cerebral artery occlusion model, as it is widely used in translational pre-clinical research (Xie *et al.,* 2016).

One limitation is that stroke was performed under light isoflurane anesthesia. Although the standard for neuroscience research, isoflurane is a neuroprotective volatile vasodilator (Miura *et al.,* 1998; Sun *et al.,* 2015; Raub *et al.,* 2021; Sullender *et al.,* 2021) and may mask the effect of stroke through increasing cerebral blood flow (Sullender *et al.,* 2022). One way to avoid anesthesia during stroke induction is to use an awake and freely moving model, such as in Seto *et al.,* 2014. Future experiments could integrate awake stroke induction to gain more clinically relevant techniques. Additionally, due to repetitive mapping, stroke was performed in young adult male and female mice (approximately three months in age). In the clinical representations, females recover worse following a stroke (Kim *et al.,* 2010; Gargano & Reeves, 2007). While our study did not specifically investigate sex-related effects, it is crucial to note that male and female mice were thoughtfully included in both the sham and stroke groups, as detailed in Section 2.1. Furthermore, age is a major risk factor for stroke in clinical populations (Kelly-Hayes, 2010). Experiments utilized mice roughly three months old at the experimental

start. As a result, our results make inferences about spontaneous recovery in a healthy population, affecting the rate and potential recovery effects (Yoo *et al.,* 2020). Further investigations using LBMM may be necessary to explore age-specific recovery patterns.

5. Conclusion

5.1. Significance

Currently, there is an unclear understanding of stroke impairment and recovery timelines and how they relate to functional recovery. We aimed to clarify how stroke impacted cortical circuits directly at the stroke site through LBMM and neighbouring sensory regions through ISOI. Although we were not the first to combine sensory and motor mapping, we are the first to characterize them using longitudinal non-invasive stimulation paradigms in rodent models. Additionally, we utilized bilateral and bi-hemispheric cortex recordings and combined these findings with behavioural assessments for functional relevance.

LBMM identified motor impairment for three weeks post-stroke and spatial recovery plateauing at post-stroke week four. We demonstrated how connected sensory regions recovered faster and evoked responses similar to baseline, whereas motor cortices recovered slower and showed more widespread spatial reorganization. Using a novel experimental paradigm (LBMM), we reiterated the findings of other mapping researchers' results (such as ICMS) while providing insight into potential time points for recovery and its relationship to behaviour. Interestingly, although LBMM was bilateral at baseline, LBMM demonstrated different recovery effects for each forelimb following chronic period recovery. The impaired forelimb recovery did not recover to baseline in the ipsilesional hemisphere, but the nonimpaired forelimb did. When compared to behaviour, a battery of tasks indicated a spontaneous recovery in the impaired forelimb that was delayed relative to motor map recovery. Specifically, the grid walking task highlighted the complexity of sensorimotor coordination in which forelimb movement recovery occurred weeks after motor map recovery had plateaued as reported by LBMM. Overall, LBMM, ISOI, and the battery of sensorimotor tasks highlight the brain's capacity to undergo adaptive changes following focal ischemic events, which can affect neurorehabilitation strategies.

5.2. Limitations

5.2.1. Mesoscopic imaging

All in-vivo experiments were acquired with mesoscopic imaging for the duration of the experiment. LDI/LDF generated blood flow maps to visualize stroke impairments, and LBMM and ISOI generated spatial-temporal imaging for longitudinal motor and sensory cortices neural reorganization, respectively. As a result, imaging of live neuronal recordings was not acquired in this project's scope. Although an increasing body of scientific literature is utilizing techniques such as multiphoton to image peri-infarct reorganization, it would have been beneficial to image neurons in key regions such as ipsilesional tissue and contralesional CFA. Future directions could utilize multiphoton imaging to provide a comprehensive analysis of spontaneously occurring reorganization versus iTBS stimulation-promoted recovery as relayed by LBMM.

5.2.2. Evoked motor movements and cognitive representations

As briefly covered throughout the discussion section, some limitations remain for the project. Regarding LBMM, it remains unknown how the relationship that forelimb-evoked movements generated from motor mapping compares to normal conscious movements. Although forelimb-evoked movements are functionally relevant biomarkers in clinical studies for impairment and recovery trends, their relevancy remains unclear.

5.2.3. Longitudinal sensory and motor map assessment was not blindly performed

The investigation in longitudinal sensory and motor mapping are designed to permit non-invasive investigation of the cortex through a minimally invasive transparent window. Since LBMM is a neuroimaging tool, mapping execution of condition and time post-condition could not be blind to the investigator. ISOI provides blood flow imaging following forelimb stimulation, resulting in clearly defined regions of decreased blood flow in stroke cohorts. Furthermore, strokes can be seen with the naked eye as decreased blood flow, resulting in white tissue, through the transcranial window implanted on the skull for longitudinal investigation. As a result, mapping experiments were conducted with researchers knowing

which animals were stroke or sham and how long it had been since stroke induction due to pre-existing technique experiences.

5.2.4. LBMM individualized assessment

One of the key advantages of LBMM is the ability to assess individual mice longitudinally, as ICMS requires animal sacrifice, and clinical paradigms cannot focalize stimulation sites small enough for rodent models. Due to the large scope of the project, cohort analyses were conducted for all conditions and time points. Future work could be conducted to expand on individualized recovery trends for mapping and behavioural recordings.

5.2.5. Sham impairments

In addition to increasing the sham cohort population for statistical means, adding a naïve group would be essential as sham animals may be impaired following Thy1-ChR2-eYFP photothrombotic stroke. Although hypothetically, channel rhodopsin should not interact with the green stroke-inducing light; sham animals appear acutely impaired post-sham. This was determined through LDI blood flow decreases, less contralaterally post-sham for ISOI and LBMM, post-sham decreases in participation in the cylinder task, and minor impairments observed in the grid walking task. As a result, future studies are required to investigate further the relationship between channel rhodopsin mice and photothrombotic stroke.

5.2.6. Required anesthesia

Stroke induction and ISOI were performed under light isoflurane, and LBMM was performed under ketamine and xylazine. Although the standard for neuroscience research, these are limitations and have potentially significant impacts on the values obtained. Mice were anesthetized with isoflurane during stroke induction; however, isoflurane is a neuroprotective volatile vasodilator (Sun *et al.,* 2015; Raub *et al.,* 2021; Sullender *et al.,* 2021) and may mask the effect of potential paradigms (Seto *et al.,* 2014). Additionally, Isoflurane may have chronic effects on behaviour (Hohlbaum *et al.,* 2017), impacting the results found in this study. However, the usage of sham animals suggests that behaviour is not altered by chronic isoflurane or ketamine xylazine. As for motor mapping, all motor mapping experiments in

rodents use ketamine-xylazine combinations to assess the state of the cortex. As a result, we performed all motor mapping tasks as such. Although strict protocols were in place to ensure similar motor map anesthetic planes across animals, it should be noted that this work was not blinded, as results were analyzed in real time. Future work is investigating the use of LBMM with automatic ketamine top-ups. Finally, mice underwent LBMM weekly, where due to the repetitive exposure to ketamine and xylazine, mice reacted to anesthesia differently from baseline versus experimental endpoints. As a result, criteria were set to ensure that mice were stable before motor mapping, which increased experimental duration.

5.2.7. Transcranial windows

Because LBMM and ISOI require access to the dorsal cortex for imaging, mice require a head-fixing mount and transcranial window to undergo mapping experiments. Although current experimental protocols are substantially less invasive than traditional experiments, where craniotomy or thinning of the skull would be required, mice still require skin removal and window and head-fixing placement. These minimal effects may affect mice in ways yet to be quantified. Additionally, transcranial windows were manually aligned against Bregma. Positioning was ideally placed completely flat and filled with dental cement. Occasionally, window quality fluctuated as windows were not correctly aligned against Bregma or became slightly opaque across the experimental timeline due to animals picking at the transcranial window. As a result, some degree of variability in aligning data for averaging is present due to transcranial window placement or sealing.

5.2.8. Lesion localization

On average, lesion localization was consistent. However, slight alterations occur across individuals. This occurs as mice are head-fixed, stereotaxically aligned to bregma, and then manually adjusted to the stroke induction site. Therefore, slight differences in Bregma's position and human error in alignment cause small location changes. For this reason, Bregma was defined as the curvature point of frontal bones at the midline to reduce variability. Quantification occurred traditionally, manually scoring the lesion and aligning against Allen Mouse Brain Atlas. Future protocols could utilize semi-automation processes to score lesions by

contrast comparison against a registered Atlas. This would permit structural or functional comparisons concerning motor or sensory map longitudinal alterations.

5.2.9. Stroke and age

Overall, one of the strongest risk factors for stroke is age and occurs in both male and female populations (Appelros *et al.,* 2002). In this study, we utilized male and female mice approximately three months old. The rationale is the rapid ability of young adult mice to recover following stroke induction permits for investigation of spontaneous recovery models. Additionally, almost no mice died from stroke induction or across the 10-week experimental timeline. As a result, displayed results make inferences about spontaneous recovery in a healthy population, which may not be as prevalent in clinical studies.

The photothrombotic stroke model is a tightly localized stroke induction model, which enables the induction of stroke at a specific and reliable location. This is key, as we aimed to determine how the cortex responds in group investigations. Although there is some degree of variability, this is a relatively stable and controlled stroke induction method. However, this model is known to have a small amount of penumbral tissue, resulting in a minimal chance of recovering stroke tissue immediately following induction (Carmichael, 2005; Clark *et al.,* 2019). It would prove beneficial to perform LBMM on mice which have undergone different stroke induction types, such as middle cerebral artery occlusion, to provide different stroke model representations for impairment and recovery.

6. Supplemental Figures and Data

Appendix A: Laser Doppler Imaging

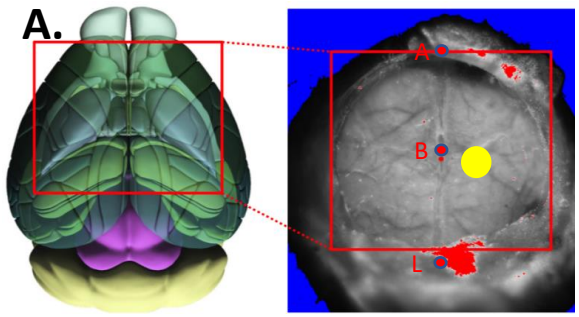

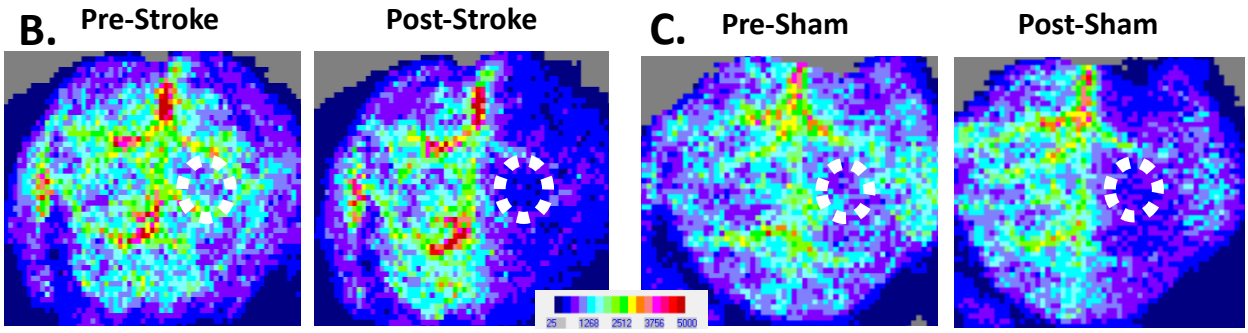

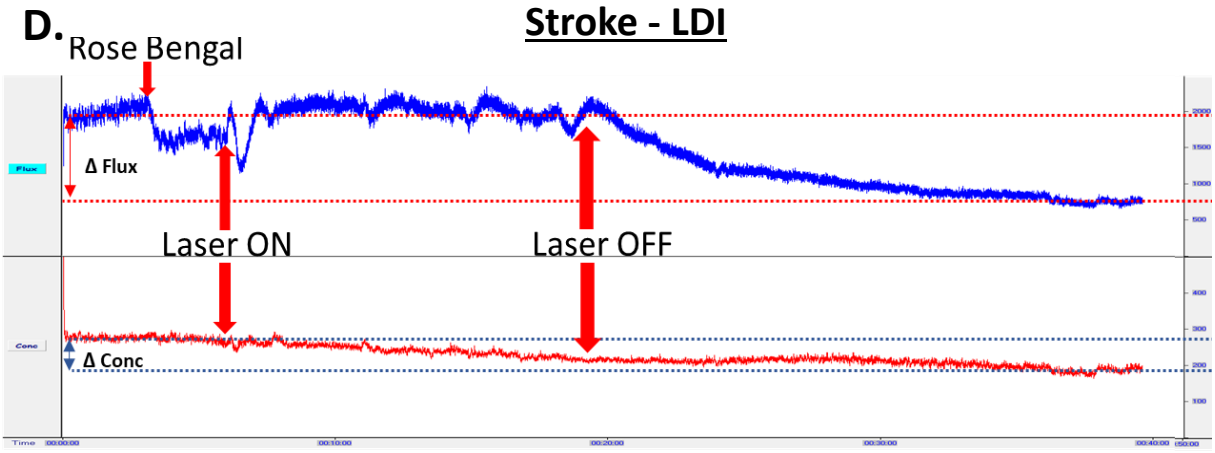

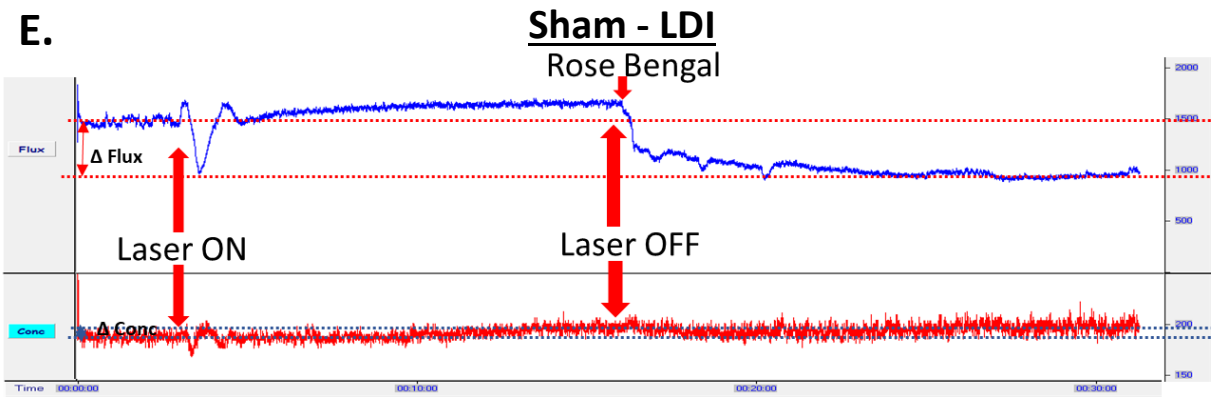

Supplemental Figure 1. Laser Doppler Imaging representations. Figure displays the laser Doppler imaging (LDI) recordings for blood flow changes in the dorsal cortex post-condition. Animals were anesthetized with isoflurane (1.5% in a 0.3 L/min oxygen flow rate). **A.** Reference of the cortex analyzed by LDI visible through the transcranial window. Labels include: Bregma (B), Lambda (L), anterior sinus (A), and the laser site (yellow, ML: 1.5 mm, AP: -0.5 mm). **B/C.** LDI scans illustrate blood flow visualization. Scale depicted in flux perfusion units (PU). Pre- and post-condition scans were taken one hour apart. The white dashed circle represents the laser induction site (1.1 mm laser diameter, 22 mW). **D/E.** LDI recordings at the stroke site. The top trace (blue) showed blood flux, while the bottom trace (red) displayed blood concentration.

Appendix B: Light-Based Motor Mapping

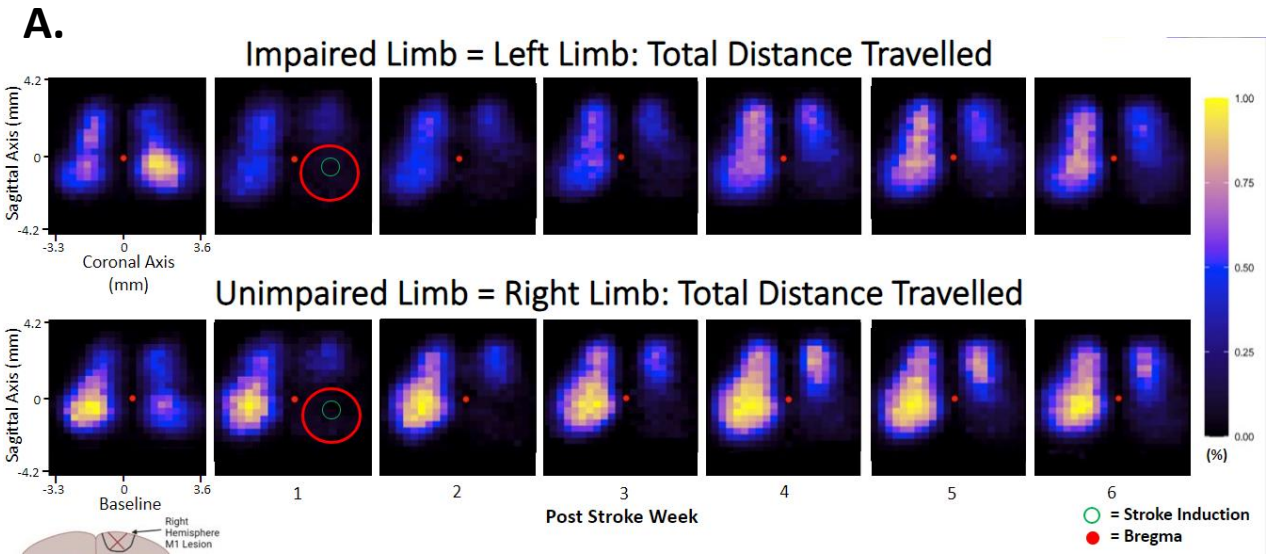

Supplemental Figure 2. Total distance forelimb motor maps. Adult Thy1-ChR2-eYFP mice (n=21) were anesthetized with 40 mg/kg ketamine and 2 mg/kg xylazine. Sites were stimulated with a 50 µm laser at each grid point, spaced 300 µm apart. Movement onset must have started within 10-60 ms following stimulation. Forelimb movement was quantified for the total distance travelled per stimulation site for both forelimbs independently. The movement was recorded using a high-frame-rate camera and analyzed through MATLAB. Distance travelled was averaged across repetitions per stimulus site, normalized per session, averaged then normalized per timepoint. The stroke site is labelled in green on post-stroke week one in green.

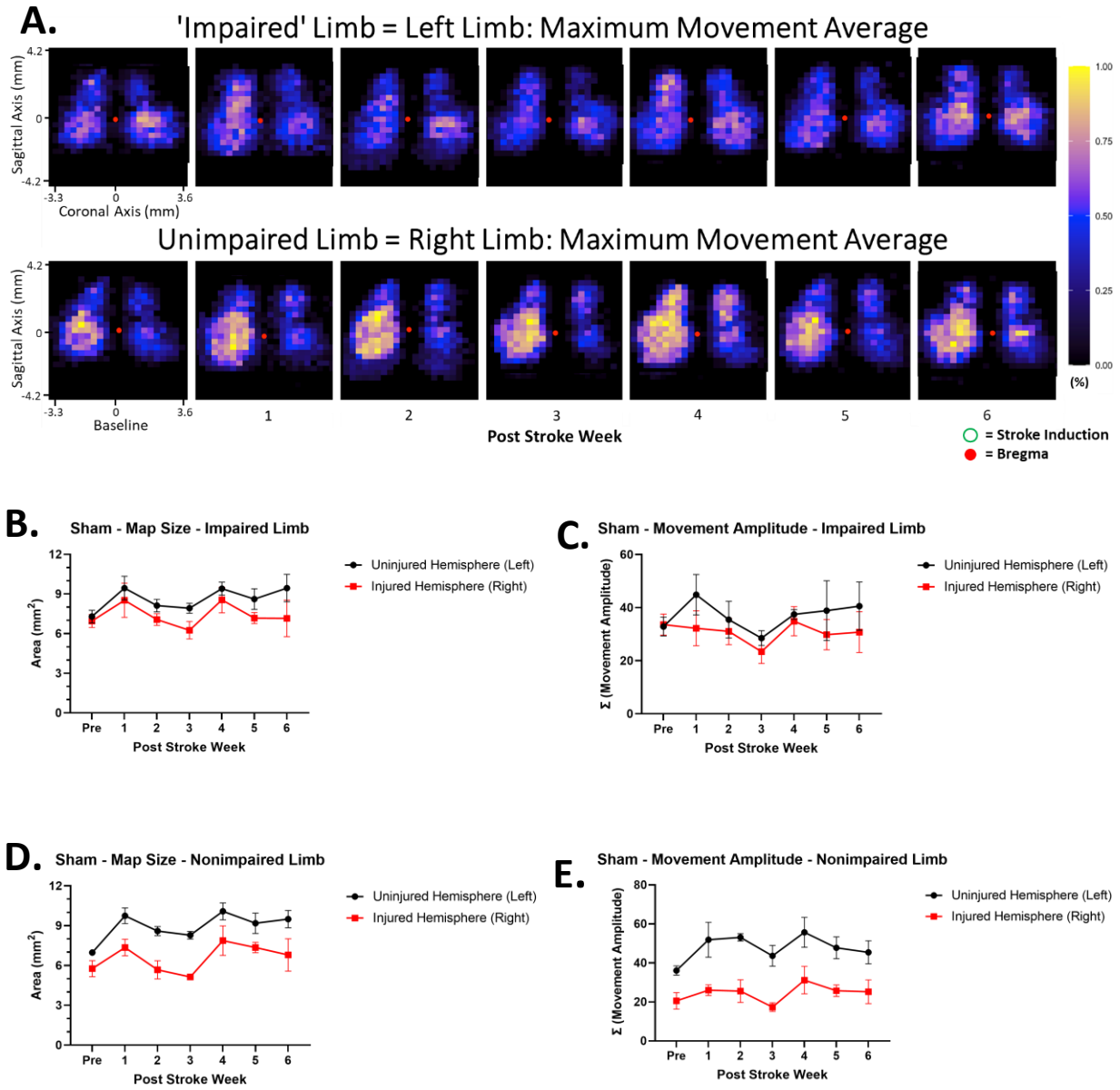

Supplemental Figure 3. Sham group Light-Based Motor Mapping of forelimbs. Adult Thy1-ChR2-eYFP mice (n=4) were anesthetized with 40 mg/kg ketamine and 2 mg/kg xylazine. **A.** Motor sites were stimulated with a 50 µm laser at each grid point with a spacing of 300 µm (red). Bregma is indicated in yellow. **B.** Forelimb-evoked movement was quantified to determine the maximum movement per stimulation site. Forelimb movements were recorded using a high-frame-rate camera and analyzed through MATLAB to obtain averaged evoked responses per stimulation site. **C.** Motor maps were normalized to the maximum response per session, averaged per timepoint, and normalized per timepoint. Bregma was indicated as a red dot. The photothrombotic stroke site (ML: 1.5 mm; AP: -0.5 mm) was labelled in green at post-stroke week one. **D-G.** Data was summed per hemisphere and presented as mean ± SEM. **D.** Hemisphere-summed movement amplitude for the impaired forelimb. **E.** Hemisphere-summed movement amplitude for the nonimpaired forelimb. **F.** Hemisphere-summed map size for the impaired forelimb. **G.** Hemisphere-summed map size for the nonimpaired forelimb. Statistical analysis was performed using repeated measures two-way ANOVA with Greenhouse-Geisser correction and Tukey's multiple comparisons tests. * indicated significance per the labelled time point.

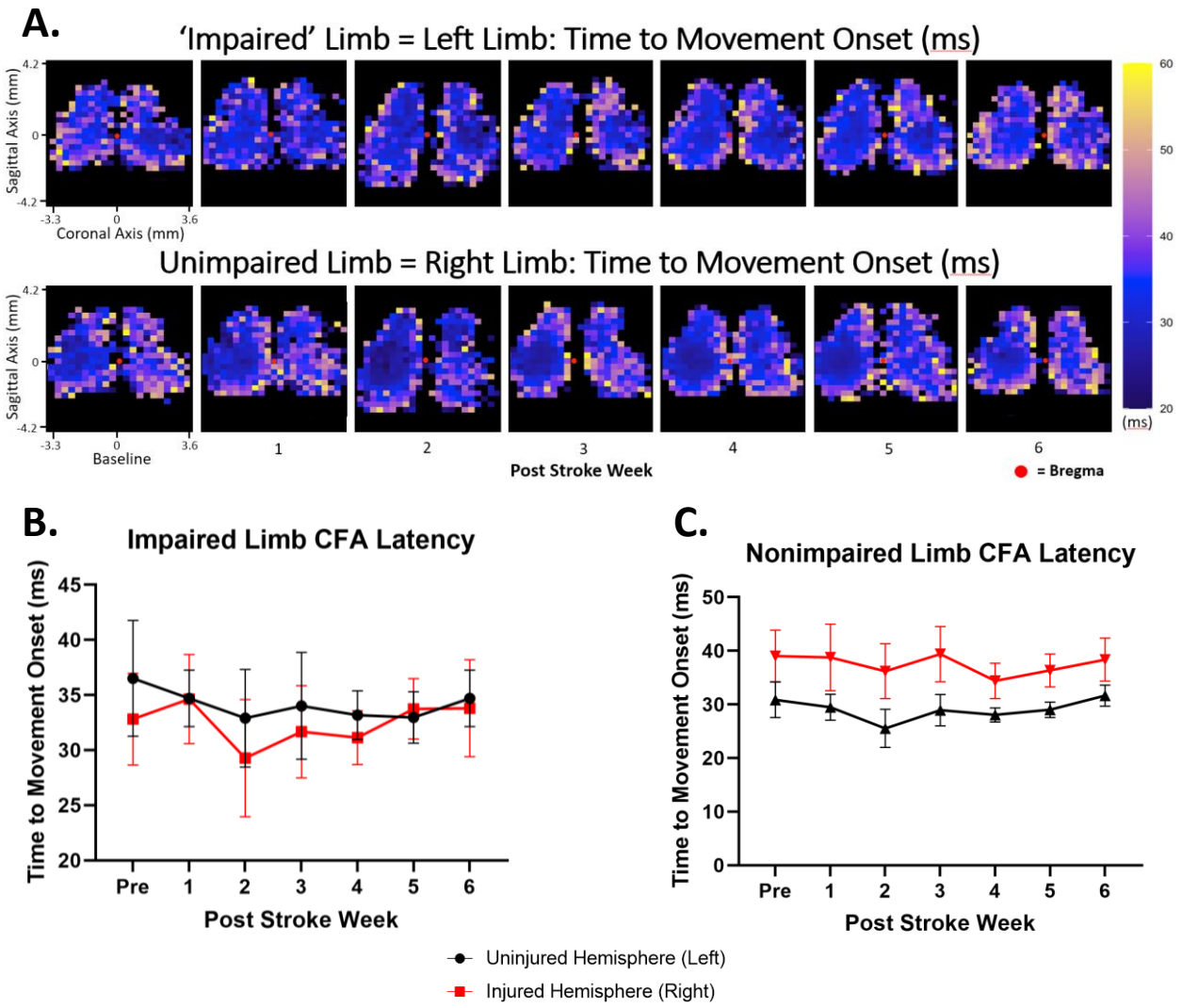

Supplemental Figure 4. Averaged latency for motor maps following sham procedure. Data presents the averaged latency for motor maps following the sham procedure in adult mice (n=4). The average time to movement onset was calculated, and exclusion criteria were applied, requiring movement to be continuous for 5 frames within 10-60ms post-stimulation. **A.** Bregma is indicated as a red dot for reference. The data was sampled across repetitions (2) and averaged across the cohort for each timepoint. The sham procedure was induced at ML: 1.5 mm and AP: -0.5 mm relative to the bregma. **B.** Impaired limb time to movement onset for the caudal forelimb area (CFA). The interior half of all CFA was included for data. **C.** Nonimpaired limb time to movement onset for the caudal forelimb area (CFA). The interior half of all CFA was included for data. Data are depicted as SEM. Statistical analysis was conducted through a mixed-model two-way ANOVA with Greenhouse-Geisser correction and Tukey's multiple comparisons tests.

Left Forelimb Sensory and Motor Maps

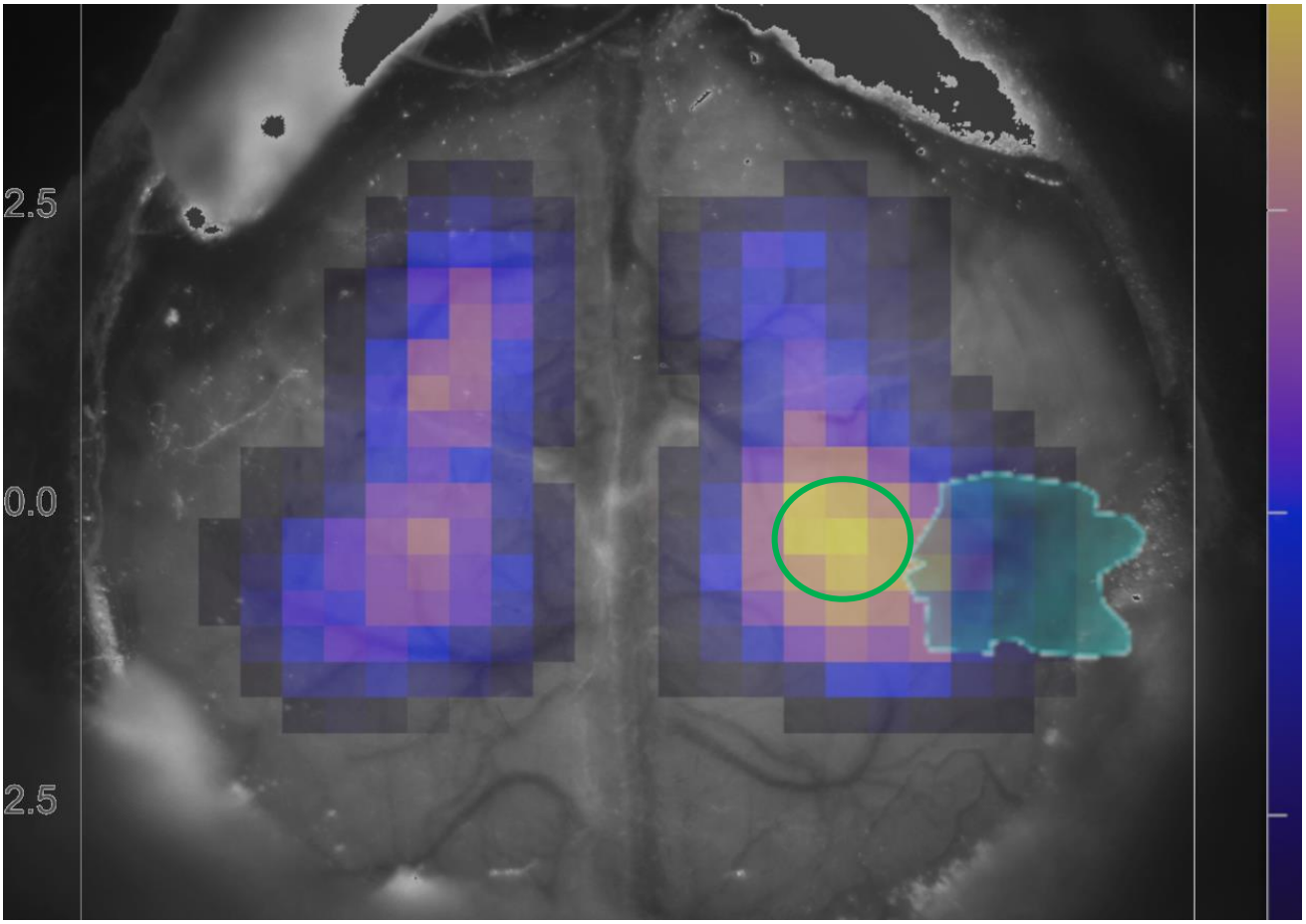

Supplemental Figure 5. Averaged baseline widefield macroscope image with motor and sensory maps. A widefield macroscope image was acquired using green light (520 nm) as the background. The image meshed with the cohort average (n=21) left forelimb maximum amplitude motor map illustrated using a normalized scale on the right-hand side. The group average (n=17, three averaged sessions) sensory map of the left forelimb was shown in teal. The green circle indicates the hypothetical site of stroke induction. This comprehensive figure allowed for simultaneous visualization of the motor and sensory responses in the left forelimb. A scale bar is depicted on the left-hand in centimeters.

Appendix C: Intrinsic Signal Optical Imaging

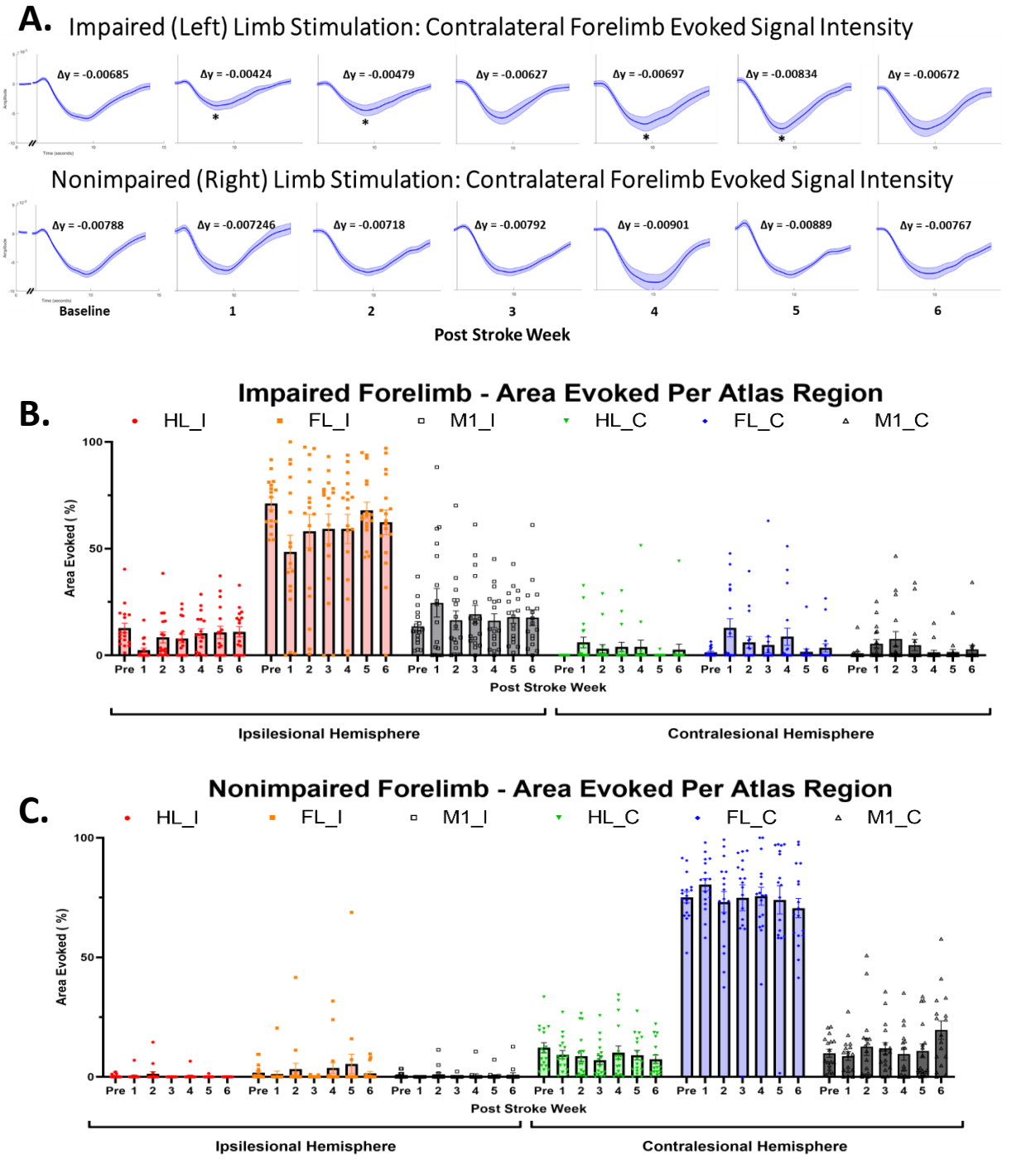

Supplemental Figure 6. Intrinsic Signal Optical Imaging alternative representation. A. Sensory evoked response in the atlas-defined contralateral area displayed per forelimb. Top: Impaired forelimb; Bottom: Nonimpaired forelimb. The change in amplitude (Δy) was manually calculated as the change from peak to trough. The vertical line displays the vibrotactile stimulus. Significant recovery between post-stroke weeks one-two against four-five was observed for the impaired limb. **B/C.** Evoked area as percentage of the total atlas area above threshold following stimulation. The threshold was 55% ± 15%. **B.** Impaired forelimb area per atlas region. **C.** Nonimpaired forelimb area evoked per atlas region.

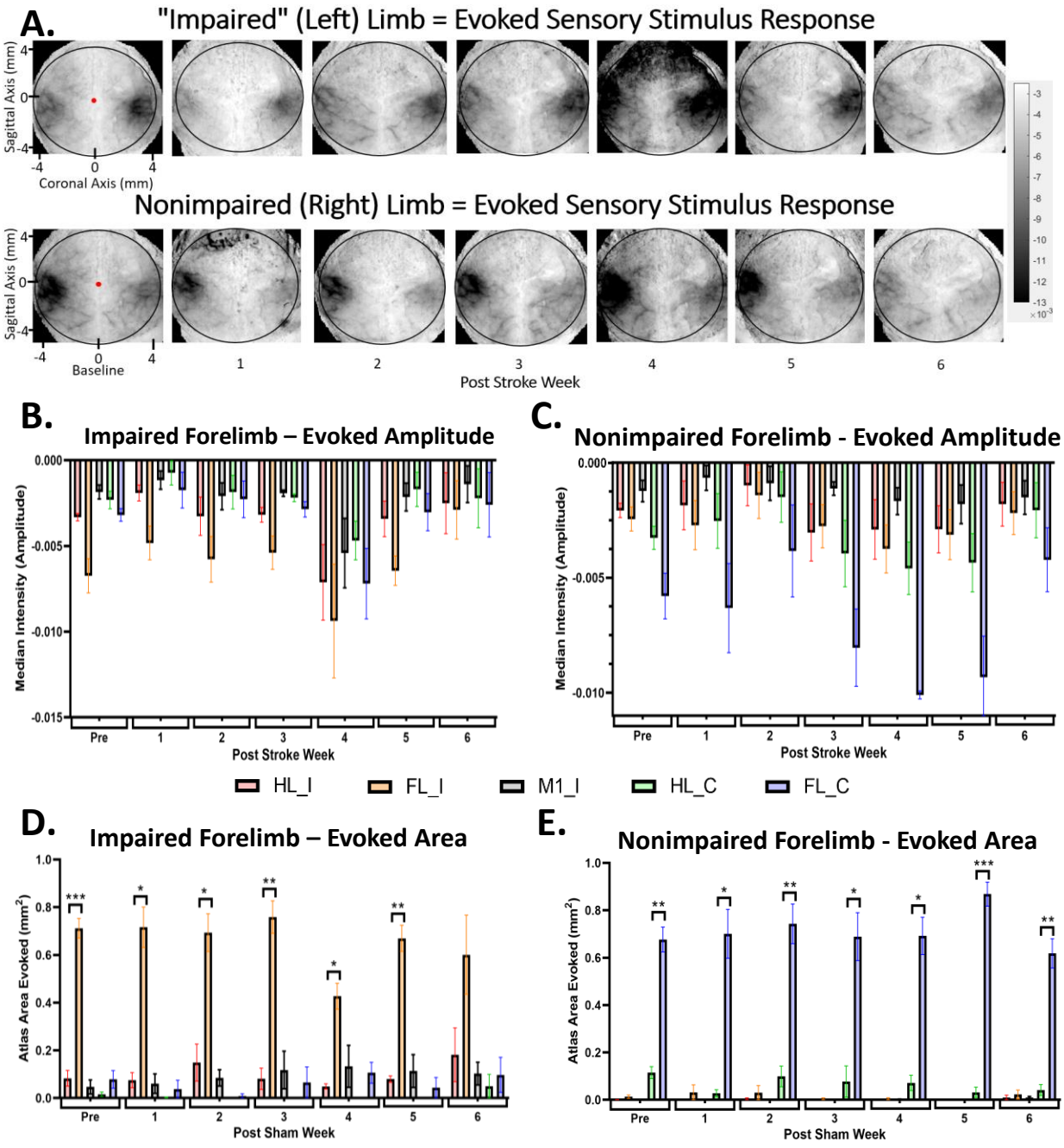

Supplemental Figure 7. Intrinsic Signal Optical Imaging following motor cortex photothrombotic sham. Evoked blood flow following sensory stimulation. The analysis frame was automatically generated as the maximum signal amplitude change relative to baseline. Images were aligned to Bregma (red label), stretched to overlap, and averaged across the sham group (n=4). Sham was induced at ML: 1.5 mm, AP: -0.5 mm relative to bregma. **A.** Impaired forelimb (top) and nonimpaired forelimb (bottom). The average window location was represented as a black outline. **B-E**. Atlas-defined regions of interest were displayed for each forelimb as a predetermined mask per individual animal transcranial window. Impaired forelimb (left side), nonimpaired forelimb (right side). **B/C**. Maximum signal amplitude relative to the baseline. Data is depicted as median amplitude ± SEM. **D/E**. The threshold area evoked is displayed per atlas region. Threshold was set to 55% ± 15% of the maximum amplitude per session average. Displayed as mean area evoked ± SEM. Statistical analysis was conducted through repeated measures two-way ANOVA with Greenhouse-Geisser correction and Tukey's multiple comparisons tests. Significance is indicated as follows: (*) $p < 0.05$, (*) $p < 0.01$, (***) $p < 0.001$, (****) $p < 0.0001$.

Appendix D: Behaviour

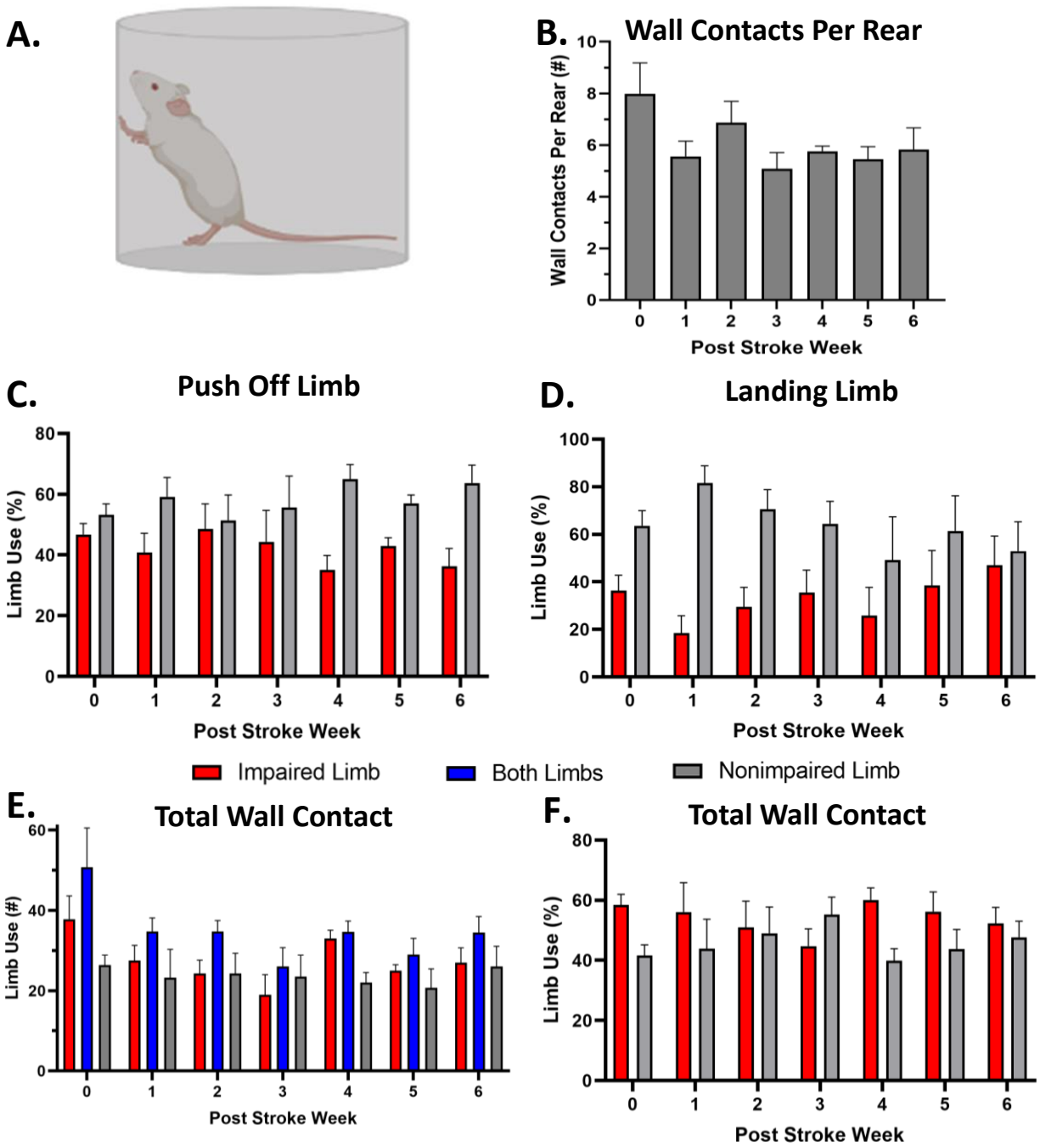

Supplemental Figure 8. Cylinder task forelimb usage post-sham. Adult mice (n=4) were analyzed for three baselines followed by weekly sessions post-sham. Each session was a minimum of 10 rears, with a maximum of 25 rears analyzed. **A.** Graphic representation of the cylinder task. **B.** The average number of wall contacts per rear. **C.** Percentage of each forelimb last in contact with the ground at the start of a rear. **D.** Percentage of each forelimb first in the contact with the ground when landing from a rear. **E.** Total number of wall contacts per individual and combined forelimb-wall contacts. F. The total wall contacts displayed as a relative left-right forelimb usage. All data was depicted as mean ± SEM. Statistical analysis was conducted through a repeated measures two-way ANOVA with Greenhouse-Geisser correction and Tukey's multiple comparisons tests. * indicated significance per labelled timepoint. # indicated significance relative to baseline.

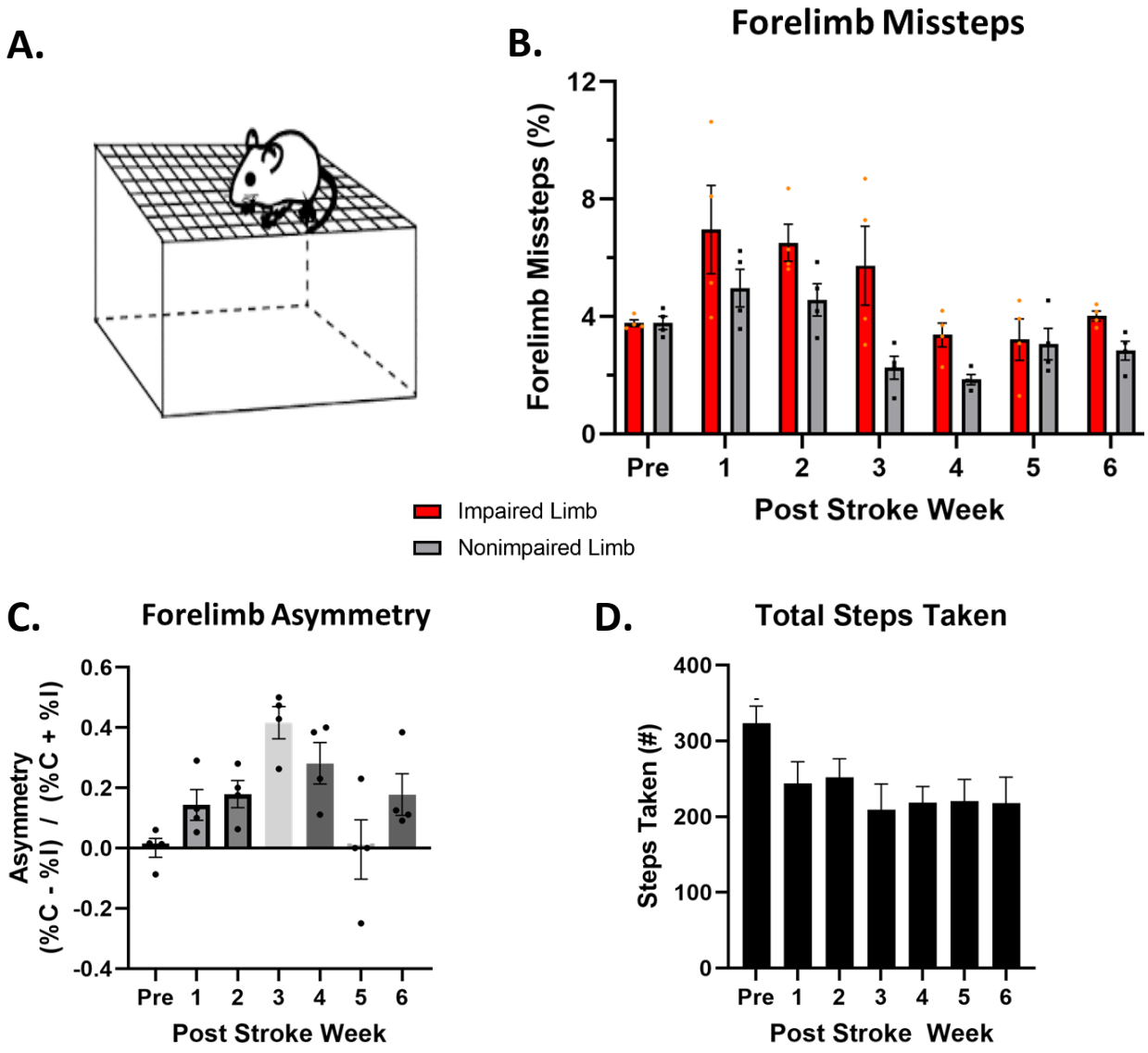

Supplemental Figure 9. Grid walking task forelimb analysis post-sham. Adult mice (n=4) were placed on a thin mess wire for five minutes and recorded for forelimb missteps. Three baseline sessions were averaged, followed by one post-stroke session per week. A minimum of 75 steps was required. **A.** Graphic representation of the grid walk task. **B.** The number of forelimb missteps over the total session steps taken. Missteps were included if the wrist went past the wire mesh. Steps were counted if the forelimb moved at least one mesh square in distance (1.0 cm). **C.** Forelimb asymmetry was the difference in forelimb missteps as a percentage divided by the summed forelimb percent missteps as a percentage. **D.** The total number of steps taken was manually counted using the impaired forelimb post-stroke. All data are depicted as mean ± SEM. Statistical analysis was conducted through repeated measures two-way ANOVA with Greenhouse-Geisser correction and Tukey's multiple comparisons tests. Significance is indicated as follows: * denotes significance per labelled timepoint, and # denotes significance within the forelimb relative to baseline.

Bibliography

AbuHasan Q, Munakomi S. Neuroanatomy, Pyramidal Tract. [Updated 2022 Jul 4]. In: StatPearls [Internet]. Treasure Island (FL): StatPearls Publishing; 2023 Jan-. Available from: https://www.ncbi.nlm.nih.gov/books/NBK545314/

Adkins, D., Campos, P., Quach, Borromeo, M., Schallert, K., Jones T.A., Epidural cortical stimulation enhances motor function after sensorimotor cortical infarcts in rats, *Experimental Neurology.* **200**(2), 356-370, (2006). ISSN 0014-4886, https://doi.org/10.1016/j.expneurol.2006.02.131.

Aghamiri, S. H., Mansouri, B., Mehrpour, M., Karani, S. M. H., Ghaffari, M., Lima, B. S., & Komlakh, K. (2022). Efficacy of mechanical thrombectomy in stroke patients with large vessel involvement. *European journal of translational myology*, *32*(2), 10456. https://doi.org/10.4081/ejtm.2022.10456

Alawieh, A., Zhao, J., & Feng, W. Factors affecting post-stroke motor recovery: Implications on neurotherapy after brain injury. *Behavioural brain research*, *340*, 94–101, (2018). https://doi.org/10.1016/j.bbr.2016.08.029

Allred, R. P., & Jones, T. A. (2008). Maladaptive effects of learning with the less-affected forelimb after focal cortical infarcts in rats. *Experimental neurology*, *210*(1), 172–181. https://doi.org/10.1016/j.expneurol.2007.10.010

Alyahyay Mansour, Kalweit Gabriel, Kalweit Maria, Karvat Golan, Ammer Julian, Schneider Artur, Adzemovic Ahmed, Vlachos Andreas, Boedecker Joschka, Diester Ilka. Mechanisms of Premotor-Motor Cortex Interactions during Goal Directed Behavior. bioRxiv 2023.01.20.524944; doi: https://doi.org/10.1101/2023.01.20.524944

Appelros P, Nydevik I, Seiger A, Terént A. Predictors of Severe Stroke. Influence of Preexisting Dementia and Cardiac Disorders. *Stroke.* 2002; 33:2357–2362. https://doi.org/10.1161/01.STR.0000030318.99727.FA

Arenkiel BR, Peca J, Davison IG, Feliciano C, Deisseroth K, Augustine GJ, Ehlers MD, Feng G. In vivo light-induced activation of neural circuitry in transgenic mice expressing channelrhodopsin-2. *Neuron*. **54**(2), 205-18, (2007). doi: 10.1016/j.neuron.2007.03.005. PMID: 17442243; PMCID: PMC3634585.

Asanuma H., Sakata H., Functional Organization of a Cortical Efferent System Examined with Focal Depth Stimulation in Cats, *Journal of Neurophysiology*, **30**(1), 35-54 (1967). https://doi.org/10.1152/jn.1967.30.1.35

Asanuma H., Ward J.E., Patterns of contraction of distal forelimb muscles produced by intracortical stimulation in cats, *Brain Research*, **27**(1), Pages 97-109, (1971), ISSN 0006-8993. https://doi.org/10.1016/0006-8993(71)90374-X.

Assaf, Y., Bouznach, A., Zomet, O., Marom, A., & Yovel, Y. (2020). Conservation of brain connectivity and wiring across the mammalian class. *Nature neuroscience*, *23*(7), 805–808. https://doi.org/10.1038/s41593-020-0641-7

Ayling, O., Harrison, T., Boyd, J. *et al.* Automated light-based mapping of motor cortex by photoactivation of channelrhodopsin-2 transgenic mice. *Nat Methods* **6,** 219–224 (2009). https://doi.org/10.1038/nmeth.1303

Bajwa, NM, Lee, JB, Halavi, S, Hartman, RE, Obenaus, A. Repeated isoflurane in adult male mice leads to acute and persistent motor decrements with long-term modifications in corpus callosum microstructural integrity. J Neuro Res. 2019; 97: 332–345. https://doi.org/10.1002/jnr.24343

Baker A, Kalmbach B, Morishima M, Kim J, Juavinett A, Li N, Dembrow N. Specialized Subpopulations of Deep-Layer Pyramidal Neurons in the Neocortex: Bridging Cellular Properties to Functional Consequences. J Neurosci. 2018 Jun 13;38(24):5441-5455. doi: 10.1523/JNEUROSCI.0150-18.2018. Epub 2018 May 21. PMID: 29798890; PMCID: PMC6001033.

Bakken, T.E., Jorstad, N.L., Hu, Q. *et al.* Comparative cellular analysis of motor cortex in human, marmoset and mouse. *Nature* **598**, 111–119 (2021). https://doi.org/10.1038/s41586-021-03465-8

Baldwin, M. K., Cooke, D. F., & Krubitzer, L. (2017). Intracortical Microstimulation Maps of Motor, Somatosensory, and Posterior Parietal Cortex in Tree Shrews (Tupaia belangeri) Reveal Complex Movement Representations. *Cerebral cortex (New York, N.Y. : 1991)*, *27*(2), 1439–1456. https://doi.org/10.1093/cercor/bhv329

Ballester Belén Rubio, Maier Martina, Duff Armin, Cameirão Mónica, Bermúdez Sergi, Duarte Esther,

Cuxart Ampar, Rodríguez Susana, Rosa María San Segundo Mozo, and Verschure Paul F. M. J. A critical time window for recovery extends beyond one-year post-stroke. Journal of Neurophysiology 2019 122:1, 350-357. https://doi.org/10.1152/jn.00762.2018

Barber PA, Davis SM, Infeld B, Baird AE, Donnan GA, Jolley D, Lichtenstein M. Spontaneous reperfusion after ischemic stroke is associated with improved outcome. Stroke. 1998 Dec;29(12):2522-8. doi: 10.1161/01.str.29.12.2522. PMID: 9836763.

Basil B, Mahmud J, Mathews M, Rodriguez C, Adetunji B. Is there evidence for effectiveness of transcranial magnetic stimulation in the treatment of psychiatric disorders? *Psychiatry (Edgmont)*. **2**(11):64-69, (2005). https://www.ncbi.nlm.nih.gov/pmc/articles/PMC2993526/

Bauer AQ, Kraft AW, Wright PW, Snyder AZ, Lee JM, Culver JP. Optical imaging of disrupted functional connectivity following ischemic stroke in mice. Neuroimage. 2014 Oct 1;99:388-401. doi: 10.1016/j.neuroimage.2014.05.051. Epub 2014 May 24. PMID: 24862071; PMCID: PMC4332714.

Bernheisel CR, Schlaudecker JD, Leopold K. Subacute management of ischemic stroke. Am Fam Physician. 2011 Dec 15;84(12):1383-8. PMID: 22230273.

Bice RA, Xiao Q, Kong J, Yan P, Rosenthal ZP, Kraft AW, Smith KP, Wieloch T, Lee JM, Culver JP, Bauer AQ. (2022) Homotopic contralesional excitation suppresses spontaneous circuit repair and global network reconnections following ischemic stroke eLife 11:e68852.

Biernaskie, J., Chernenko, G., & Corbett, D. (2004). Efficacy of rehabilitative experience declines with time after focal ischemic brain injury. *The Journal of neuroscience : the official journal of the Society for Neuroscience*, *24*(5), 1245–1254. https://doi.org/10.1523/JNEUROSCI.3834-03.2004

Blackwell AA, Banovetz MT, Qandeel, Whishaw IQ, Wallace DG. The structure of arm and hand movements in a spontaneous and food rewarded on-line string-pulling task by the mouse. Behav Brain Res. 2018 Jun 1;345:49-58. doi: 10.1016/j.bbr.2018.02.025. Epub 2018 Feb 21. PMID: 29474809.

Blackwell, A. A., Schell, B. D., Osterlund Oltmanns, J. R., Whishaw, I. Q., Ton, S. T., Adamczyk, N. S., Kartje, G. L., Britten, R. A., & Wallace, D. G. (2021). Skilled movement and posture deficits in rat string-pulling behavior following low dose space radiation (^{28}Si) exposure. *Behavioural brain research*, *400*, 113010. https://doi.org/10.1016/j.bbr.2020.113010

Blumberger, D. M., Vila-Rodriguez, F., Thorpe, K. E., Feffer, K., Noda, Y., Giacobbe, P., Knyahnytska, Y., Kennedy, S. H., Lam, R. W., Daskalakis, Z. J., & Downar, J. (2018). Effectiveness of theta burst versus high-frequency repetitive transcranial magnetic stimulation in patients with depression (THREE-D): a randomised non-inferiority trial. *Lancet (London, England)*, *391*(10131), 1683–1692. https://doi.org/10.1016/S0140-6736(18)30295-2

Boychuk, J. A., Adkins, D. L., & Kleim, J. A. Distributed versus focal cortical stimulation to enhance motor function and motor map plasticity in a rodent model of ischemia. *Neurorehabilitation and neural repair*, ***25***(1), 88–97, (2011). https://doi.org/10.1177/1545968310385126

Boychuk JA, Schwerin SC, Thomas N, Roger A, Silvera G, Liverpool M, Adkins DL, Kleim JA. Enhanced Motor Recovery After Stroke With Combined Cortical Stimulation and Rehabilitative Training Is Dependent on Infarct Location. Neurorehabil Neural Repair. 2016 Feb;30(2):173-81. doi: 10.1177/1545968315624979. Epub 2015 Dec 29. PMID: 26719353; PMCID: PMC5800516.

Boyd, L. A., Hayward, K. S., Ward, N. S., Stinear, C. M., Rosso, C., Fisher, R. J., Carter, A. R., Leff, A. P., Copland, D. A., Carey, L. M., Cohen, L. G., Basso, D. M., Maguire, J. M., & Cramer, S. C. (2017). Biomarkers of stroke recovery: Consensus-based core recommendations from the Stroke Recovery and Rehabilitation Roundtable. *International journal of stroke : official journal of the International Stroke Society*, *12*(5), 480–493. https://doi.org/10.1177/1747493017714176

Broughton BR, Reutens DC, Sobey CG. Apoptotic mechanisms after cerebral ischemia. Stroke. 2009 May;40(5):e331-9. doi: 10.1161/STROKEAHA.108.531632. Epub 2009 Jan 29. PMID: 19182083.

Brown CE, Aminoltejari K, Erb H, Winship IR, Murphy TH. In vivo voltage-sensitive dye imaging in adult mice reveals that somatosensory maps lost to stroke are replaced over weeks by new structural and functional circuits with prolonged modes of activation within both the peri-infarct zone and distant sites. J Neurosci. 2009 Feb 11;29(6):1719-34. doi: 10.1523/JNEUROSCI.4249-08.2009. PMID: 19211879; PMCID: PMC6666293.

Brown AR & Martinez M. Ipsilesional Motor Cortex Plasticity Participates in Spontaneous Hindlimb Recovery after Lateral Hemisection of the Thoracic Spinal Cord in the Rat. (2018). Journal of Neuroscience*. 38 (46) 9977-9988; DOI: https://doi.org/10.1523/JNEUROSCI.1062-18.2018*

Brown, A. R., Mitra, S., Teskey, G. C., & Boychuk, J. A. (2023). Complex forelimb movements and cortical topography evoked by intracortical microstimulation in male and female mice. *Cerebral cortex (New York, N.Y. : 1991)*, *33*(5), 1866–1875. https://doi.org/10.1093/cercor/bhac178

Brown, A. R., & Teskey, G. C. Motor cortex is functionally organized as a set of spatially distinct representations for complex movements. *The Journal of neuroscience: the official journal of the Society for Neuroscience*, **34**(41), 13574–13585, (2014). https://doi.org/10.1523/JNEUROSCI.2500-14.2014

Buetefisch CM. Role of the Contralesional Hemisphere in Post-Stroke Recovery of Upper Extremity Motor Function. *Front Neurol*. **16**(6), 214, (2015). doi: 10.3389/fneur.2015.00214. PMID: 26528236; PMCID: PMC4607877.

Buetefisch CM, Haut MW, Revill KP, Shaeffer S, Edwards L, Barany DA, Belagaje SR, Nahab F, Shenvi N, Easley K. Stroke Lesion Volume and Injury to Motor Cortex Output Determines Extent of Contralesional Motor Cortex Reorganization. Neurorehabil Neural Repair. 2023 Feb-Mar;37(2-3):119-130. doi: 10.1177/15459683231152816. Epub 2023 Feb 14. PMID: 36786394; PMCID: PMC10079613.

Bütefisch, C. M., Netz, J., Wessling, M., Seitz, R. J., & Hömberg, V. (2003). Remote changes in cortical excitability after stroke. *Brain : a journal of neurology*, *126*(Pt 2), 470–481. https://doi.org/10.1093/brain/awg044

Bütefisch, C. M., Wessling, M., Netz, J., Seitz, R. J., & Hömberg, V. (2008). Relationship between interhemispheric inhibition and motor cortex excitability in subacute stroke patients. *Neurorehabilitation and neural repair*, *22*(1), 4–21. https://doi.org/10.1177/1545968307301769

Bundy, D. T., & Leuthardt, E. C. (2019). The Cortical Physiology of Ipsilateral Limb Movements. Trends in neurosciences, 42(11), 825–839. https://doi.org/10.1016/j.tins.2019.08.008

Carlson C., Devinsky O., The excitable cerebral cortex: Fritsch G, Hitzig E. Über die elektrische Erregbarkeit des Grosshirns. Arch Anat Physiol Wissen 1870;37:300–32., *Epilepsy & Behavior.* **15**(2), 131-132 (2009), ISSN 1525-5050. https://doi.org/10.1016/j.yebeh.2009.03.002.

Carmichael S. T. Brain excitability in stroke: the yin and yang of stroke progression. *Archives of neurology*, (2012). *69*(2), 161–167. https://doi.org/10.1001/archneurol.2011.1175

Carmichael, S. T. Plasticity of cortical projections after stroke. Neuroscientist, 2003;9(1), 64-75.

Carmichael, S.T. Rodent models of focal stroke: Size, mechanism, and purpose. Neurotherapeutics 2, 396–409 (2005). https://doi.org/10.1602/neurorx.2.3.396

Carolee J. Winstein, PhD, *et al*., A Guideline for Healthcare Professionals From the American Heart Association/American Stroke Association. 47(6), 98-160, (2016). https://doi.org/10.1161/STR.0000000000000098

Carson, R. G., & Kennedy, N. C. (2013). Modulation of human corticospinal excitability by paired associative stimulation. *Frontiers in human neuroscience*, *7*, 823. https://doi.org/10.3389/fnhum.2013.00823

Cassidy JM, Cramer SC. Spontaneous and Therapeutic-Induced Mechanisms of Functional Recovery After Stroke. Transl Stroke Res. 2017 Feb;8(1):33-46. doi: 10.1007/s12975-016-0467-5. Epub 2016 Apr 25. PMID: 27109642; PMCID: PMC5079852.

Castel-Lacanal, E., Marque, P., Tardy, J., de Boissezon, X., Guiraud, V., Chollet, F., Loubinoux, I., & Moreau, M. S. (2009). Induction of cortical plastic changes in wrist muscles by paired associative stimulation in the recovery phase of stroke patients. *Neurorehabilitation and neural repair*, *23*(4), 366–372. https://doi.org/10.1177/1545968308322841

Chail, A., Saini, R. K., Bhat, P. S., Srivastava, K., & Chauhan, V. Transcranial magnetic stimulation: A review of its evolution and current applications. *Industrial psychiatry journal*, **27**(2), 172–180 (2018). https://doi.org/10.4103/ipj.ipj_88_18

Chen Huanwen, Jindal Gaurav, Miller Timothy, Gandhi Dheeraj, and Chaturvedi Seemant. Stroke Thrombectomy in the Elderly: Efficacy, Safety, and Special Considerations. *Stroke: Vascular and Interventional Neurology*. 2023;3:e000634. https://doi.org/10.1161/SVIN.122.000634

Chen J, Zhang C, Jiang H, Li Y, Zhang L, Robin A, Katakowski M, Lu M, Chopp M. Atorvastatin induction of VEGF and BDNF promotes brain plasticity after stroke in mice. J Cereb Blood Flow Metab. 2005 Feb;25(2):281-90. doi: 10.1038/sj.jcbfm.9600034. PMID: 15678129; PMCID: PMC2804085.

Chen, T. W., Li, N., Daie, K., & Svoboda, K. (2017). A Map of Anticipatory Activity in Mouse Motor Cortex. *Neuron*, *94*(4), 866–879.e4. https://doi.org/10.1016/j.neuron.2017.05.005

Cheney, P. D., Griffin, D. M., & Van Acker, G. M., 3rd (2013). Neural hijacking: action of high-frequency electrical stimulation on cortical circuits. *The Neuroscientist : a review journal bringing neurobiology, neurology and psychiatry*, *19*(5), 434–441. https://doi.org/10.1177/1073858412458368

Cicinelli, P., Traversa, R., & Rossini, P. M. (1997). Post-stroke reorganization of brain motor output to the hand: a 2-4 month follow-up with focal magnetic transcranial stimulation. *Electroencephalography and clinical neurophysiology*, *105*(6), 438–450. https://doi.org/10.1016/s0924-980x(97)00052-0

Cirillo, C., Brihmat, N., Castel-Lacanal, E., Le Friec, A., Barbieux-Guillot, M., Raposo, N., Pariente, J., Viguier, A., Simonetta-Moreau, M., Albucher, J. F., Olivot, J. M., Desmoulin, F., Marque, P., Chollet, F., & Loubinoux, I. (2020). Post-stroke remodeling processes in animal models and humans. *Journal of cerebral blood flow and metabolism : official journal of the International Society of Cerebral Blood Flow and Metabolism*, *40*(1), 3–22. https://doi.org/10.1177/0271678X19882788

Citri, A., Malenka, R. Synaptic Plasticity: Multiple Forms, Functions, and Mechanisms. *Neuropsychopharmacol* **33,** 18–41 (2008). https://doi.org/10.1038/sj.npp.1301559

Clark KL, Armstrong KM, Moore T. Probing neural circuitry and function with electrical microstimulation. Proc Biol Sci. 2011 Apr 22;278(1709):1121-30. doi: 10.1098/rspb.2010.2211. Epub 2011 Jan 19. PMID: 21247952; PMCID: PMC3049083.

Clark, T.A., Sullender, C., Kazmi, S.M. *et al*. Artery targeted photothrombosis widens the vascular penumbra, instigates peri-infarct neovascularization and models forelimb impairments. Sci Rep 9, 2323 (2019). https://doi.org/10.1038/s41598-019-39092-7

Clarkson, A., Huang, B., MacIsaac, S. *et al*. Reducing excessive GABA-mediated tonic inhibition promotes functional recovery after stroke. Nature 468, 305–309 (2010). https://doi.org/10.1038/nature09511

Classen J, Knorr U, Werhahn KJ, Schlaug G, Kunesch E, Cohen LG, Seitz RJ, Benecke R. Multimodal output mapping of human central motor representation on different spatial scales. J Physiol. 1998 Oct 1;512 (Pt 1):163-79. doi: 10.1111/j.1469-7793.1998.163bf.x. PMID: 9729626; PMCID: PMC2231178.

Coleman ER, Moudgal R, Lang K, Hyacinth HI, Awosika OO, Kissela BM, Feng W. Early Rehabilitation After Stroke: a Narrative Review. Curr Atheroscler Rep. 2017 Nov 7;19(12):59. doi: 10.1007/s11883-017-0686-6. PMID: 29116473; PMCID: PMC5802378.

Cooke, D. F., Taylor, C. S., Moore, T., & Graziano, M. S. (2003). Complex movements evoked by microstimulation of the ventral intraparietal area. *Proceedings of the National Academy of Sciences of the United States of America*, *100*(10), 6163–6168. https://doi.org/10.1073/pnas.1031751100

Cramer SC, Nelles G, Benson RR, Kaplan JD, Parker RA, Kwong KK, Kennedy DN, Finklestein SP, Rosen BR. A functional MRI study of subjects recovered from hemiparetic stroke. *Stroke*. **28**(12), 2518-27, 1997. doi: 10.1161/01.str.28.12.2518. PMID: 9412643.

Cuccione E, Versace A, Cho TH, Carone D, Berner LP, Ong E, Rousseau D, Cai R, Monza L, Ferrarese C, Sganzerla EP, Berthezène Y, Nighoghossian N, Wiart M, Beretta S, Chauveau F. Multi-site laser Doppler flowmetry for assessing collateral flow in experimental ischemic stroke: Validation of outcome prediction with acute MRI. J Cereb Blood Flow Metab. 2017 Jun;37(6):2159-2170. doi: 10.1177/0271678X16661567. Epub 2016 Jan 1. PMID: 27466372; PMCID: PMC5464709.

Dancause, N., Barbay, S., Frost, S. B., Plautz, E. J., Chen, D., Zoubina, E. V., Stowe, A. M., & Nudo, R. J. (2005). Extensive cortical rewiring after brain injury. *The Journal of neuroscience : the official journal of the Society for Neuroscience*, *25*(44), 10167–10179. https://doi.org/10.1523/JNEUROSCI.3256-05.2005

Daskalakis, Z. J., Christensen, B. K., Fitzgerald, P. B., Roshan, L., & Chen, R. (2002). The mechanisms of interhemispheric inhibition in the human motor cortex. *The Journal of physiology*, *543*(Pt 1), 317–326. https://doi.org/10.1113/jphysiol.2002.017673

Deffeyes, J E *et al*. "Interactions between rostral and caudal cortical motor areas in the rat." *Journal of neurophysiology.* **13**(10) 3893-904, (2015). doi:10.1152/jn.00760.2014

Deleglise, B., Lassus, B., Soubeyre, V., Doulazmi, M., Brugg, B., Vanhoutte, P., & Peyrin, J. M. (2018). Dysregulated Neurotransmission induces Trans-synaptic degeneration in reconstructed Neuronal Networks. *Scientific reports*, *8*(1), 11596. https://doi.org/10.1038/s41598-018-29918-1

Di Pino, G., Pellegrino, G., Assenza, G. *et al.* Modulation of brain plasticity in stroke: a novel model for neurorehabilitation. *Nat Rev Neurol* **10,** 597–608 (2014). https://doi.org/10.1038/nrneurol.2014.162

Diao, X., Lu, Q., Qiao, L., Gong, Y., Lu, X., Feng, M., Su, P., Shen, Y., Yuan, T. F., & He, C. (2022). Cortical Inhibition State-Dependent iTBS Induced Neural Plasticity. *Frontiers in neuroscience*, *16*, 788538. https://doi.org/10.3389/fnins.2022.788538

Dickins, D. S., Sale, M. V., & Kamke, M. R. (2015). Plasticity Induced by Intermittent Theta Burst Stimulation in

Bilateral Motor Cortices Is Not Altered in Older Adults. *Neural plasticity*, *2015*, 323409. https://doi.org/10.1155/2015/323409

Dodd KC, Nair VA, Prabhakaran V. Role of the Contralesional vs. Ipsilesional Hemisphere in Stroke Recovery. Front Hum Neurosci. 2017 Sep 21;11:469. doi: 10.3389/fnhum.2017.00469. PMID: 28983244; PMCID: PMC5613154.

Donnan GA, Fisher M, Macleod M, Davis SM. Stroke. Lancet. 2008 May 10;371(9624):1612-23. doi: 10.1016/S0140-6736(08)60694-7. PMID: 18468545.

Duncan PW, Goldstein LB, Matchar D, Divine GW, Feussner J. Measurement of motor recovery after stroke. Outcome assessment and sample size requirements. Stroke. 1992 Aug;23(8):1084-9. doi: 10.1161/01.str.23.8.1084. PMID: 1636182.

Duncan PW, Lai SM, Keighley J. Defining post-stroke recovery: implications for design and interpretation of drug trials. Neuropharmacology. 2000 Mar 3;39(5):835-41. doi: 10.1016/s0028-3908(00)00003-4. PMID: 10699448.

Ebbesen, C., Brecht, M. Motor cortex — to act or not to act?. *Nat Rev Neurosci* **18**, 694–705 (2017). https://doi.org/10.1038/nrn.2017.119

Efron, Chapter 16 - Corneal staining, Contact Lens Complications (Third Edition), W.B. Saunders, 2012, Pages 155-166, ISBN 9780702042690, https://doi.org/10.1016/B978-0-7020-4269-0.00016-X.

Escudero, J. V., Sancho, J., Bautista, D., Escudero, M., & López-Trigo, J. (1998). Prognostic value of motor evoked potential obtained by transcranial magnetic brain stimulation in motor function recovery in patients with acute ischemic stroke. *Stroke*, *29*(9), 1854–1859. https://doi.org/10.1161/01.str.29.9.1854

Ferbert, A., Priori, A., Rothwell, J. C., Day, B. L., Colebatch, J. G., & Marsden, C. D. (1992). Interhemispheric inhibition of the human motor cortex. *The Journal of physiology*, *453*, 525–546. https://doi.org/10.1113/jphysiol.1992.sp019243

Friel, K. M., Kuo, H., Fuller, J., Ferre, C. L., Brandão, M., Carmel, J. B., ... Gordon, A. M. Skilled Bimanual Training Drives Motor Cortex Plasticity in Children With Unilateral Cerebral Palsy. *Neurorehabilitation and Neural Repair*, **30**(9), 834–844, (2016). https://doi.org/10.1177/1545968315625838

Fritsch, G. and Hitzig, E. (1870) über die elektrische Erregbarkeit des Grosshirns. von Bonin, G., Trans. In: The Cerebral Cortex, Thomas, Springfield, IL, 73-96.

Frostig RD, Chen-Bee CH. Visualizing Adult Cortical Plasticity Using Intrinsic Signal Optical Imaging. In: Frostig RD, editor. In Vivo Optical Imaging of Brain Function. 2nd edition. Boca Raton (FL): CRC Press/Taylor & Francis; 2009. Chapter 9. https://www.ncbi.nlm.nih.gov/books/NBK20227/

Fujito, Y., Aoki, M. Monosynaptic rubrospinal projections to distal forelimb motoneurons in the cat. *Exp Brain Res* **105**, 181–190 (1995). https://doi.org/10.1007/BF00240954

Gargango Julia, Reeves Mathew. Sex Differences in Stroke Recovery and Stroke-Specific Quality of Life. 2007. *Stroke*.38:2541–2548. https://doi.org/10.1161/STROKEAHA.107.485482

Gerbaud E, Cochet H, Bullier E, Ragot C, Gilbert SH, Douard H, Pucheu Y, Laurent F, Coste P, Bordenave L, Montaudon M. Peri-infarct ischaemia assessed by cardiovascular MRI: comparison with quantitative perfusion single photon emission CT imaging. Br J Radiol. 2014 Jul;87(1039):20130774. doi: 10.1259/bjr.20130774. Epub 2014 Apr 29. PMID: 24779410; PMCID: PMC4075581.

Gharbawie, O. A., Gonzalez, C. L., Williams, P. T., Kleim, J. A., & Whishaw, I. Q. Middle cerebral artery (MCA) stroke produces dysfunction in adjacent motor cortex as detected by intracortical microstimulation in rats. *Neuroscience*, **130**(3), 601–610, (2005). https://doi.org/10.1016/j.neuroscience.2004.10.010

Gharbawie, O. A., Stepniewska, I., & Kaas, J. H. (2011). Cortical connections of functional zones in posterior parietal cortex and frontal cortex motor regions in new world monkeys. *Cerebral cortex (New York, N.Y. : 1991)*, *21*(9), 1981–2002. https://doi.org/10.1093/cercor/bhq260

Gharbawie OA, Whishaw PA, Whishaw IQ. The topography of three-dimensional exploration: a new quantification of vertical and horizontal exploration, postural support, and exploratory bouts in the cylinder test. *Behavioral Brain Research*. **151**, 125–135, (2004). doi: 10.1016/j.bbr.2003.08.009.

Grafton ST, Mazziotta JC, Presty S, Friston KJ, Frackowiak RS, Phelps ME. Functional anatomy of human procedural learning determined with regional cerebral blood flow and PET. J Neurosci. 1992 Jul;12(7):2542-8. doi: 10.1523/JNEUROSCI.12-07-02542.1992. PMID: 1613546; PMCID: PMC6575851.

Gravanis, I., & Tsirka, S. E. (2008). Tissue-type plasminogen activator as a therapeutic target in stroke. *Expert opinion on therapeutic targets*, *12*(2), 159–170. https://doi.org/10.1517/14728222.12.2.159

Graziano, M. S., Taylor, C. S., & Moore, T. (2002). Complex movements evoked by microstimulation of precentral cortex. Neuron, 34(5), 841–851. https://doi.org/10.1016/s0896-6273(02)00698-0

Graziano, M. S., Aflalo, T. N., & Cooke, D. F. (2005). Arm movements evoked by electrical stimulation in the motor cortex of monkeys. *Journal of neurophysiology*, *94*(6), 4209–4223. https://doi.org/10.1152/jn.01303.2004

Grigoras IF, Stagg CJ. Recent advances in the role of excitation-inhibition balance in motor recovery post-stroke. Fac Rev. 2021 Jun 23;10:58. doi: 10.12703/r/10-58. PMID: 34308424; PMCID: PMC8265564.

Gu, Z., Kalambogias, J., Yoshioka, S., Han, W., Li, Z., Kawasawa, Y. I., Pochareddy, S., Li, Z., Liu, F., Xu, X., Wijeratne, H. R. S., Ueno, M., Blatz, E., Salomone, J., Kumanogoh, A., Rasin, M. R., Gebelein, B., Weirauch, M. T., Sestan, N., Martin, J. H., … Yoshida, Y. (2017). Control of species-dependent cortico-motoneuronal connections underlying manual dexterity. *Science (New York, N.Y.)*, *357*(6349), 400–404. https://doi.org/10.1126/science.aan3721

Guo L., Kondapavulur S., Lemke S.M., Won S.J., Ganguly K., Coordinated increase of reliable cortical and striatal ensemble activations during recovery after stroke, *Cell Reports*, **36**(2), 109370, ISSN 2211-1247, (2021). https://doi.org/10.1016/j.celrep.2021.109370.

Hall RD, Lindholm EP. Organization of motor and somatosensory neocortex in the albino rat. Brain Res. 1974;66:23–38 ISSN 0006-8993, https://doi.org/10.1016/0006-8993(74)90076-6.

Hallett M. Plasticity of the human motor cortex and recovery from stroke. Brain Res Brain Res Rev. 2001 Oct;36(2-3):169-74. doi: 10.1016/s0165-0173(01)00092-3. PMID: 11690613.

Hallett M. (2007). Transcranial magnetic stimulation: a primer. *Neuron*, *55*(2), 187–199. https://doi.org/10.1016/j.neuron.2007.06.026

Han, L., Savalia, N. K., Chan, M. Y., Agres, P. F., Nair, A. S., & Wig, G. S. (2018). Functional Parcellation of the Cerebral Cortex Across the Human Adult Lifespan. *Cerebral cortex (New York, N.Y. : 1991)*, *28*(12), 4403–4423. https://doi.org/10.1093/cercor/bhy218

Hanajima, R., Ugawa, Y., Terao, Y., Sakai, K., Furubayashi, T., Machii, K., & Kanazawa, I. (1998). Paired-pulse magnetic stimulation of the human motor cortex: differences among I waves. The Journal of physiology, 509 (Pt 2)(Pt 2), 607–618. https://doi.org/10.1111/j.1469-7793.1998.607bn.x

Harms, K. J., Rioult-Pedotti, M. S., Carter, D. R., & Dunaevsky, A. (2003). Transient spine expansion and learning-induced plasticity in layer 1 primary motor cortex. The Journal of Neuroscience, 23(6), 2250-2257.

Harrison, T. C., & Murphy, T. H. (2014). Motor maps and the cortical control of movement. *Current opinion in neurobiology*, *24*(1), 88–94. https://doi.org/10.1016/j.conb.2013.08.018

Harrison TC, Silasi G, Boyd JD, Murphy TH. Displacement of sensory maps and disorganization of motor cortex after targeted stroke in mice. *Stroke*, **44**(8), 2300-6, (2013). doi: 10.1161/STROKEAHA.113.001272. Epub 2013 Jun 6. PMID: 23743973.

Hatem, S. M., Saussez, G., Della Faille, M., Prist, V., Zhang, X., Dispa, D., & Bleyenheuft, Y. Rehabilitation of Motor Function after Stroke: A Multiple Systematic Review Focused on Techniques to Stimulate Upper Extremity Recovery. *Frontiers in human neuroscience*, **10**, 442, (2016). https://doi.org/10.3389/fnhum.2016.00442

Hayley, P., Tuchek, C., Dalla, S., Borrell, J., Murphy, M. D., Nudo, R. J., & Guggenmos, D. J. (2023). Post-Ischemic Reorganization of Sensory Responses in Cerebral Cortex. *bioRxiv : the preprint server for biology*, 2023.01.18.524583. https://doi.org/10.1101/2023.01.18.524583

Hira R, Ohkubo F, Tanaka YR, Masamizu Y, Augustine GJ, Kasai H, Matsuzaki M. In vivo optogenetic tracing of functional corticocortical connections between motor forelimb areas. Front Neural Circuits. 2013 Apr 1;7:55. doi: 10.3389/fncir.2013.00055. PMID: 23554588; PMCID: PMC3612597.

Hohlbaum K, Bert B, Dietze S, Palme R, Fink H, Thöne-Reineke C. Impact of repeated anesthesia with ketamine and xylazine on the well-being of C57BL/6JRj mice. PLoS One. 2018 Sep 19;13(9):e0203559. doi: 10.1371/journal.pone.0203559. PMID: 30231081; PMCID: PMC6145541.

Hohlbaum K, Bert B, Dietze S, Palme R, Fink H, Thöne-Reineke C. Severity classification of repeated isoflurane anesthesia in C57BL/6JRj mice-Assessing the degree of distress. PLoS One. 2017 Jun 15;12(6):e0179588. doi: 10.1371/journal.pone.0179588. PMID: 28617851; PMCID: PMC5472303.

Hoyer E. H., Celnik P. A. (2011). Understanding and enhancing motor recovery after stroke using transcranial magnetic stimulation. Restor. Neurol. Neurosci. 29, 395–409. 10.3233/RNN-2011-061

Huang, W., Chen, J., Zheng, Y., Zhang, J., Li, X., Su, L., Li, Y., & Dou, Z. (2022). The Effectiveness of Intermittent

Theta Burst Stimulation for Stroke Patients With Upper Limb Impairments: A Systematic Review and Meta-Analysis. *Frontiers in neurology*, *13*, 896651. https://doi.org/10.3389/fneur.2022.896651

Huang, Y. Z., Edwards, M. J., Rounis, E., Bhatia, K. P., & Rothwell, J. C. (2005). Theta burst stimulation of the human motor cortex. *Neuron*, *45*(2), 201–206. https://doi.org/10.1016/j.neuron.2004.12.033

Hughes RE, Tadi P, Bollu PC. TPA Therapy. [Updated 2023 Jul 4]. In: StatPearls [Internet]. Treasure Island (FL): StatPearls Publishing; 2023 Jan-. Available from: https://www.ncbi.nlm.nih.gov/books/NBK482376/

Hui C, Tadi P, Patti L. Ischemic Stroke. [Updated 2021 Jul 19]. *StatPearls* [Internet]. Treasure Island (FL): StatPearls Publishing; *2021.* https://www.ncbi.nlm.nih.gov/books/NBK499997/

Hussin AT, Boychuk JA, Brown AR, Pittman QJ, Teskey GC. Intracortical Microstimulation (ICMS) Activates Motor Cortex Layer 5 Pyramidal Neurons Mainly Transsynaptically. *Brain Stimul*. **8**(4):742-50, (2015). doi: 10.1016/j.brs.2015.03.003. Epub 2015 Mar 27. PMID: 25892002.

Hwang FJ, Roth RH, Wu YW, Sun Y, Kwon DK, Liu Y, Ding JB. Motor learning selectively strengthens cortical and striatal synapses of motor engram neurons. Neuron. 2022 Sep 7;110(17):2790-2801.e5. doi: 10.1016/j.neuron.2022.06.006. Epub 2022 Jul 8. PMID: 35809573; PMCID: PMC9464700.

Hylin, M. J., Kerr, A. L., & Holden, R. (2017). Understanding the Mechanisms of Recovery and/or Compensation following Injury. *Neural plasticity*, *2017*, 7125057. https://doi.org/10.1155/2017/7125057

Ingram Lewis A., Butler Annie A., Brodie Matthew A., Lord Stephen R., and Gandevia Simon C. (2021). Quantifying upper limb motor impairment in chronic stroke: a physiological profiling approach. *Journal of Applied Physiology.* Vol. 131, No. 3. https://doi.org/10.1152/japplphysiol.00078.2021

Ito, K. L., Kim, B., Liu, J., Soekadar, S. R., Winstein, C., Yu, C., Cramer, S. C., Schweighofer, N., & Liew, S. L. (2022). Corticospinal Tract Lesion Load Originating From Both Ventral Premotor and Primary Motor Cortices Are Associated With Post-stroke Motor Severity. Neurorehabilitation and neural repair, 36(3), 179–182. https://doi.org/10.1177/15459683211068441

Jeong, M., Kim, Y., Kim, J. *et al.* Comparative three-dimensional connectome map of motor cortical projections in the mouse brain. *Sci Rep* **6**, 20072 (2016). https://doi.org/10.1038/srep20072

Jingsong Ruan, Yao Yao, Behavioral tests in rodent models of stroke, Brain Hemorrhages, Volume 1, Issue 4, 2020, Pages 171-184, ISSN 2589-238X, https://doi.org/10.1016/j.hest.2020.09.001.

Jones TA. Motor compensation and its effects on neural reorganization after stroke. Nat Rev Neurosci. 2017 May;18(5):267-280. doi: 10.1038/nrn.2017.26. Epub 2017 Mar 23. PMID: 28331232; PMCID: PMC6289262.

Jones, T. A., & Adkins, D. L. Motor System Reorganization After Stroke: Stimulating and Training Toward Perfection. Physiology. *Bethesda, Md*. **30**(5), 358–370, (2015). https://doi.org/10.1152/physiol.00014.2015

Jones TH, Morawetz RB, Crowell RM, Marcoux FW, FitzGibbon SJ, DeGirolami U, Ojemann RG. Thresholds of focal cerebral ischemia in awake monkeys. J Neurosurg. 1981 Jun;54(6):773-82. doi: 10.3171/jns.1981.54.6.0773. PMID: 7241187.

Kang DW, Latour LL, Chalela JA, Dambrosia JA, Warach S. Early and late recurrence of ischemic lesion on MRI: evidence for a prolonged stroke-prone state? Neurology. 2004 Dec 28;63(12):2261-5. doi: 10.1212/01.wnl.0000147295.50029.67. PMID: 15623684.

Kaas, J. H., Gharbawie, O. A., & Stepniewska, I. (2013). Cortical networks for ethologically relevant behaviors in primates. *American journal of primatology*, *75*(5), 407–414. https://doi.org/10.1002/ajp.22065

Kelly-Hayes M. (2010). Influence of age and health behaviors on stroke risk: lessons from longitudinal studies. *Journal of the American Geriatrics Society*, *58 Suppl 2*(Suppl 2), S325–S328. https://doi.org/10.1111/j.1532-5415.2010.02915.x

Kim, J. S., Lee, K. B., Roh, H., Ahn, M. Y., & Hwang, H. W. (2010). Gender differences in the functional recovery after acute stroke. *Journal of clinical neurology (Seoul, Korea)*, *6*(4), 183–188. https://doi.org/10.3988/jcn.2010.6.4.183

Kim SG, Ashe J, Georgopoulos AP, Merkle H, Ellermann JM, Menon RS, Ogawa S, Ugurbil K. Functional imaging of human motor cortex at high magnetic field. J Neurophysiol. 1993 Jan;69(1):297-302. doi: 10.1152/jn.1993.69.1.297. PMID: 8433133.

Kim YW. Update on Stroke Rehabilitation in Motor Impairment. Brain Neurorehabil. 2022 Jul 20;15(2):e12. doi: 10.12786/bn.2022.15.e12. PMID: 36743199; PMCID: PMC9833472.

Klapoetke, N. C., Murata, Y., Kim, S. S., Pulver, S. R., Birdsey-Benson, A., Cho, Y. K., Morimoto, T. K., Chuong, A. S.,

Carpenter, E. J., Tian, Z., Wang, J., Xie, Y., Yan, Z., Zhang, Y., Chow, B. Y., Surek, B., Melkonian, M., Jayaraman, V., Constantine-Paton, M., Wong, G. K., … Boyden, E. S. (2014). Independent optical excitation of distinct neural populations. *Nature methods*, *11*(3), 338–346. https://doi.org/10.1038/nmeth.2836

Kleim JA, Barbay S, Nudo RJ. Functional reorganization of the rat motor cortex following motor skill learning. J Neurophysiol. 1998 Dec;80(6):3321-5. doi: 10.1152/jn.1998.80.6.3321. PMID: 9862925.

Kleim, J. A., Bruneau, R., VandenBerg, P., MacDonald, E., Mulrooney, R., & Pocock, D. (2003). Motor cortex stimulation enhances motor recovery and reduces peri-infarct dysfunction following ischemic insult. *Neurological research*, *25*(8), 789–793. https://doi.org/10.1179/016164103771953862

Kleim JA, Hogg TM, VandenBerg PM, Cooper NR, Bruneau R, Remple M. Cortical synaptogenesis and motor map reorganization occur during late, but not early, phase of motor skill learning. J Neurosci. 2004 Jan 21;24(3):628-33. doi: 10.1523/JNEUROSCI.3440-03.2004. PMID: 14736848; PMCID: PMC6729261.

Ko, S. H., Kim, T., Min, J. H., Kim, M., Ko, H. Y., & Shin, Y. I. (2021). Corticoreticular Pathway in Post-Stroke Spasticity: A Diffusion Tensor Imaging Study. Journal of personalized medicine, 11(11), 1151. https://doi.org/10.3390/jpm11111151

Kowalski, J. L., Nemanich, S. T., Nawshin, T., Chen, M., Peyton, C., Zorn, E., Hickey, M., Rao, R., Georgieff, M., Rudser, K., & Gillick, B. T. (2019). Motor Evoked Potentials as Potential Biomarkers of Early Atypical Corticospinal Tract Development in Infants with Perinatal Stroke. *Journal of clinical medicine*, *8*(8), 1208. https://doi.org/10.3390/jcm8081208

Krisa, L., Runyen, M., & Detloff, M. R. (2018). Translational Challenges of Rat Models of Upper Extremity Dysfunction After Spinal Cord Injury. *Topics in spinal cord injury rehabilitation*, *24*(3), 195–205. https://doi.org/10.1310/sci2403-195

Kubis N. Non-Invasive Brain Stimulation to Enhance Post-Stroke Recovery. Front Neural Circuits. 2016 Jul 27;10:56. doi: 10.3389/fncir.2016.00056. PMID: 27512367; PMCID: PMC4961863.

Küchler, M., Fouad, K., Weinmann, O., Schwab, M. E., & Raineteau, O. (2002). Red nucleus projections to distinct motor neuron pools in the rat spinal cord. *The Journal of comparative neurology*, *448*(4), 349–359. https://doi.org/10.1002/cne.10259

Kunori, N., & Takashima, I. (2016). High-order motor cortex in rats receives somatosensory inputs from the primary motor cortex via cortico-cortical pathways. *The European journal of neuroscience*, *44*(11), 2925–2934. https://doi.org/10.1111/ejn.13427

Kurth, F., Mayer, E. A., Toga, A. W., Thompson, P. M., & Luders, E. (2013). The right inhibition? Callosal correlates of hand performance in healthy children and adolescents callosal correlates of hand performance. *Human brain mapping*, *34*(9), 2259–2265. https://doi.org/10.1002/hbm.22060

Kuroiwa T, Xi G, Hua Y, Nagaraja TN, Fenstermacher JD, Keep RF. Development of a rat model of photothrombotic ischemia and infarction within the caudoputamen. Stroke. 2009 Jan;40(1):248-53. doi: 10.1161/STROKEAHA.108.527853. Epub 2008 Nov 26. PMID: 19038913; PMCID: PMC2692300.

Kwon, B. K., Streijger, F., Hill, C. E., Anderson, A. J., Bacon, M., Beattie, M. S., Blesch, A., Bradbury, E. J., Brown, A., Bresnahan, J. C., Case, C. C., Colburn, R. W., David, S., Fawcett, J. W., Ferguson, A. R., Fischer, I., Floyd, C. L., Gensel, J. C., Houle, J. D., Jakeman, L. B., … Tetzlaff, W. (2015). Large animal and primate models of spinal cord injury for the testing of novel therapies. *Experimental neurology*, *269*, 154–168. https://doi.org/10.1016/j.expneurol.2015.04.008

Labat-gest V, Tomasi S. Photothrombotic ischemia: A minimally invasive and reproducible photochemical cortical lesion model for mouse stroke studies. *J Vis Exp.* **9**(76), 50370, (2013). doi: 10.3791/50370. PMID: 23770844; PMCID: PMC3727176.

Lai TW, Zhang S, Wang YT. Excitotoxicity and stroke: identifying novel targets for neuroprotection. Prog Neurobiol. 2014 Apr;115:157-88. doi: 10.1016/j.pneurobio.2013.11.006. Epub 2013 Dec 17. PMID: 24361499.

Lansberg Maarten, MD; O'Brien Michael, MD, PhD; Tong David, MD; *et al*., Evolution of Cerebral Infarct Volume Assessed by Diffusion-Weighted Magnetic Resonance Imaging. *Arch Neurol*. 2001;58(4):613-617. doi:10.1001/archneur.58.4.613

Larivière, S., Ward, N. S., & Boudrias, M. H. (2018). Disrupted functional network integrity and flexibility after stroke: Relation to motor impairments. NeuroImage. Clinical, 19, 883–891. https://doi.org/10.1016/j.nicl.2018.06.010

Lee KB, Lim SH, Kim KH, Kim KJ, Kim YR, Chang WN, Yeom JW, Kim YD, Hwang BY. Six-month functional recovery of

stroke patients: a multi-time-point study. Int J Rehabil Res. 2015 Jun;38(2):173-80. doi: 10.1097/MRR.0000000000000108. PMID: 25603539; PMCID: PMC4415968.
Lemke SM, Ramanathan DS, Darevksy D, Egert D, Berke JD, Ganguly K. Coupling between motor cortex and striatum increases during sleep over long-term skill learning. Elife. 2021 Sep 10;10:e64303. doi: 10.7554/eLife.64303. PMID: 34505576; PMCID: PMC8439654.
Lemke SM, Ramanathan DS, Guo L, Won SJ, Ganguly K. Emergent modular neural control drives coordinated motor actions. Nat Neurosci. 2019 Jul;22(7):1122-1131. doi: 10.1038/s41593-019-0407-2. Epub 2019 May 27. PMID: 31133689; PMCID: PMC6592763.
Lemon R. (2019). Recent advances in our understanding of the primate corticospinal system. *F1000Research*, *8*, F1000 Faculty Rev-274. https://doi.org/10.12688/f1000research.17445.1
Leutenegger M, Martin-Williams E, Harbi P, Thacher T, Raffoul W, André M, Lopez A, Lasser P, Lasser T. Real-time full field laser Doppler imaging. Biomed Opt Express. 2011 Jun 1;2(6):1470-7. doi: 10.1364/BOE.2.001470. Epub 2011 May 9. PMID: 21698011; PMCID: PMC3114216.
Liang H, Paxinos G, Watson C. The red nucleus and the rubrospinal projection in the mouse. Brain Struct Funct. 2012 Apr;217(2):221-32. doi: 10.1007/s00429-011-0348-3. Epub 2011 Sep 17. PMID: 21927901.
Lin David, MD, Cloutier Alison, MS, Erler Kimberly, OTR/L, PhD, Cassidy Jessica, PhD, DPT, Snider Samuel, MD, Ranford Jessica, OTR/L, MS, Parlman Kristin, PT, DPT, Giatsidis Fabio, MD, Burke James, MD, MS, Schwamm Lee, MD, Finklestein Seth, MD, Hochberg Leigh, MD, PhD, Cramer Steven, MD. Corticospinal Tract Injury Estimated From Acute Stroke Imaging Predicts Upper Extremity Motor Recovery After Stroke. Stroke. 2019;50:3569–3577. https://doi.org/10.1161/STROKEAHA.119.025898
Lin J. Y. (2011). A user's guide to channelrhodopsin variants: features, limitations and future developments. *Experimental physiology*, *96*(1), 19–25. https://doi.org/10.1113/expphysiol.2009.051961
Liu NW, Ke CC, Zhao Y, Chen YA, Chan KC, Tan DT, Lee JS, Chen YY, Hsu TW, Hsieh YJ, Chang CW, Yang BH, Huang WS, Liu RS. Evolutional Characterization of Photochemically Induced Stroke in Rats: a Multimodality Imaging and Molecular Biological Study. Transl Stroke Res. 2017 Jun;8(3):244-256. doi: 10.1007/s12975-016-0512-4. Epub 2016 Dec 1. PMID: 27910074; PMCID: PMC5435782.
Liu, S., Levine, S. R., & Winn, H. R. (2010). Targeting ischemic penumbra: part I - from pathophysiology to therapeutic strategy. *Journal of experimental stroke & translational medicine*, *3*(1), 47–55. https://doi.org/10.6030/1939-067x-3.1.47
Liu Z, Zhang RL, Li Y, Cui Y, Chopp M. Remodeling of the corticospinal innervation and spontaneous behavioral recovery after ischemic stroke in adult mice. Stroke. 2009 Jul;40(7):2546-51. doi: 10.1161/STROKEAHA.109.547265. Epub 2009 May 28. Erratum in: Stroke. 2009 Dec;40(12):e719. PMID: 19478220; PMCID: PMC2704262.
Lo, M. C., Younk, R., & Widge, A. S. (2020). Paired Electrical Pulse Trains for Controlling Connectivity in Emotion-Related Brain Circuitry. *IEEE transactions on neural systems and rehabilitation engineering : a publication of the IEEE Engineering in Medicine and Biology Society*, *28*(12), 2721–2730. https://doi.org/10.1109/TNSRE.2020.3030714
Lu HD, Chen G, Cai J, Roe AW. Intrinsic signal optical imaging of visual brain activity: Tracking of fast cortical dynamics. Neuroimage. 2017 Mar 1;148:160-168. doi: 10.1016/j.neuroimage.2017.01.006. Epub 2017 Jan 4. PMID: 28063974; PMCID: PMC5344706.
Magno, L. A. V., Collodetti, M., Tenza-Ferrer, H., & Romano-Silva, M. A. (2019). Cylinder Test to Assess Sensory-motor Function in a Mouse Model of Parkinson's Disease. *Bio-protocol*, *9*(16), e3337. https://doi.org/10.21769/BioProtoc.3337
Maraka S, Jiang Q, Jafari-Khouzani K, Li L, Malik S, Hamidian H, Zhang T, Lu M, Soltanian-Zadeh H, Chopp M, Mitsias PD. Degree of corticospinal tract damage correlates with motor function after stroke. Ann Clin Transl Neurol. 2014 Nov;1(11):891-9. doi: 10.1002/acn3.132. Epub 2014 Oct 31. PMID: 25540803; PMCID: PMC4265060.
Mathews S, De Jesus O. Thrombectomy. [Updated 2023 Aug 14]. In: StatPearls [Internet]. Treasure Island (FL): StatPearls Publishing; 2023 Jan-. Available from: https://www.ncbi.nlm.nih.gov/books/NBK562154/
Merino J. G. Clinical stroke challenges: A practical approach. Neurology. Clinical practice, **4**(5), 376–377, (2014). https://doi.org/10.1212/CPJ.0000000000000082
Metz, GA, and Whishaw, IQ, Cortical and subcortical lesions impair skilled walking in the ladder rung walking test: a

new task to evaluate fore- and hindlimb stepping, placing, and co-ordination, Journal of Neuroscience Methods, Volume 115, Issue 2, 2002, Pages 169-179, ISSN 0165-0270, https://doi.org/10.1016/S0165-0270(02)00012-2.

Meyer, B. U., Röricht, S., & Woiciechowsky, C. (1998). Topography of fibers in the human corpus callosum mediating interhemispheric inhibition between the motor cortices. *Annals of neurology*, *43*(3), 360–369. https://doi.org/10.1002/ana.410430314

Miura, Y., Grocott, H. P., Bart, R. D., Pearlstein, R. D., Dexter, F., & Warner, D. S. (1998). Differential effects of anesthetic agents on outcome from near-complete but not incomplete global ischemia in the rat. *Anesthesiology*, *89*(2), 391–400. https://doi.org/10.1097/00000542-199808000-00016

Morandell, K., Huber, D. The role of forelimb motor cortex areas in goal directed action in mice. *Sci Rep* **7**, 15759 (2017). https://doi.org/10.1038/s41598-017-15835-2

Moreno-Lopez Yunuen, Bichara Charlotte, Delbecq Gilles, Isope Philippe, Cordero-Erausquin Matilde. (2021) The corticospinal tract primarily modulates sensory inputs in the mouse lumbar cord eLife 10:e65304. https://doi.org/10.7554/eLife.65304

Morishita, T., Timmermann, J.E., Schulz, R. *et al.* Impact of interhemispheric inhibition on bimanual movement control in young and old. *Exp Brain Res* **240**, 687–701 (2022). https://doi.org/10.1007/s00221-021-06258-7

Muñoz-Castañeda, R., Zingg, B., Matho, K.S. *et al*. Cellular anatomy of the mouse primary motor cortex. Nature 598, 159–166 (2021). https://doi.org/10.1038/s41586-021-03970-w

Murphy, T., Corbett, D. Plasticity during stroke recovery: from synapse to behaviour. *Nat Rev Neurosci* **10,** 861–872 (2009). https://doi.org/10.1038/nrn2735

Nathan P. W. (1994). Effects on movement of surgical incisions into the human spinal cord. *Brain : a journal of neurology*, *117 (Pt 2)*, 337–346. https://doi.org/10.1093/brain/117.2.337

Neafsey, E. J., Bold, E. L., Haas, G., Hurley-Gius, K. M., Quirk, G., Sievert, C. F., & Terreberry, R. R. (1986). The organization of the rat motor cortex: a microstimulation mapping study. *Brain research*, *396*(1), 77–96. https://doi.org/10.1016/s0006-8993(86)80191-3

Neafsey EJ, Sievert C. A second forelimb motor area exists in rat frontal cortex. Brain Res. 1982 Jan 28;232(1):151-6. doi: 10.1016/0006-8993(82)90617-5. PMID: 7055691.

Newton, J. M., Sunderland, A., & Gowland, P. A. (2005). fMRI signal decreases in ipsilateral primary motor cortex during unilateral hand movements are related to duration and side of movement. *NeuroImage*, *24*(4), 1080–1087. https://doi.org/10.1016/j.neuroimage.2004.10.003

Nilsson, T. Tenland and P. A. Oberg, "Evaluation of a Laser Doppler Flowmeter for Measurement of Tissue Blood Flow," in IEEE Transactions on Biomedical Engineering, vol. BME-27, no. 10, pp. 597-604, Oct. 1980, doi: 10.1109/TBME.1980.326582.

Nishibe, M., Barbay, S., Guggenmos, D., & Nudo, R. J. (2010). Reorganization of motor cortex after controlled cortical impact in rats and implications for functional recovery. *Journal of neurotrauma*, *27*(12), 2221–2232. https://doi.org/10.1089/neu.2010.1456

Nishibe, M., Urban, E. T., 3rd, Barbay, S., & Nudo, R. J. Rehabilitative training promotes rapid motor recovery but delayed motor map reorganization in a rat cortical ischemic infarct model. *Neurorehabilitation and neural repair*, *29*(5), 472–482, (2015) https://doi.org/10.1177/1545968314543499

Nogles TE, Galuska MA. Middle Cerebral Artery Stroke. [Updated 2023 Apr 3]. In: StatPearls [Internet]. Treasure Island (FL): StatPearls Publishing; 2023 Jan-. Available from: https://www.ncbi.nlm.nih.gov/books/NBK556132/

Nowak, D. A., Grefkes, C., Dafotakis, M., Eickhoff, S., Küst, J., Karbe, H., & Fink, G. R. Effects of low-frequency repetitive transcranial magnetic stimulation of the contralesional primary motor cortex on movement kinematics and neural activity in subcortical stroke. *Archives of neurology*, **65**(6), 741–747, (2008). https://doi.org/10.1001/archneur.65.6.741.

Nudo R.J, Mechanisms for recovery of motor function following cortical damage, Current Opinion in Neurobiology, Volume 16, Issue 6, 2006, Pages 638-644, ISSN 0959-4388, https://doi.org/10.1016/j.conb.2006.10.004.

Nudo R. J. Recovery after brain injury: mechanisms and principles. *Frontiers in human neuroscience*. 2013. *7*, 887. https://doi.org/10.3389/fnhum.2013.00887

Nudo RJ. The Role of Skill versus Use in the Recovery of Motor Function after Stroke. OTJR: Occupational Therapy Journal of Research. 2007;27(1_suppl):24S-32S. doi:10.1177/15394492070270S104

Nudo, R. J., Jenkins, W. M., & Merzenich, M. M. (1990). Repetitive microstimulation alters the cortical representation of movements in adult rats. *Somatosensory & motor research*, *7*(4), 463–483. https://doi.org/10.3109/08990229009144720

Nudo RJ, Milliken GW. Reorganization of movement representations in primary motor cortex following focal ischemic infarcts in adult squirrel monkeys. *Journal of Neurophysiology*. (1996). Vol. 75, No. 5. https://doi.org/10.1152/jn.1996.75.5.2144

Nudo RJ, Plautz EJ, Frost SB. Role of adaptive plasticity in recovery of function after damage to motor cortex. Muscle Nerve. 2001 Aug;24(8):1000-19. doi: 10.1002/mus.1104. PMID: 11439375.

Nudo, R. J., Wise, B. M., SiFuentes, F., & Milliken, G. W. (1996). Neural substrates for the effects of rehabilitative training on motor recovery after ischemic infarct. Science (New York, N.Y.), 272(5269), 1791–1794. https://doi.org/10.1126/science.272.5269.1791

Okabe N, Shiromoto T, Himi N, Lu F, Maruyama-Nakamura E, Narita K, Iwachidou N, Yagita Y, Miyamoto O. Neural network remodeling underlying motor map reorganization induced by rehabilitative training after ischemic stroke. *Neuroscience*, **339,** 338-362, (2016). doi: 10.1016/j.neuroscience.2016.10.008. Epub 2016 Oct 8. PMID: 27725217.

Ontario Stroke Repot 2019/20 Overview – CorHealth Ontario. CorHealthOntario.ca, https://www.corhealthontario.ca/data-&-reporting/ontario-stroke-reports

Papale, Andrew E, and Bryan M Hooks. Circuit changes in motor cortex during motor skill learning. *Neuroscience*. **368,** 283-297 (2018). https://doi.org/10.1016/j.neuroscience.2017.09.010

Patil, C. G., Long, E. F., & Lansberg, M. G. (2009). Cost-effectiveness analysis of mechanical thrombectomy in acute ischemic stroke. *Journal of neurosurgery*, *110*(3), 508–513. https://doi.org/10.3171/2008.8.JNS08133

Pilgram-Pastor, S. M., Piechowiak, E. I., Dobrocky, T., Kaesmacher, J., Den Hollander, J., Gralla, J., & Mordasini, P. (2021). Stroke thrombectomy complication management. *Journal of neurointerventional surgery*, *13*(10), 912–917. https://doi.org/10.1136/neurintsurg-2021-017349

Poomalai G, Prabhakar S, Sirala Jagadesh N. Functional Ability and Health Problems of Stroke Survivors: An Explorative Study. Cureus. 2023 Jan 4;15(1):e33375. doi: 10.7759/cureus.33375. PMID: 36751244; PMCID: PMC9898797.

Prabhakaran S, Zarahn E, Riley C, Speizer A, Chong JY, Lazar RM, Marshall RS, Krakauer JW. Inter-individual variability in the capacity for motor recovery after ischemic stroke. Neurorehabil Neural Repair. 2008 Jan-Feb;22(1):64-71. doi: 10.1177/1545968307305302. Epub 2007 Aug 8. PMID: 17687024.

Public Health Agency of Canada, using Canadian Chronic Disease Surveillance System data files contributed by provinces and territories, as of February 2021 (data up to 2017–2018). Data from Nunavut and the Northwest Territories were not available for 2017–2018.

Puig, B., Brenna, S., & Magnus, T. (2018). Molecular Communication of a Dying Neuron in Stroke. *International journal of molecular sciences*, *19*(9), 2834. https://doi.org/10.3390/ijms19092834

Quallo, M. M., Kraskov, A., & Lemon, R. N. (2012). The activity of primary motor cortex corticospinal neurons during tool use by macaque monkeys. *The Journal of neuroscience : the official journal of the Society for Neuroscience*, *32*(48), 17351–17364. https://doi.org/10.1523/JNEUROSCI.1009-12.2012

Raghavan P. (2015). Upper Limb Motor Impairment After Stroke. *Physical medicine and rehabilitation clinics of North America*, *26*(4), 599–610. https://doi.org/10.1016/j.pmr.2015.06.008

Raub Dana, *et al*., Effects of Volatile Anesthetics on Postoperative Ischemic Stroke Incidence. Journal of the American Heart Association. 2021 Feb; 10:e018952. https://doi.org/10.1161/JAHA.120.018952.

Riva M, Pappadà GB, Papadakis M, Cuccione E, Carone D, Menendez VR, Sganzerla EP, Beretta S. Hemodynamic monitoring of intracranial collateral flow predicts tissue and functional outcome in experimental ischemic stroke. Exp Neurol. 2012 Feb;233(2):815-20. doi: 10.1016/j.expneurol.2011.12.006. Epub 2011 Dec 13. PMID: 22193110.

Robinson, T., Zaheer, Z., & Mistri, A. K. (2011). Thrombolysis in acute ischaemic stroke: an update. *Therapeutic advances in chronic disease*, *2*(2), 119–131. https://doi.org/10.1177/2040622310394032

Roger VL, Go AS, Lloyd-Jones DM, Benjamin EJ, Berry JD, Borden WB, Bravata DM, Dai S, Ford ES, Fox CS, Fullerton HJ, Gillespie C, Hailpern SM, Heit JA, Howard VJ, Kissela BM, Kittner SJ, Lackland DT, Lichtman JH, Lisabeth LD, Makuc DM, Marcus GM, Marelli A, Matchar DB, Moy CS, Mozaffarian D, Mussolino ME, Nichol G, Paynter NP, Soliman EZ, Sorlie PD, Sotoodehnia N, Turan TN, Virani SS, Wong ND, Woo D, Turner MB; American Heart Association Statistics Committee and Stroke Statistics Subcommittee. Heart disease and

stroke statistics--2012 update: a report from the American Heart Association. Circulation. 2012 Jan 3;125(1):e2-e220. doi: 10.1161/CIR.0b013e31823ac046. Epub 2011 Dec 15. Erratum in: Circulation. 2012 Jun 5;125(22):e1002. PMID: 22179539; PMCID: PMC4440543.

Rothstein, S., Simkins, T., & Nunez, J. L. (2008). Response to neonatal anesthesia: Effect of sex on anatomical and behavioral outcome. Neuroscience, 152(4), 959–969. https://doi.org/10.1016/j.neuroscience.2008.01.0

Rouiller EM, Moret V, Liang F. Comparison of the connectional properties of the two forelimb areas of the rat sensorimotor cortex: support for the presence of a premotor or supplementary motor cortical area. Somatosens Mot Res. 1993;10(3):269-89. doi: 10.3109/08990229309028837. PMID: 8237215.

Rousselet E, Kriz J, Seidah NG. Mouse model of intraluminal MCAO: cerebral infarct evaluation by cresyl violet staining. J Vis Exp. 2012 Nov 6;(69):4038. doi: 10.3791/4038. PMID: 23168377; PMCID: PMC3520579.

Rudd AG, Bowen A, Young GR, James MA. The latest national clinical guideline for stroke. Clin Med (Lond). 2017 Apr;17(2):154-155. doi: 10.7861/clinmedicine.17-2-154. PMID: 28365628; PMCID: PMC6297617.

Saini V, Guada L, Yavagal DR. Global Epidemiology of Stroke and Access to Acute Ischemic Stroke Interventions. Neurology. 2021 Nov 16;97(20 Suppl 2):S6-S16. doi: 10.1212/WNL.0000000000012781. PMID: 34785599.

Salim S. (2017). Oxidative Stress and the Central Nervous System. *The Journal of pharmacology and experimental therapeutics*, *360*(1), 201–205. https://doi.org/10.1124/jpet.116.237503

Samsoon Inayat, Surjeet Singh, Arashk Ghasroddashti, Qandeel, Pramuka Egodage, Ian Q Whishaw, Majid H Mohajerani (2020) A Matlab-based toolbox for characterizing behavior of rodents engaged in string-pulling eLife 9:e54540

Schaar KL, Brenneman MM, Savitz SI. Functional assessments in the rodent stroke model. Exp Transl Stroke Med. 2010 Jul 19;2(1):13. doi: 10.1186/2040-7378-2-13. PMID: 20642841; PMCID: PMC2915950.

Schlaug G, Knorr U, Seitz R. Inter-subject variability of cerebral activations in acquiring a motor skill: a study with positron emission tomography. Exp Brain Res. 1994;98(3):523-34. doi: 10.1007/BF00233989. PMID: 8056072.

Schrandt CJ, Kazmi SM, Jones TA, Dunn AK. Chronic monitoring of vascular progression after ischemic stroke using multiexposure speckle imaging and two-photon fluorescence microscopy. J Cereb Blood Flow Metab. 2015 Jun;35(6):933-42. doi: 10.1038/jcbfm.2015.26. Epub 2015 Feb 25. PMID: 25712498; PMCID: PMC4640252.

Schwamm Lee, Koroshetz Walter, Sorensen Gregory, Wang Bing, Copen William, Budzik Ronald, Rordorf Guy, Buonanno Fernando, Schaefer Pamela and Gonzalez Gilberto. Time Course of Lesion Development in Patients With Acute Stroke. *Stroke*. 1998;29:2268–2276. https://doi.org/10.1161/01.STR.29.11.2268

Seto A, Taylor S, Trudeau D, Swan I, Leung J, Reeson P, Delaney KR, Brown CE. Induction of ischemic stroke in awake freely moving mice reveals that isoflurane anesthesia can mask the benefits of a neuroprotection therapy. Front Neuroenergetics. 2014 Apr 3;6:1. doi: 10.3389/fnene.2014.00001. PMID: 24765075; PMCID: PMC3982055.

Shen J, Huber M, Zhao EY, Peng C, Li F, Li X, Geng X, Ding Y. Early rehabilitation aggravates brain damage after stroke via enhanced activation of nicotinamide adenine dinucleotide phosphate oxidase (NOX). Brain Res. 2016 Oct 1;1648(Pt A):266-276. doi: 10.1016/j.brainres.2016.08.001. Epub 2016 Aug 2. PMID: 27495986.

Shin, H., Han, T., & Paik, N. Effect of Consecutive Application of Paired Associative Stimulation on Motor Recovery in a Rat Stroke Model: A Preliminary Study. *International Journal of Neuroscience*. **118**(6), 807–820, (2009). https://doi.org/10.1080/00207450601123480

Shiromoto, T., Okabe, N., Lu, F., Maruyama-Nakamura, E., Himi, N., Narita, K., Yagita, Y., Kimura, K., & Miyamoto, O. The Role of Endogenous Neurogenesis in Functional Recovery and Motor Map Reorganization Induced by Rehabilitative Therapy after Stroke in Rats. *Journal of stroke and cerebrovascular diseases: the official journal of National Stroke Association*, ***26***(2), 260–272 (2017). https://doi.org/10.1016/j.jstrokecerebrovasdis.2016.09.016

Silasi Gergely, Boyd Jamie, LeDue Jeffrey, Murphy Tim. Improved methods for chronic light-based motor mapping in mice: automated movement tracking with accelerometers, and chronic EEG recording in a bilateral thin-skull preparation. *Frontiers in Neural Circuits*. 2013. 7. 1662-5110. DOI=10.3389/fncir.2013.00123

Silasi, G., Xiao, D., Vanni, M. P., Chen, A. C. N., & Murphy, T. H. Intact skull chronic windows for mesoscopic wide-field imaging in awake mice. J*ournal of Neuroscience Methods*. **267**, 141–149, (2016). https://doi.org/10.1016/j.jneumeth.2016.04.012

Singleton AC., Brown AR., Teskey GC. Development and plasticity of complex movement representations. (2021).

Journal of Neurophysiology. 125:2, 628-637. https://doi.org/10.1152/jn.00531.2020
Sliwinska, M. W., Vitello, S., & Devlin, J. T. (2014). Transcranial magnetic stimulation for investigating causal brain-behavioral relationships and their time course. *Journal of visualized experiments : JoVE*, (89), 51735. https://doi.org/10.3791/51735
Spruston, N. Pyramidal neurons: dendritic structure and synaptic integration. *Nat Rev Neurosci* **9,** 206–221 (2008). https://doi.org/10.1038/nrn2286
Stefan, K., Kunesch, E., Cohen, L. G., Benecke, R., & Classen, J. (2000). Induction of plasticity in the human motor cortex by paired associative stimulation. *Brain : a journal of neurology*, *123 Pt 3*, 572–584. https://doi.org/10.1093/brain/123.3.572
Stepniewska, I., Friedman, R. M., Gharbawie, O. A., Cerkevich, C. M., Roe, A. W., & Kaas, J. H. (2011). Optical imaging in galagos reveals parietal-frontal circuits underlying motor behavior. Proceedings of the National Academy of Sciences of the United States of America, 108(37), E725–E732. https://doi.org/10.1073/pnas.1109925108
Stoykov, M. E., Lewis, G. N., & Corcos, D. M. (2009). Comparison of bilateral and unilateral training for upper extremity hemiparesis in stroke. *Neurorehabilitation and neural repair*, *23*(9), 945–953. https://doi.org/10.1177/1545968309338190
Stroke in Canada: Highlights from the Canadian Chronic Disease Surveillance System. *2017 - Canada.ca*, Public Health Agency of Canada, 9 Dec. 2019, https://www.canada.ca/en/public-health/services/publications/diseases-conditions/stroke-canada-fact-sheet.html.
Sullender CT, Richards LM, He F, Luan L, Dunn AK. Dynamics of isoflurane-induced vasodilation and blood flow of cerebral vasculature revealed by multi-exposure speckle imaging. J Neurosci Methods. 2022 Jan 15;366:109434. doi: 10.1016/j.jneumeth.2021.109434. Epub 2021 Dec 1. PMID: 34863840; PMCID: PMC9258779.
Summers, J. J., Kagerer, F. A., Garry, M. I., Hiraga, C. Y., Loftus, A., & Cauraugh, J. H. (2007). Bilateral and unilateral movement training on upper limb function in chronic stroke patients: A TMS study. *Journal of the neurological sciences*, *252*(1), 76–82. https://doi.org/10.1016/j.jns.2006.10.011
Sun, M., Deng, B., Zhao, X. *et al*. Isoflurane preconditioning provides neuroprotection against stroke by regulating the expression of the TLR4 signalling pathway to alleviate microglial activation. Sci Rep 5, 11445 (2015). https://doi.org/10.1038/srep11445
Sunil Smrithi, Jiang John, Shah Shashwat, Kura Sreekanth, Kilic Kivilcim, Erdener Sefik, Ayata Cenk, Devor Anna, Boas David, Neurovascular coupling is preserved in chronic stroke recovery after targeted photothrombosis, NeuroImage: Clinical, Volume 38, 2023, 103377, ISSN 2213-1582, https://doi.org/10.1016/j.nicl.2023.103377.
Takeuchi, N., & Izumi, S. (2012). Maladaptive plasticity for motor recovery after stroke: mechanisms and approaches. *Neural plasticity*, *2012*, 359728. https://doi.org/10.1155/2012/359728
Taub, E., Uswatte, G., Mark, V. W., Morris, D. M., & Barman, J. (2013). The motor deficit attributable to the lesion in the contralesional hemisphere of the chronic stroke patient. Brain, 136(5), 1288-1308.
Taylor JL, Gandevia SC. Noninvasive stimulation of the human corticospinal tract. Journal of Applied Physiology. 2004; Vol. 96, No. 4. https://doi.org/10.1152/japplphysiol.01116.2003
Tennant KA, Adkins DL, Donlan NA, Asay AL, Thomas N, Kleim JA, Jones TA. The organization of the forelimb representation of the C57BL/6 mouse motor cortex as defined by intracortical microstimulation and cytoarchitecture. Cereb Cortex. 2011 Apr;21(4):865-76. doi: 10.1093/cercor/bhq159. Epub 2010 Aug 25. PMID: 20739477; PMCID: PMC3059888.
Tennant KA, Adkins DL, Scalco MD, Donlan NA, Asay AL, Thomas N, Kleim JA, Jones TA. Skill learning induced plasticity of motor cortical representations is time and age-dependent. Neurobiol Learn Mem. 2012 Oct;98(3):291-302. doi: 10.1016/j.nlm.2012.09.004. Epub 2012 Sep 23. PMID: 23010138; PMCID: PMC3491094.
Tennant, K. A., Kerr, A. L., Adkins, D. L., Donlan, N., Thomas, N., Kleim, J. A., & Jones, T. A. (2015). Age-dependent reorganization of peri-infarct "premotor" cortex with task-specific rehabilitative training in mice. *Neurorehabilitation and neural repair*, *29*(2), 193–202. https://doi.org/10.1177/1545968314541329
Tehovnik EJ. Electrical stimulation of neural tissue to evoke behavioral responses. J Neurosci Methods. 1996 Mar;65(1):1-17. doi: 10.1016/0165-0270(95)00131-x. PMID: 8815302.

Teskey, G. C., Monfils, M. H., VandenBerg, P. M., & Kleim, J. A. (2002). Motor map expansion following repeated cortical and limbic seizures is related to synaptic potentiation. *Cerebral cortex (New York, N.Y. : 1991)*, *12*(1), 98–105. https://doi.org/10.1093/cercor/12.1.98

Thair, H., Holloway, A. L., Newport, R., & Smith, A. D. Transcranial Direct Current Stimulation (tDCS): A Beginner's Guide for Design and Implementation. *Frontiers in neuroscience*, **11**, 641, (2017). https://doi.org/10.3389/fnins.2017.00641

Timothy M. Barth, Theresa A. Jones, Timothy Schallert, Functional subdivisions of the rat somatic sensorimotor cortex, *Behavioural Brain Research*. **39**(1), 73-95, (1990). ISSN 0166-4328, https://doi.org/10.1016/0166-4328(90)90122-U

Toshihiko Kuroiwa, MD , Guohua Xi, MD , Ya Hua, MD , Tavarekere N. Nagaraja, PhD , Joseph D. Fenstermacher, PhD , and Richard F. Keep, PhD. Development of a Rat Model of Photothrombotic Ischemia and Infarction Within the Caudoputamen. Stroke. 2009;40:248–253. https://doi.org/10.1161/STROKEAHA.108.527853

Touvykine, B., Elgbeili, G., Quessy, S., & Dancause, N. (2020). Interhemispheric modulations of motor outputs by the rostral and caudal forelimb areas in rats. *Journal of neurophysiology*, *123*(4), 1355–1368. https://doi.org/10.1152/jn.00591.2019

Traversa Raimondo, MD , Cicinelli Paola, MD , Bassi Andrea, MD , Rossini Paolo, MD , and Bernardi Giorgio, MD. Mapping of Motor Cortical Reorganization After Stroke. 1997;28:110–117. https://doi.org/10.1161/01.STR.28.1.110

Tsuboyama, M., Lee Kaye, H., & Rotenberg, A. (2019). Biomarkers Obtained by Transcranial Magnetic Stimulation of the Motor Cortex in Epilepsy. *Frontiers in integrative neuroscience*, *13*, 57. https://doi.org/10.3389/fnint.2019.00057

Tung CE., Win SS, and Lansberg MG, Cost-Effectiveness of Tissue-Type Plasminogen Activator in the 3- to 4.5-Hour Time Window for Acute Ischemic Stroke. (2011), *Stroke*;42:2257–2262 https://doi.org/10.1161/STROKEAHA.111.615682

Vahdat *et al*, Brain-wide neural dynamics of poststroke recovery induced by optogenetic stimulation, *Science Advances.* **7**(33), (2021). DOI: 10.1126/sciadv.abd9465

Välisuo P, Optical methods for assessing skin flap survival, In Woodhead Publishing Series in Biomaterials, Biophotonics for Medical Applications, Woodhead Publishing, 2015, Pages 331-346, ISBN 9780857096623, https://doi.org/10.1016/B978-0-85709-662-3.00012-9.

Van Wittenberghe IC, Peterson DC. Corticospinal Tract Lesion. [Updated 2023 Jan 20]. In: StatPearls [Internet]. Treasure Island (FL): StatPearls Publishing; 2023 Jan-. Available from: https://www.ncbi.nlm.nih.gov/books/NBK542201/

Veldema, J., Gharabaghi, A. Non-invasive brain stimulation for improving gait, balance, and lower limbs motor function in stroke. J NeuroEngineering Rehabil 19, 84 (2022). https://doi.org/10.1186/s12984-022-01062-y

Wang, Tiannan & Cui, Wenju & Xie, Yicheng & Zhang, Weiping & Ding, Shinghua. Controlling the Volume of the Focal Cerebral Ischemic Lesion through Photothrombosis. *Am. J. Biomed. Sci*. **2**. 33-42, (2010). Doi: 10.5099/aj100100033.

Wang Q, Ding SL, Li Y, Royall J, Feng D, Lesnar P, Graddis N, Naeemi M, Facer B, Ho A, Dolbeare T, Blanchard B, Dee N, Wakeman W, Hirokawa KE, Szafer A, Sunkin SM, Oh SW, Bernard A, Phillips JW, Hawrylycz M, Koch C, Zeng H, Harris JA, Ng L. The Allen Mouse Brain Common Coordinate Framework: A 3D Reference Atlas. Cell. 2020 May 14;181(4):936-953.e20. doi: 10.1016/j.cell.2020.04.007. Epub 2020 May 7. PMID: 32386544; PMCID: PMC8152789.

Wang RY, Wang FY, Huang SF, Yang YR. High-frequency repetitive transcranial magnetic stimulation enhanced treadmill training effects on gait performance in individuals with chronic stroke: A double-blinded randomized controlled pilot trial. Gait Posture. 2019 Feb;68:382-387. doi: 10.1016/j.gaitpost.2018.12.023. Epub 2018 Dec 18. PMID: 30586670.

Ward, N. S., Brander, F., & Kelly, K. (2017). Intensive upper limb neurorehabilitation in chronic stroke: outcomes from the Queen Square programme. Journal of Neurology, Neurosurgery & Psychiatry, 88(6), 498-506.

Watson BD, Dietrich WD, Busto R, Wachtel MS, Ginsberg MD. Induction of reproducible brain infarction by photochemically initiated thrombosis. *Ann Neurol*. **17**(5), 497-504, (1985). doi: 10.1002/ana.410170513. PMID: 4004172.

Weber RZ, Mulders G, Kaiser J, Tackenberg C, Rust R. Deep learning-based behavioral profiling of rodent stroke

recovery. BMC Biol. 2022 Oct 15;20(1):232. doi: 10.1186/s12915-022-01434-9. PMID: 36243716; PMCID: PMC9571460.

Winship, I. R., & Murphy, T. H. (2008). In vivo calcium imaging reveals functional rewiring of single somatosensory neurons after stroke. *The Journal of neuroscience : the official journal of the Society for Neuroscience*, *28*(26), 6592–6606. https://doi.org/10.1523/JNEUROSCI.0622-08.2008

Winship, I. R., & Murphy, T. H. (2009). Remapping the somatosensory cortex after stroke: insight from imaging the synapse to network. *The Neuroscientist : a review journal bringing neurobiology, neurology and psychiatry*, *15*(5), 507–524. https://doi.org/10.1177/1073858409333076

Włodarczyk L, Cichon N, Saluk-Bijak J, Bijak M, Majos A, Miller E. Neuroimaging Techniques as Potential Tools for Assessment of Angiogenesis and Neuroplasticity Processes after Stroke and Their Clinical Implications for Rehabilitation and Stroke Recovery Prognosis. Journal of Clinical Medicine. 2022; 11(9):2473. https://doi.org/10.3390/jcm11092473

Xie, L., Kang, H., & Nedergaard, M. (2016). A Novel Model of Transient Occlusion of the Middle Cerebral Artery in Awake Mice. *Journal of nature and science*, *2*(2), e176.

Xu, N., LaGrow, T. J., Anumba, N., Lee, A., Zhang, X., Yousefi, B., Bassil, Y., Clavijo, G. P., Khalilzad Sharghi, V., Maltbie, E., Meyer-Baese, L., Nezafati, M., Pan, W. J., & Keilholz, S. (2022). Functional Connectivity of the Brain Across Rodents and Humans. *Frontiers in neuroscience*, *16*, 816331. https://doi.org/10.3389/fnins.2022.816331

Xu, T., Yu, X., Perlik, A. J., Tobin, W. F., Zweig, J. A., Tennant, K., ... & Zuo, Y. (2009). Rapid formation and selective stabilization of synapses for enduring motor memories. Nature, 462(7275), 915-919.

Yarossi M, Patel J, Qiu Q, Massood S, Fluet G, Merians A, Adamovich S, Tunik E. The Association Between Reorganization of Bilateral M1 Topography and Function in Response to Early Intensive Hand Focused Upper Limb Rehabilitation Following Stroke Is Dependent on Ipsilesional Corticospinal Tract Integrity. Front Neurol. 2019 Mar 26;10:258. doi: 10.3389/fneur.2019.00258. PMID: 30972004; PMCID: PMC6443957.

Yew KS, Cheng EM. Diagnosis of acute stroke. Am Fam Physician. 2015 Apr 15;91(8):528-36. PMID: 25884860.

Yi, J. H., & Hazell, A. S. (2006). Excitotoxic mechanisms and the role of astrocytic glutamate transporters in traumatic brain injury. *Neurochemistry international*, *48*(5), 394–403. https://doi.org/10.1016/j.neuint.2005.12.001

Yoo, J. W., Hong, B. Y., Jo, L., Kim, J. S., Park, J. G., Shin, B. K., & Lim, S. H. (2020). Effects of Age on Long-Term Functional Recovery in Patients with Stroke. *Medicina (Kaunas, Lithuania)*, *56*(9), 451. https://doi.org/10.3390/medicina56090451

Young, N. A., Vuong, J., Flynn, C., & Teskey, G. C. (2011). Optimal parameters for microstimulation derived forelimb movement thresholds and motor maps in rats and mice. *Journal of neuroscience methods*, *196*(1), 60–69. https://doi.org/10.1016/j.jneumeth.2010.12.028

Zeiger, W.A., Marosi, M., Saggi, S. *et al.* Barrel cortex plasticity after photothrombotic stroke involves potentiating responses of pre-existing circuits but not functional remapping to new circuits. *Nat Commun* **12,** 3972 (2021). https://doi.org/10.1038/s41467-021-24211-8

Zeiler, S. R., Hubbard, R., Gibson, E. M., Zheng, T., Ng, K., O'Brien, R., ... & Muir, D. (2016). Paradoxical motor recovery from a first stroke after induction of a second stroke: reopening a postischemic sensitive period. Neurorehabilitation and Neural Repair, 30(8), 794-800.

Zhang, J. J., Sánchez Vidaña, D. I., Chan, J. N., Hui, E. S. K., Lau, K. K., Wang, X., Lau, B. W. M., & Fong, K. N. K. (2023). Biomarkers for prognostic functional recovery poststroke: A narrative review. *Frontiers in cell and developmental biology*, *10*, 1062807. https://doi.org/10.3389/fcell.2022.1062807

Zhang, S. Y., Jeffers, M. S., Lagace, D. C., Kirton, A., & Silasi, G. (2021). Developmental and interventional plasticity of motor maps after perinatal stroke. *The Journal of neuroscience : the official journal of the Society for Neuroscience*, *41*(28), 6157–6172. Advance online publication. https://doi.org/10.1523/JNEUROSCI.3185-20.2021

Zhao LR, Willing A. Enhancing endogenous capacity to repair a stroke-damaged brain: An evolving field for stroke research. Prog Neurobiol. 2018 Apr-May;163-164:5-26. doi: 10.1016/j.pneurobio.2018.01.004. Epub 2018 Feb 21. PMID: 29476785; PMCID: PMC6075953.